SECURITY MARKING

The classified or limited status of this report applies to each page, unless otherwise marked.

Separate page printouts MUST be marked accordingly.

THIS DOCUMENT CONTAINS INFORMATION AFFECTING THE NATIONAL DEFENSE OF THE UNITED STATES WITHIN THE MEANING OF THE ESPIONAGE LAWS, TITLE 18, U.S.C., SECTIONS 793 AND 794. THE TRANSMISSION OR THE REVELATION OF ITS CONTENTS IN ANY MANNER TO AN UNAUTHORIZED PERSON IS PROHIBITED BY LAW.

NOTICE: When government or other drawings, specifications or other data are used for any purpose other than in connection with a definitely related government procurement operation, the U. S. Government thereby incurs no responsibility, nor any obligation whatsoever; and the fact that the Government may have formulated, furnished, or in any way supplied the said drawings, specifications, or other data is not to be regarded by implication or otherwise as in any manner licensing the holder or any other person or corporation, or conveying any rights or permission to manufacture, use or sell any patented invention that may in any way be related thereto.

AFRPL-TR-65-176

FINAL REPORT

EFFECT OF ROCKET ENGINE COMBUSTION ON CHAMBER MATERIALS, PART II: TWO-DIMENSIONAL COMPUTER PROGRAM

Technical Documentary Report No. AFRPL-TR-65-176

September 1965

Air Force Rocket Propulsion Laboratory
Edwards, California

Project No. 3058
Task No. 305802
Program Structure No. 750G

Prepared Under Contract No. AF04(611)-9714

H. A. Friedman
S. F. Persselin
B. L. McFarland
J. D. Seader

By
Research Department of Rocketdyne,
A Division of North American Aviation, Inc.
Canoga Park, California

AFRPL-TR-65-1?

FINAL REPORT

EFFECT OF ROCKET ENGINE COMBUSTION ON CHAMBER MATERIALS, PART II: TWO-DIMENSIONAL COMPUTER PROGRAM

September 1965

Air Force Rocket Propulsion Laboratory

Edwards, California

by

H. A. Friedman
S. F. Persselin
B. L. McFarland
J. D. Seader

Research Department of Rocketdyne
A Division of North American Aviation, Inc.
Canoga Park, California

FOREWORD

This technical report was prepared for the Air Force Rocket Propulsion Laboratory, Edwards Air Force Base, California, by Rocketdyne, a Division of North American Aviation, Inc. The report covers Phase II of Contract AF04(611)-9714 in accordance with Part I, paragraph B.2.b.(3) under Project No. 3058, Task No. 305802, and Program Structure No. 750G. The Air Force Project Monitor was Lt. L. A. Barlock, office symbol RPREE. The research reported was conducted during the period 1 June 1964 through 31 May 1965 by the Research Department, R. J. Thompson, Jr., Vice President and Director. The Rocketdyne Program Manager was R. B. Lawhead, with J. M. Zimmerman and T. A. Coultas as responsible supervisors. J. D. Seader was technically responsible for the overall effort. H. A. Friedman was the Principal Investigator, and with B. L. McFarland developed the mathematical procedures utilized in the resulting digital computer program. S. Persselin and the Principal Investigator were responsible for coding the program.

This report has been given the Rocketdyne identification number R-6050-2.

This report contains no classified information extracted from other classified documents.

Publication of this report does not constitute Air Force approval of the report, findings, or conclusions. It is published only for the exchange and stimulation of ideas.

ABSTRACT

An alternating direction implicit finite difference procedure is developed for solving a general class of two-dimensional transient non-linear ablation and heat conduction problems for rocket engine thrust chamber walls. Engine firing may be steady or can consist of multiple start or pulsing type modes. The analysis is performed in cylindrical coordinates (axial and radial) assuming an axisymmetric multi-material wall having arbitrarily curved boundaries and interfaces. A maximum (due only to computer storage limitations) of five different wall materials may be treated in a given problem including one charring ablative material. Temperature dependent properties may be specified for each material. Chemical reactions within the ablative material are handled in depth; also surface erosion due to chemical reactions or melting at the hot gas boundary is treated and the resulting surface recession is predicted. The numerical procedures have been programmed in Fortran IV for automatic computation on the IBM 7094 digital computer. Comparison of the results of sample computations with actual engine test firing data is included in this report.

TABLE OF CONTENTS

ILLUSTRATIONS

TABLES

SYMBOLS

$a_\ell, b_\ell, c_\ell, d_\ell$	coefficients used to illustrate general tridiagonal system of equations, $\ell=1,\ldots,n$
B	input constant characteristic of the blocking phenomenon
C(T)	specific heat of wall material
C_p	specific heat at constant pressure
d	distance between adjacent points used in definition of first and second differences
$F(x,y,\tau)$	arbitrary function used in definition of first and second differences
$F_{dec}(T)$	fraction of mass converted from solid product (of char-reinforcement reaction) to gas by further decomposition
$F_{py}(T)$	fraction of mass converted from resin to vapor by the pyrolysis reaction
F_{res}	fraction of resin in the virgin laminate
$F_{sc}(T)$	fraction of mass remaining as the solid product of the char-reinforcement reaction
$F_{on}(\tau)$	multiplicative constant (in [0,1]) used to simulate intermittent firing in representative periods
$f(x,\tau)$	radial position of receding hot gas boundary
f_o	initial position of receding hot gas boundary
$G(x,y,\tau)$	mass flowrate of gases generated in charring material
G_x	axial component of $G(x,y,\tau)$
G_y	radial component of $G(x,y,\tau)$

$G_i(x,\tau)$	mass flowrate of gas or liquid species i ejected from wall at hot gas boundary
$H(T)$	enthalpy of gases generated in charring material
ΔH_i	heat of decomposition mode i at eroding wall surface
$h(x,\tau,T)$	heat transfer coefficient
h	value of distance increment when $\Delta x = \Delta y$
$\bar{h}_{conv}(x)$	basic convective heat transfer coefficient prior to modification for intermittent firing or blocking
$K(T)$	thermal conductivity of wall material
N_z	modulus, $h_{eff}\Delta z/K$, where $\Delta z = \min(\Delta x, \Delta y)$
n,s	outward normal, counterclockwise tangential directions, respectively, at boundary of material region (s also used to weight radial differences as r is used for axial differences)
n_j	input constant characteristic of gaseous species j ejected at hot gas boundary
Q	reference heat of reaction
$\Delta Q(T)$	heat of reaction
$q(x,\tau)$	heat flux
$R(x,y,\tau)$	ratio, $\frac{\partial T}{\partial x}\Big/\frac{\partial T}{\partial y}$, assumed equal, within limits, to G_x/G_y
R	modulus, $\alpha\Delta\tau/h^2$, used in stability analysis of linear conduction analog
r	parameter (in $[0,1]$) used for temporal weighting of axial differences in linear conduction analog

r_ℓ, z_ℓ	recursively defined quantities in solution of general tridiagonal system of equations, $\ell=1,\ldots,n$
$T(x,y,\tau)$	temperature of wall material
$T_{aw}(x)$	adiabatic wall temperature
T_{dec}	minimum decomposition temperature of wall material exposed to hot combustion gas
T_{env}	temperature of the environment
T_{py}	minimum pyrolysis temperature of the charring material
T_o	initial wall temperature
x	axial coordinate
Δx	axial distance increment
y	radial coordinate
Δy	radial distance increment
$\alpha(T)$	thermal diffusivity of wall material
$\beta_f(x)$	radiation shape factor
$\Gamma_{i,j}$	weight ratio of species i and j taking part in chemical reaction
ϵ	emissivity of radiating wall material
$\epsilon_{m,n,k}$	cumulative initial, truncation, and roundoff error introduced in numerical solution of linear conduction analog
$\rho(T)$	spatial density
ρ^*	true density of component present in charring material

σ	Stefan-Boltzmann constant
τ	time
$\Delta\tau$	time increment used for time step calculations

SUBSCRIPTS

A,B,C,D	points adjacent to interior point O (to right, above, left, and below, respectively) used with point O in 5-point analog of energy equation
B_i	points on exposed hot gas boundary
c	char
conv	due to convection
eff	effective
env	due to environmental heating
g_1, g_2, g_3	gases generated by pyrolysis, char-reinforcement reaction, and decomposition of solid product of char-reinforcement reaction, respectively
O	interior point (x_i, y_j)
P,Q	interface point on horizontal, vertical mesh lines, respectively
r	reinforcement
rad	due to radiation
res	resin
s	solid product of the char-reinforcement reaction
v	virgin laminate

1,2,3,4	regular points (x_i, y_j), (x_{i+1}, y_j), (x_i, y_{j+1}), (x_{i+1}, y_{j+1}), respectively, used in 4-point analog of continuity equation
∞	free stream conditions

INTRODUCTION AND SUMMARY

In order to effectively design rocket engine thrust chambers which are partly or completely cooled by heat sink or ablative techniques or evaluate engine firing data from such chambers, it is necessary to adequately predict the effect of combustion gas products upon the wall materials for the particular geometrical configurations of interest. In 1963, in conjunction with Contract No. AF04(611)-8190 (Ref. 1), Rocketdyne formulated a transient one-dimensional mathematical model of the mechanisms affecting charring-ablative wall materials, i.e., heat transfer, erosion, and corrosion. However, a detailed solution of the equations was not attempted at that time.

In April 1964, Rocketdyne initiated a 12-month two-phase program entitled "Effect of Rocket Engine Combustion on Chamber Materials" under Contract AF04(611)-9714. In Phase I of this program, which is reported in detail in Ref. 2 , two goals were achieved. First of all, the equations of the 1963 model were verified. Secondly, a computer code based on an augmented non-linear transient one-dimensional model was written to relate the combustion environment to its effect on ablative thrust chamber materials.

In Phase II, as described in detail in this report, a finite difference procedure and accompanying computer program was developed for solving

a general two-dimensional extension of the Phase I problem. The analysis was performed in cylindrical coordinates (axial and radial) assuming an axisymmetric multi-material solid with temperature dependent properties and arbitrarily curved boundaries and interfaces. A maximum of five wall materials can be handled in the computer program including no more than one charring ablative material. Surface erosion of the materials due to chemical reactions or melting at the hot gas boundary is also treated in the program and the resulting surface recession is predicted. All heat fluxes at the boundaries and material interfaces are expressed in terms of normally directed temperature gradients.

There are already in existence several one-dimensional and two-dimensional programs for analyzing ablation and heat conduction problems, but none it is felt provides adequate methods for handling these normal gradient conditions at curved boundaries and interfaces. Furthermore, in most previously existing programs, an explicit forward difference analog is used to simulate the energy equation in each time step. In order to avoid numerical instability with this method, it is often necessary to employ prohibitively small time steps. In the present program, on the other hand, a generalization of the unconditionally stable implicit Peaceman-Rachford alternating direction method (see Ref. 3 for basic technique) has been employed to discretize the energy equation in conjunction with special second-order accurate techniques for simulating normal gradient conditions at curved surfaces. Coupled to the solution

of the energy equation for the temperature distribution in each time step is a finite difference solution to the first order two-dimensional mass continuity equation for the mass flow rate of the generated pyrolysic gases in the internally charring ablative material. The gas mass flow is assumed to be zero at each interface separating the region from other solid materials.

In formulating the model and developing the numerical solution, the following assumptions were made concerning the charring ablative material:

1. There is assumed to be a single continuous charring material which is described by a continuous rather than an interface model. Thus, the moving pyrolysis zone, which separates the virgin material from the char residue, is distinguishable only by the temperature range within which the pyrolysis reaction takes place.

2. Chemical reactions occurring in the charring region are treated in depth but are simulated thermodynamically in the heat storage and gas enthalpy terms of the energy equation. They include a maximum of three gas generation reactions plus cracking of the generated gases. In addition to pyrolysis, a char-reinforcement reaction and a further decomposition of the solid product of this reaction can also be handled.

3. The porous char is cooled convectively by the pyrolysis gases, the gas and char temperatures at any point being assumed identical. Conduction of heat within the gas is taken to be negligible in comparison with that in the char.

4. All momentum effects and thus consideration of a momentum equation are neglected due to the two following assumptions:

a) negligible gas density relative to that of the solid material

b) orientation of the gas mass flow vector in the char with the temperature gradient rather than the pressure gradient vector (under certain conditions, further restrictions are placed on the direction of flow).

The heating and cooling mechanisms incorporated in the model and handled by the program include engine firing, environmental heating, radiation to the environment, insulation, chemical reaction and melting of the hot gas wall surface, blocking of the hot gas by the generated and transpiring gases at the boundaries, chemical reaction and convective cooling (discussed above) in the charring material and conduction within each wall material and across each material interface. Intermittent engine firing with soakback is also treated including both steady firing and high frequency pulsing. The latter is simulated in representative time periods by reduced values of the convective heat transfer coefficient.

The principal parameters computed and printed out at preassigned time levels are the temperature distribution throughout the wall materials, the gas mass flow rate at the hot surface of the charring ablator, and the new surface positions of the receding hot gas boundary. Also computed and optionally printed out are effective heat transfer coefficients at the

wall boundaries and (both axial and radial) mass flow rates within the region of charring. Finally, a matrix is supplied at the termination of the calculation of the maximum temperature achieved at each computational point within the charring material. This is particularly useful in case of multiple start or pulsing operations. Input requirements include the temperature dependence of the physical and chemical properties of the wall materials, the axial variation of the various surface heat flux and hot gas surface erosion parameters, and explicit piecewise quadratic functions describing the nozzle wall configuration. Also required are the initial thermal conditions as well as the composition of the charring material.

Program options include: (1) up to 5 wall materials, only one of which may char internally, (2) erosion of the hot gas surface of any of the materials exposed to firing, (3) omission of either charring or eroding materials which results in a straight conduction analysis.

In this report a brief description is given of previous work in the area of two-dimensional transient ablation calculations and a comparison is drawn with the present program, a discussion and derivation are presented of the ablation and heat conduction equations, the numerical procedures developed to solve the equations are described, and the essentials of the computer program are discussed. The results of several program computations are presented and compared with available experimental

test data, and typical examples of computer runs are described in detail. Finally, recommendations are given for further development and implementation of the two-dimensional program.

PREVIOUS INVESTIGATIONS

The widespread utilization of ablative materials for nose cones of re-entry vehicles and for rocket engine thrust chambers has stimulated the development of analytical methods for predicting the transient behavior of such materials. As described in Ref. 2, a number of analytical methods have been developed for handling one-dimensional models in either rectangular or radial coordinates.

On the other hand, relatively little effort has gone into the development of multi-dimensional models which are needed for a more accurate description of heat transfer phenomena in the complex geometry of actual multi-material thrust chamber walls. In what follows we give a brief summary of previously developed multi-dimensional models, as discussed in available literature, including the use of thermal analyzer computer programs, models developed primarily for nose-cone applications, and a recent two-dimensional nozzle model. A comparison is then drawn of the capabilities of the computer code developed in the present Phase II program with the others described.

THERMAL ANALYZER COMPUTER PROGRAMS

Rocketdyne has made extensive use of modified versions of two thermal analyzer digital computer programs, namely TIGER (Ref. 4) and TAP (Ref. 5). Both of these programs permit the solution of multi-

dimensional heat conduction problems for multi-material walls and structures. Surface boundary conditions may consist of radiation and/or convective modes of heat transfer. An explicit finite difference solution technique, subject to the usual stability criteria, is utilized in both programs.

The TAP program is the more versatile of the two since it can handle temperature-dependent physical properties, a wider variety of surface boundary conditions, and can more easily approximate cylindrical coordinate systems. However, like the TIGER program, it is not sufficiently versatile to solve the problems of interest to the present program, namely those involving solid materials which are subject to internal charring and/or surface ablation, without considerably oversimplifying the actual physical and chemical processes. Furthermore, the user of the TAP program must, after selecting the positions of the nodes, submit as input to the program the coordinates of each node as well as all the corresponding capacitances and conductances. For complex geometries, the necessary pre-calculations as well as the writing of data sheets can be quite time-consuming. As will be discussed in detail later, the computer program presented in this report automatically sets up the node points so as to minimize the required pre-calculations.

MULTI-DIMENSIONAL COMPUTATION METHODS FOR NOSE CONE TYPE PROBLEMS

Hurwicz, et.al. (Ref. 6 and 7) have described multi-dimension computation

schemes for electronic analog computation which have been developed to solve particular simultaneous ablation and heat conduction problems for re-entry structures. In order to handle surface recession, a shrinking coordinate system is utilized in conjunction with the usual finite difference equations. Typical calculations for several structures indicate the significant differences between more exact multi-dimension calculations and one-dimensional approximations.

TWO-DIMENSIONAL NOZZLE MODEL?

McCuen, et.al. (Ref. 8) have developed a two-dimensional single-material computer program primarily for application to non-melting, non-charring nozzle throat inserts. The surface exposed to the hot combustion gases can, however, recede due to chemical reactions controlled either by mass transfer or reaction kinetics. A moving coordinate system is used in conjunction with an explicit finite difference technique. Only one wall material may be specified, but a variety of internal wall boundary conditions are possible. Temperature-dependent material properties can be utilized including directional thermal conductivities to simulate anisotropic materials.

COMPARISON WITH PRESENT PROGRAM

The numerical procedures described below and the resulting computer code developed in Phase II of the present program are more comprehensive

in many important respects than those previously available programs discussed above. Charring, for example, is handled in the present program as a two-dimensional continuous process and not as a discontinuous interface reaction; on the other hand, except for the Hurwicz program, which is not applicable to rocket nozzles, charring is omitted in the other programs. In this connection it should be mentioned that a version of TAP has been adapted at Rocketdyne to simulate charring by effectively lumping all gas generation and convection effects in the storage term of the energy equation. Of the programs discussed above, only the McCuen code includes the effect of boundary curvature in the normal temperature gradient conditions at the hot gas surface, by all means the most important region, through use of a radial curvilinear transformation. The present code can account for curvature at all boundaries. The present program employs an implicit finite difference procedure to solve the energy equation and thus avoids limiting the size of the time step used in order to insure the stability of the numerical computation. This limitation exists in the other programs available except for that of Hurwicz which requires no discretization of the time derivative at all, being an analog procedure. Usually an implicit method requires a time consuming iterative solution in each time step, but, as discussed below, the alternating direction method (ADM) used in the present program generates a tridiagonal system of equations in each time step which can be solved directly by well known recursion formulas. Although the

explicit method is between two and three times faster than the ADM in each time step, the ADM can often use a time step as much as 100 times larger than that needed for the explicit method and is therefore generally much more efficient. One excellent feature of the McCuen code not treated in the present analysis is the ability to specify different thermal conductivities in the axial and radial directions.

The comparison between the presently reported code and those discussed above is summarized in Table 1, where "2D-ABLATE" is used to designate the former. The full name of the code reported here is Two-dimensional Charring Ablation Program. The Hurwicz code is omitted from the table due to its analog rather than digital nature and its non-applicability to rocket engine thrust chambers.

Table 1

Comparison of the Present Program With Some of the Previous 2D Conduction and Ablation Codes

TABLE	TIGER	TAP	McCUEN	2D-ABLATE (presently reported code)
Transient Conduction	yes	yes	yes	yes
Charring	no	no	no	yes
Surface Ablation	no	no	yes	yes
More than one Material	yes	yes	no	yes
Temperature Dependent Properties	no	yes	yes	yes
Finite Difference Method	explicit	exp.	exp.	Implicit alternating direction method (ADM)
Numerical Stability	conditional	cond.	cond.	unconditional
Normal Flux at Curved Boundaries	no	no	yes	yes
Anisotropic Conductivity	no	no	yes	no

MATHEMATICAL MODEL

PRELIMINARY REMARKS

A two-dimensional transient mathematical model is developed below describing the coupled conduction and charring ablation mechanisms which are induced in the walls of a rocket engine thrust chamber during engine firing. It is assumed for the presentation that the reader is familiar with the descriptive motivation and discussion contained in Ref. 2 , the final report of the first phase of this program. Thus the discussion presented here will be limited to those areas in which the Phase 2 model differs from the Phase 1 one-dimensional model. These include the extra dimension, the thermodynamic simulation of the chemical reactions occurring within the ablative material, the omission of all momentum effects, and the degree of assumed knowledge of the material properties of the charring ablative material.

The general approach taken is similar to that of Ref. 2 in that internal charring is treated in depth. Both heat flow and gas mass-flow are handled in two-dimensional cylindrical coordinates, however, using the assumption of axial symmetry to restrict their spatial variation to the axial and radial directions.

In this section we will describe the major features of the mathematical model. Further details, such as the basis for the thermodynamic simulation of chemical reactions in the energy and continuity equations, are given in separate appendices at the end of the report.

The equations developed are presumed to hold in regions bounded by quite arbitrarily curved boundaries. In practice, the overall multi-region configurations are limited to those typical of the walls of rocket engine thrust chambers. Similarly the boundary conditions utilized reflect the heating and cooling mechanisms which describe the thermal environment of the chamber walls during engine operation. Figure 1 is a sketch of a typical thrust chamber wall configuration in cross-section, along with examples of the heating conditions encountered (in Fig. 1 the receding hot gas boundary is indicated as well as the normal and tangential directions assumed for the material regions).

ENERGY, CONTINUITY, AND RECESSION EQUATIONS

Using cylindrical coordinates (axial and radial), the energy and continuity equations, respectively, can be written in the following form for a charring wall material (see Appendix A for justification):

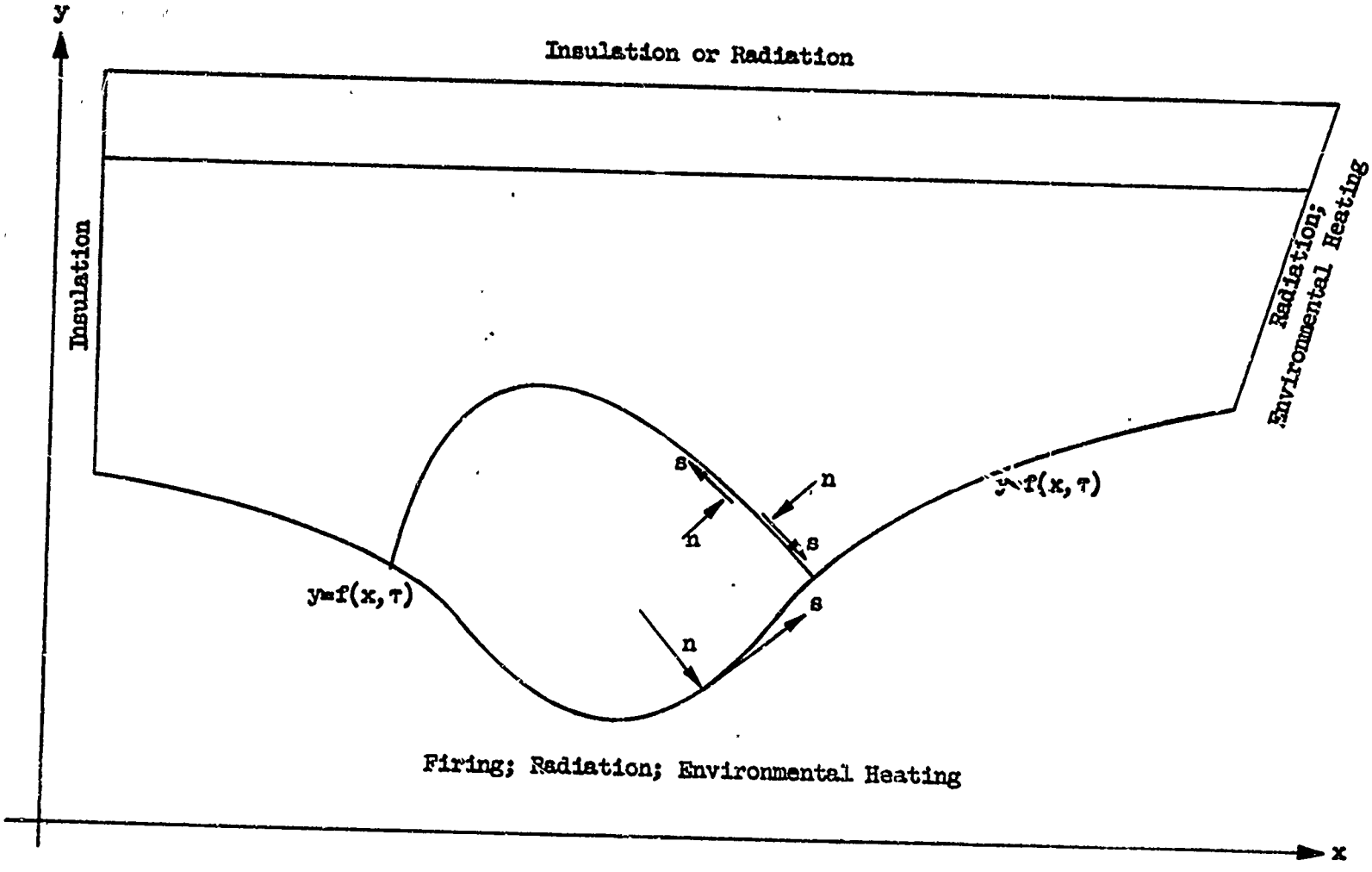

Fig. 1 Typical Thrust Chamber Configuration and Boundary Conditions

$$\left[\rho C - \sum_i Q_i \frac{\partial \rho}{\partial F_i} \frac{dF_i}{dT}\right] \frac{\partial T}{\partial \tau}$$

$$= \frac{\partial}{\partial x}\left(K \frac{\partial T}{\partial x}\right) + \frac{1}{y}\frac{\partial}{\partial y}\left(yK \frac{\partial T}{\partial y}\right) - G_x \frac{\partial H}{\partial x} - G_y \frac{\partial H}{\partial y} \quad , \qquad (1)$$

$$- \frac{\partial \rho}{\partial \tau} = - \sum_i \frac{\partial \rho}{\partial F_i} \frac{\partial F_i}{\partial \tau} = \frac{\partial G_x}{\partial x} + \frac{1}{y}\frac{\partial}{\partial y}(yG_y) \quad , \qquad (2)$$

where i ranges over the chemical reactions taking place within the material. For a non-charring material, in which no reactions and thus no gas mass flow occurs, Eq. (2) does not apply and Eq. (1) reduces to the pure conduction equation:

$$\rho C \frac{\partial T}{\partial \tau} = \frac{\partial}{\partial x}\left(K \frac{\partial T}{\partial x}\right) + \frac{1}{y}\frac{\partial}{\partial y}\left(yK \frac{\partial T}{\partial y}\right) \quad . \qquad (3)$$

Using the following expression for the density ρ of the charring material (see Appendix B for the derivation)

$$\rho = \rho_v^* (1 - F_{res} F_{py}) + \rho_s^* [(1 - \Gamma_{c,s} - \Gamma_{r,s}) F_{sc} - F_{dec} F_{sc}] \quad , \qquad (4)$$

we may substitute in Eqs. (1) and (2) to obtain the following more convenient expressions:

Energy

$$\left\{\rho C+Q_{py}\rho_v^* F_{res}\frac{dF_{py}}{dT}+\rho_s^*\left[Q_{sc}\left(\Gamma_{c,s}+\Gamma_{r,s}-1\right)\frac{dF_{sc}}{dT}\right.\right.$$
$$\left.\left.+\left(Q_{sc}F_{dec}\frac{dF_{sc}}{dT}+Q_{dec}F_{sc}\frac{dF_{dec}}{dT}\right)\right]\right\}\frac{\partial T}{\partial \tau}$$
$$=\frac{\partial}{\partial x}\left(K\frac{\partial T}{\partial x}\right)+\frac{1}{y}\frac{\partial}{\partial y}\left(yK\frac{\partial T}{\partial y}\right)-G_x\frac{\partial H}{\partial x}-G_y\frac{\partial H}{\partial y}\quad , \tag{5}$$

Continuity

$$\rho_v^* F_{res}\frac{dF_{py}}{d\tau}+\rho_s^*\left[\left(\Gamma_{c,s}+\Gamma_{r,s}-1\right)\frac{\partial F_{sc}}{\partial \tau}+F_{dec}\frac{\partial F_{sc}}{\partial \tau}+F_{sc}\frac{\partial F_{dec}}{\partial \tau}\right]$$
$$=\frac{\partial G_x}{\partial x}+\frac{1}{y}\frac{\partial}{\partial y}\left(yG_y\right)\quad . \tag{6}$$

Consideration of a momentum equation is avoided by the use of two assumptions. Strictly speaking, Eq. (4) is an expression for the density only of the porous solid material in the char region and not of the entire region. The missing term, the density of the gas, is assumed to vary so slightly with time that the derivative of this quantity can be neglected in the continuity equation. Its elimination from the energy equation, on the other hand, is effected algebraically as shown in Appendix A. The only remaining dependent variables (other than those parameters with known temperature dependence) are T, G_x, and G_y.

The second basis upon which momentum considerations can be eliminated is the assumption that the orientation of the gas mass flowrate in the char

region is in the direction of the temperature gradient vector,* rather than the pressure gradient vector, as indicated in the following equation:

$$G_x/G_y = \frac{\partial T}{\partial x} \Big/ \frac{\partial T}{\partial y} \; (\equiv R(x,y,\tau)) \quad . \tag{7}$$

In the energy equation, the gas cracking reaction is simulated in the convection terms by rewriting $\frac{\partial H}{\partial x}$ and $\frac{\partial H}{\partial y}$ as $\frac{dH}{dT}\frac{\partial T}{\partial x}$ and $\frac{dH}{dT}\frac{\partial T}{\partial y}$ where H is assumed to be a known function of temperature and includes the effective heat of cracking as well as the integral with respect to temperature of the gas specific heat at constant pressure.

All physical and chemical material properties appearing in Eqs. (1) - (6), i.e., F_{py}, F_{sc}, F_{dec}, K, ρC, and H, are assumed to be known functions of temperature.

In the case of surface erosion, one more dependent variable of the analysis must be accounted for, namely, the changing radial position, $y = f(x,\tau)$, of the receding hot gas boundary (see Fig. 1). The following differential equation relates surface recession to the surface erosion mechanisms:

$$\frac{\partial f}{\partial \tau} = \left(\sum_i G_i\right) \sqrt{1+\left(\frac{\partial f}{\partial x}\right)^2} \Big/ \rho \quad , \tag{8}$$

where i ranges over the species of gas or liquid generated at the surface and does not include those generated within the material and ejected

*The direction of flow may be further restricted as discussed on page 65 below.

at the surface. The values of G_1 are determined through a temperature coupled analysis of the erosive mechanisms occurring at the surface. This is discussed below in the section on initial and boundary conditions. In Eq. (8), ρ is the density of the decomposing wall material. The minus sign on the right side of Eq. (8) is required because of the negative orientation of the mass flowrates, G_1.

INITIAL AND BOUNDARY CONDITIONS

In order to complete the specification of the model, given in part by Eqs. (5) - (8), which determines the temperature distribution throughout the wall materials and the mass flowrate distribution in the ablative material, and in order to calculate the positions of the receding hot gas boundary due to surface erosion, it is necessary to specify initial values for these parameters and boundary conditions which describe the thermal exchange between the wall materials and their immediate environment.

For purposes of the present analysis, all wall materials are taken initially to be at some uniform temperature. After firing commences, the wall materials are assumed to be heated at the hot gas boundary by convection, but are permitted to radiate to the surroundings. The other boundaries may be either insulated or radiating surfaces.

In addition, allowance is made for the possibility of a known heat flux at certain portions of the boundary due to heating or cooling by the outside environment (e.g., aerodynamic heating by the atmosphere during re-entry). Finally, perfect thermal contact is assumed at interfaces common to two adjoining materials, which implies continuous temperature and heat flux distributions across the interface. Heat is transferred through the walls by conduction only until some point within the interior of the charring material reaches its minimum pyrolysis temperature. After subsequent generation of gas and formation of a porous char within the material, convective cooling takes place due to the flow of gas through the char. In addition, heat is lost or gained through the process of gas generation itself. Similarly, all the heat brought to the wall at the hot gas boundary is conducted away from the surface into the interior until some exposed surface point of one of the wall materials (or the char residue in the case of the charring material) reaches its minimum decomposition temperature. Then some of the heat is absorbed at the boundary as the surface erodes (or perhaps released, depending upon the reaction that takes place). In addition, the surface heating is diminished by the so-called "blocking effect" of the gases ejected into the hot gas stream, including those generated both at the surface and within the charring material.

The qualitative discussion given above of the driving mechanisms for the initial and boundary value problem under discussion can be expressed more formally in summary, as follows:

Initial Conditions

$$T(x,y,0) = T_o \tag{9}$$

$$G_y(x,y,\tau) = 0 \quad \text{for} \quad T(x,y,\tau) \leq T_{py} \tag{10}$$

$$f(x,\tau) = f_o(x) \quad \text{for} \quad T(x,f(x,\tau),\tau) \leq T_{dec} \ , \tag{11}$$

where T_o, T_{dec}, and T_{py} are known constants and $f_o(x)$ is a known function of axial distance. After the beginning of pyrolysis, Eq. (10) can also be treated as a boundary condition by restricting attention to those points (x,y) in the charring material for which $T(x,y,\tau) = T_{py}$.

Boundary Condition

If n is taken in the outward normal direction at a boundary (see Fig. 1), we may write

$$K \frac{\partial T}{\partial n} = h_{eff}(T_{aw}-T) + \sum_i (\Delta H_i)G_i \ , \tag{12}$$

where

$$h_{eff} = \begin{cases} h_{conv} + h_{rad} + h_{env} \\ 0 \text{ at insulated boundary} \end{cases} \tag{13}$$

Equations (12) and (13) comprise a convenient formulation of all the boundary conditions on the perimeter of the multi-material wall being analyzed. For example, T_{aw}, h_{conv}, and the species summation (where the range of i is the same as in Eq. (8)) have physical significance only at the hot gas surface exposed to engine firing. At other boundaries they either are zero in Eq. (12) or cancel out. For example, in the case of a surface at temperature T radiating to an environment at temperature T_{env}, we have $h_{conv} = 0$, the radiative term in Eq. (13) is expressed by

$$h_{rad} = - \frac{\alpha\epsilon\beta_f(T^4 - T_{env}^4)}{T_{aw} - T} \tag{14}$$

and (if there is any environmental heating) we have

$$h_{env} = \frac{q_{env}}{T_{aw} - T} \quad . \tag{15}$$

Thus, when Eq. (13) is substituted in (12), h_{conv} and T_{aw} do not appear. In Eq. (12), T_{aw} is a known function of x, K is a known function of T for each material, and the (ΔH_i) are known constants for each material. The G_i are determined by a method developed at Rocketdyne (see Ref. 9 and Appendix C) which combines many of the features of the Surface Kinetics Method discussed in Ref. 2 with a diffusion approach. In Eq. (13), the term h_{conv} includes the

following modifications of the basic heat transfer coefficient, $\bar{h}_{conv}$, due both to simulation of intermittent engine firing with soakback and to the "blocking" or "blowing effect" of the gases ejected at the hot gas surface:

$$h_{conv} = F_{on}(\tau)\bar{h}_{conv}(x) - BC_{p_\infty} \sum_j \left(\frac{dH_j}{dT} / C_{p_\infty}\right)^{n_j} G_j \quad . \tag{16}$$

In Eq. (16), $F_{on}(\tau)$ is a known step function which takes on constant values between 0 and 1 in order to simulate "on" time during representative time periods of intermittent steady firing or high frequency pulsing with soakback, and $\bar{h}_{conv}$ is a known function of x. The summation in Eq. (16) is taken over all gaseous (only) species ejected at the surface, including those generated internally as well as at the surface. In the blocking term, B, C_{p_∞}, and the n_j are known constants and the H_j are known functions of temperature. For the gases generated at the surface, the G_j are obtained as described in Appendix C and for the internally generated gas, we have

$$G = (G_x^2 + G_y^2)^{\frac{1}{2}} \quad . \tag{17}$$

Interface Conditions

At an interface separating material regions I and J, the continuity of temperature and normal heat flux conditions are expressed in the following form:

$$T_I = T_J , \quad K_I \left.\frac{\partial T}{\partial n}\right|_I = - K_J \left.\frac{\partial T}{\partial n}\right|_J , \tag{18}$$

where the minus sign results from the opposite senses of the outward normal directions from materials I and J.

The complete initial and boundary value problem that has been solved numerically and coded for automatic computation is given by Eqs. (5) - (18) along with subsidiary equations from Appendix C for the mass flow-rates of the gases and liquids generated at the hot gas surface.

NUMERICAL SOLUTION OF ABLATION AND CONDUCTION EQUATIONS

GENERAL APPROACH

The two-dimensional transient nonlinear boundary value problem of ablation and heat conduction defined by Eqs. (5) - (18) was solved numerically using finite difference techniques. The second order energy equation was discretized in accordance with a virtually second order generalization of the unconditionally stable implicit alternating-direction method of Peaceman and Rachford. Generalization and modification of this method were required for several reasons, including: (1) the nonlinearity of the equation and boundary conditions; (2) additional gas generation and convection terms in the equation due to charring; (3) coupling of the energy equation with the continuity and recession equations; (4) handling of more than one material; (5) the treatment of normal temperature gradient conditions at curved boundaries; and (6) the changes in boundary geometry due to surface erosion and recession. The first order continuity equation, on the other hand, was approximated to first order in time using a backward difference and to second order in distance. Because of the backward time difference, the resulting set of difference equations in each time step can be solved explicitly by proceeding from the vicinity of the char front to the hot gas surface with a four point formula.

The recession equation, i.e., Eq. (8), was discretized using a forward difference approximation for the time derivative. Due, however, to the iterative method described in Appendix C for evaluating the G_i and new values of the radial position, $y = f(x,\tau)$, of the hot gas boundary, the time difference approaches a second-order central difference approximation.

The use of essentially central or backward time differences in the finite difference version of Eqs. (5) - (8) should guarantee that the solution procedure will be unconditionally stable with respect to the time step procedure used in the interior of the material regions. (The stability of the distance step procedure, on the other hand, used within each time step to solve the continuity equation, has not been established. As a matter of fact, a homogeneous linearization of the difference equation has been shown to be unstable.)

As a result of the high values of the heat flux encountered at the hot gas boundary during periods of steady firing, limitations are imposed upon the size of the time steps utilized. In general, however, these limitations are not nearly as severe as that required for an explicit discretization of the energy equation, and are not necessary at all during periods of sparse intermittent firing or during soakback.

Uncoupling of the equations is achieved in each time step by predicting first the new position of the receding boundary (when recession occurs), then the two-dimensional temperature distribution, and finally the mass flowrates in the charring material. Only one such calculation cycle is performed in each time step. The only iterative procedures utilized are local in character, such as the recession calculation (see Appendix C) and a special routine used in the computer program for computing values of the effective heat transfer coefficient at boundaries subject to strong heat fluxes.

Spatially the discretization is achieved through imposition of a mesh on the multi-material region of interest. Mesh points are located at the intersection of the radial and axial mesh lines with each other (regularly spaced points) and with the boundaries and interfaces (irregularly spaced points). Axial mesh lines must be equidistant, but the spacing of the radial mesh lines can be variable. The latter feature permits concentration in areas of possibly strong axial heat flux (such as the nozzle throat region).

In simulating normal gradients at curved boundaries, exact relationships are employed in the usual fashion to relate the normal and tangential derivatives to the axial and radial derivatives in terms of the slope of the curve. These derivatives are used in conjunction with the

physical assumption of no local flux along the curve and second order spatial differencing to obtain an expression for the normal derivative. In the recession procedure, normal recession is actually predicted and then is converted to the equivalent radial recession, again in terms of the slope of the receding boundary.

After the iterative prediction of the new radial positions of the hot gas boundary (i.e., the new intersection of the boundary with the radial mesh lines), these values are smoothed to conform to the overall converging and diverging character of the initial boundary geometry. Then first derivatives of the new curve are obtained numerically at the radial positions. Finally, interpolation is performed to obtain both the new axial positions and the derivatives at these positions. This provides the basis for the calculations in the remainder of the time step.

In the time step procedure utilized, all systems of equations generated are at worst tridiagonal* and are easily solved directly or by well-known recursion formulas.

Explicit details of these numerical procedures are given in the following sections.

---

*A system of linear equations is tridiagonal if its nonzero coefficients appear only on the main diagonal and its immediately adjacent diagonals.

MESH PROCEDURE AND FINITE DIFFERENCE DEFINITIONS

At each level of time $\tau_k = \tau_{k-1} + \Delta\tau_{k-1}$ a rectangular mesh or network of lines, $x = x_i$ and $y = y_j$, where $x_i = x_{i-1} + \Delta x_{i-1}$ and $y_j = j\Delta y$, is imposed on the wall materials in the x-y plane. A typical example is shown in Fig. 2 . Intersections, (x_i, y_j), of the mesh lines are called regular mesh points, and intersections of mesh lines with boundaries or interfaces are called boundary or interface mesh points. Boundary and interface points are usually irregular. A regular mesh point, which is not on the boundary of the material region in which it lies or on its interface with another region, is further termed an interior point.

To approximate the continuous distributions desired, discrete temperature and mass flowrate distributions are obtained which are defined only at mesh points and at discrete times τ_k. These approximations are provided by employing finite differences to replace the time and space derivatives of Eqs. (5) - (18) at the mesh points. Three-level second order accurate differences are used for the space derivatives, centered at interior points and off-centered at boundary and interface points. Two-level differences are employed for the time derivatives, either first or second order in accuracy depending upon the weight given to the time levels used for the remaining terms of the equations

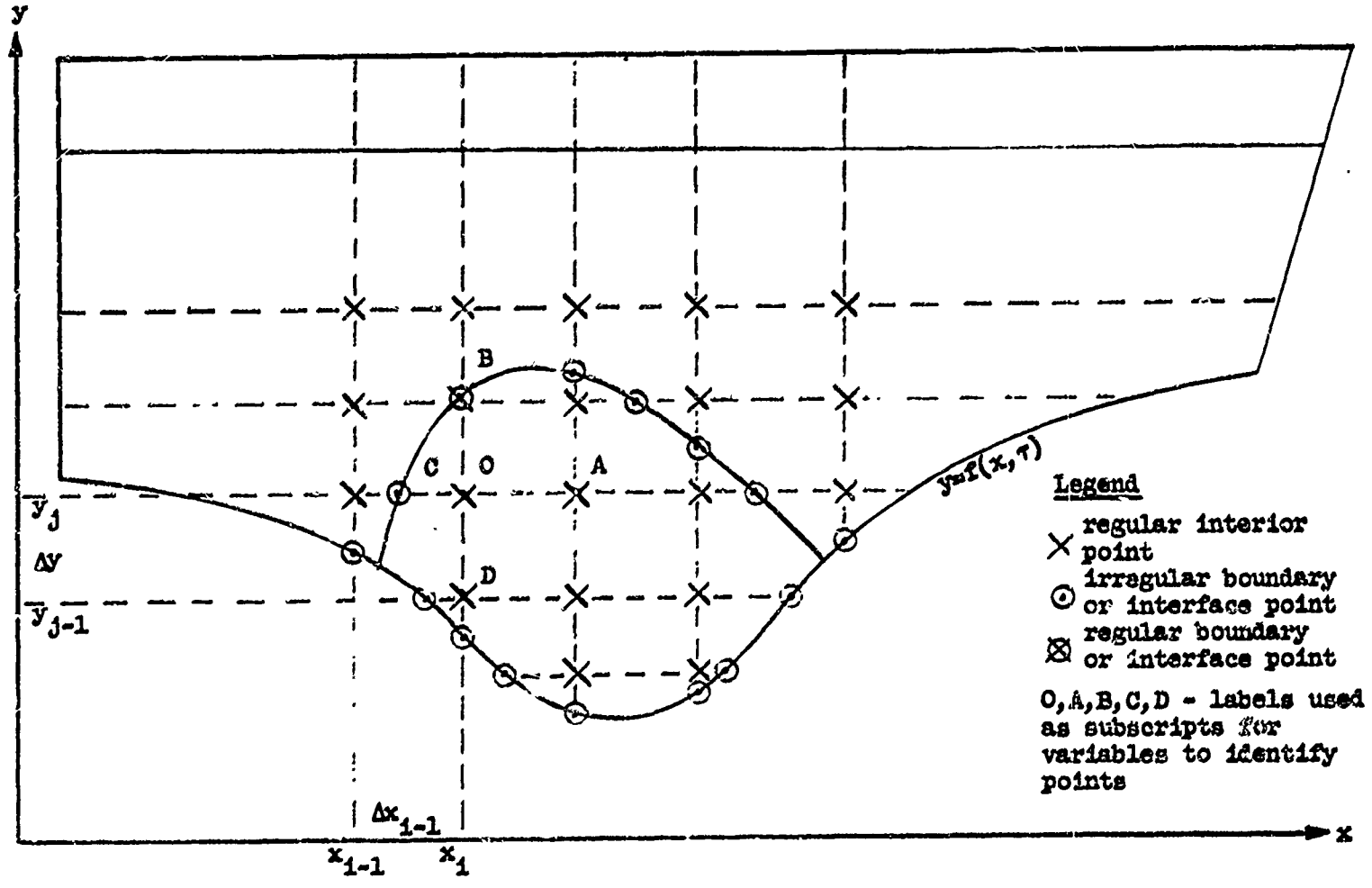

Fig. 2 Typical Mesh Configuration and Categorization of Resulting Mesh Points

in which the time derivatives appear. Equations (5) - (7) are discretized only at interior points and Eqs. (12) and (18) only at boundary and interface points. Equation (8), being only one-dimensional in distance, is differenced at the axial locations x_i.

For convenience of notation in defining centered space differences at an interior point, (x_j, y_j), we assign this point the subscript 0 and the four adjacent points the subscripts A, B, C, and D, as shown in Figs. 2 and 3, where the lettered points need not be interior points (Fig. 2). We further let d_A be the distance between points 0 and A, d_B the distance between 0 and B, etc. (see Fig. 5). Then centered finite difference approximations to the first and second axial derivatives are defined for use in Eqs. (5) - (8) as follows, where $F(x,y,\tau)$ is an arbitrary function and where $D_{A,C} = d_A + d_C$ and $P_{A,C} = d_A d_C D_{A,C}$,

$$\left.\frac{\partial F}{\partial x}\right|_{0,\tau_k} \approx \delta_x F_{0,k} = [d_C^2 F_{A,k} + (d_A^2 - d_C^2) F_{0,k} - d_A^2 F_{C,k}]/P_{A,C} \qquad (19)$$

$$\left.\frac{\partial^2 F}{\partial x^2}\right|_{0,\tau_k} \approx \delta_x^2 F_{0,k} = 2[d_C F_{A,k} - D_{A,C} F_{0,k} + d_A F_{C,k}]/P_{A,C} \quad . \qquad (20)$$

The defining formulas for centered radial differences are analogous to those of Eqs. (19) and (20) and thus have been omitted. Using the same

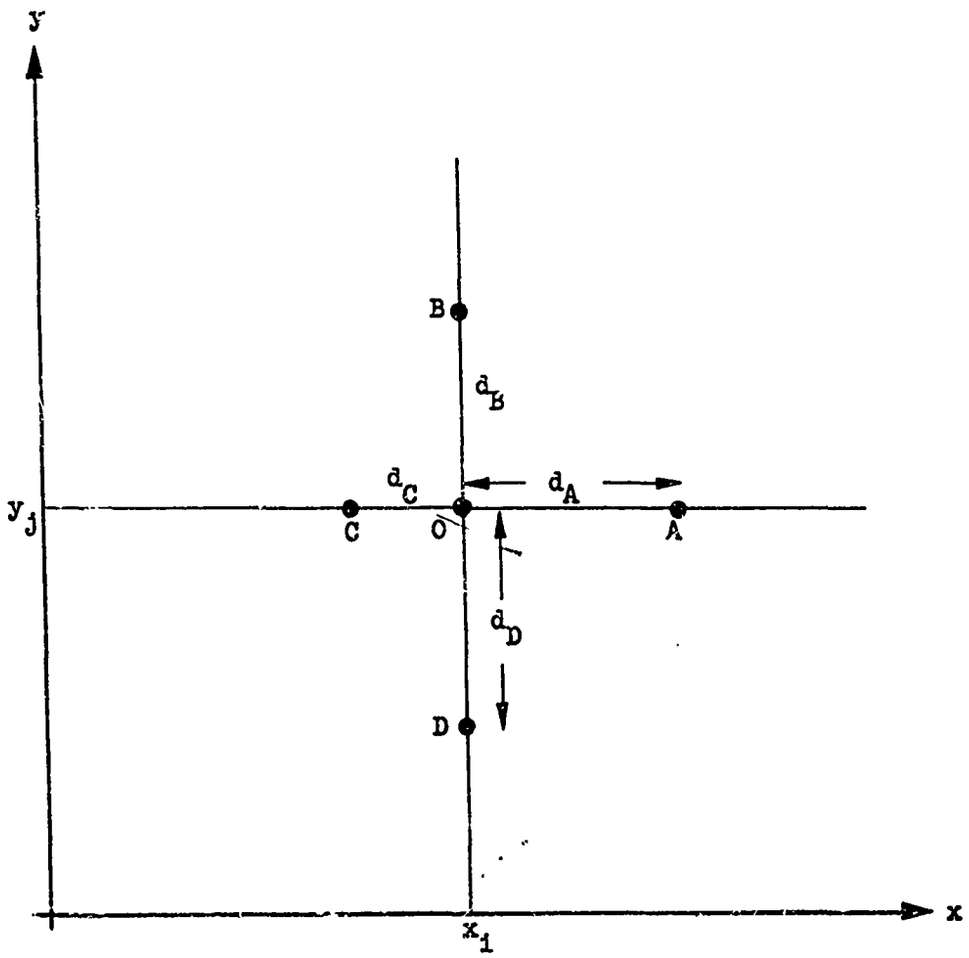

Fig. 3 Configuration Used in Defining First and Second Differences

point arrangement, the off-centered (to the left) first axial difference at point A (which is needed when A is either a boundary or interface point) is defined by the following:

$$\left.\frac{\partial F}{\partial x}\right|^{(-)}_{A,\tau_k} \cong \delta_x^{(-)} F_{A,k} = (\delta_x + d_A \delta_x^2) F_{O,k}$$

$$= [(D^2_{A,C} - d_A^2) F_{A,k} - D^2_{A,C} F_{O,k} + d_A^2 F_{C,k}] / P_{A,C} \quad . \qquad (21)$$

Similarly we obtain the off-centered (to the right) difference at C:

$$\left.\frac{\partial F}{\partial x}\right|^{(+)}_{C,\tau_k} \cong \delta_x^{(+)} F_{C,k} = (\delta_x - d_C \delta_x^2) F_{O,k}$$

$$= - [d_C^2 F_{A,k} - D^2_{A,C} F_{O,k} + (D^2_{A,C} - d_C^2) F_{C,k}] / P_{A,C} \quad . \qquad (22)$$

Both left and right off-centered temperature differences are required at an interface point separating materials of different thermal conductivities for, in such a case, the derivative is in general discontinuous at the interface. Downward and upward off-centered radial differences are defined analogously and are required for similar reasons. All the expressions defined above are accurate to second order and can be derived by manipulation of Taylor series, truncated after the quadratic term, expressed at each of the points A, B, C, and D about the point O.

The time differences used in Eqs. (5) - (8) are defined differently, being formulated as two-level rather than three-level expressions. To

approximate the derivative with respect to time at any mesh point O in the $(k+1)^{th}$ time step, i.e., in going from time τ_k to time τ_{k+1}, we use the following definition (where, for convenience, we drop the subscript on $\Delta\tau$):

$$\left.\frac{\partial F}{\partial \tau}\right|_{O,\bar{k}} \simeq \frac{F_{O,k+1} - F_{O,k}}{\Delta\tau}, \quad k \le \bar{k} \le k+1 \quad . \tag{23}$$

The derivative in Eq. (23) is taken to be at some time $\tau_{\bar{k}}$ between τ_k and τ_{k+1}. When $\bar{k}$ is k or k+1 exactly, then Eq. (23) is a forward or backward difference, respectively, and provides only first order accuracy. Only when $\bar{k} = k+\frac{1}{2}$ does the expression give full second order accuracy. The value of $\bar{k}$ is determined in a given discretization by the weighting factors assigned to the spatial differences and the other time-varying terms of the equation at each time level. If, for example, the spatial differences were assigned weight 0 at time τ_k and weight 1 at time τ_{k+1}, then $\bar{k}$ would assume the value k+1. If we term a discretization stable when errors do not grow during the calculation required for its solution and call it unconditionally stable when it is stable for any size time step used, then generally unconditional stability is assured only when $\bar{k} \ge k+\frac{1}{2}$. In the next section, through use of the simple linear two-dimensional transient heat conduction equation, the various possibilities for $\bar{k}$

are illustrated and a stability analysis is indicated. Included is a comparison of some of the commonly used difference methods with the alternating-direction method, which for the linear case, effectively yields a value for $\bar{k}$ of $k+\frac{1}{2}$.

DIFFERENCE SCHEMES FOR SOLVING THE LINEAR CONDUCTION EQUATION

As indicated above, the linear two-dimensional transient equation of heat conduction, which follows, is a convenient vehicle for illustrating some of the many two-level finite difference methods for solving parabolic partial differential equations such as the energy equation expressed by Eq. (5):

$$\frac{1}{\alpha}\frac{\partial T}{\partial \tau} = \frac{\partial^2 T}{\partial x^2} + \frac{\partial^2 T}{\partial y^2} \quad . \tag{24}$$

Most of the commonly used discretizations of Eq. (24) can be represented by the following two-parameter family of finite difference equations (for which we assume a constant mesh size $h = \Delta x = \Delta y$ and, as a matter of convenience, omit spatial subscripting):

$$\frac{1}{\alpha}\frac{T_{k+1}-T_k}{\Delta\tau} = r\delta_x^2 T_{k+1} + s\delta_y^2 T_{k+1} + (1-r)\delta_x^2 T_k + (1-s)\delta_y^2 T_k \quad . \tag{25}$$

Here r, s are weighting parameters which lie in the closed interval $[0,1]$ and whose values determine the level of the time difference,

i.e., the value of $\bar{k}$ (as defined in the last section). In general, we may write

$$\bar{k} = k + (r+s)/2 \quad . \tag{26}$$

Thus, for example, when $r = s = 0$, the most familiar form of Eq. (25) is obtained, the forward difference equation. In this case we have $\bar{k} = k$ and only first order accuracy is provided by the time differencing. The forward difference approximation is also referred to as explicit because each application of it contains only one unknown (temperature at time τ_{k+1}) and each member of the system of equations generated in each time step can be solved individually.

If we designate a numerical scheme for solving a system of finite difference equations as stable (in time) if errors do not grow during the calculation and unstable if they do grow, it can be proved that the explicit scheme ($r = s = 0$) is stable if and only if the following inequality holds:

$$\Delta\tau \leq \frac{h^2}{4\alpha} \quad . \tag{27}$$

(A stability analysis of Eq. (25) for all values of r and s is given in Appendix D.) Inequality (27) is often written in terms of the modulus $R = \frac{\alpha\Delta\tau}{h^2}$, as follows:

$$R = \frac{\alpha\Delta\tau}{h^2} \leq \frac{1}{4} \quad . \tag{28}$$

Because this condition is not met for all values of $\Delta\tau$, we say then that the explicit method is only conditionally stable. This restriction is, in some cases, more damaging than the first order truncation error incurred in using a forward difference. In fact for large values of $\frac{\alpha}{h^2}$, the scheme may not be useful because of the excessive number of time steps required despite the brevity of the calculation in each time step.

By setting $r = s = 1$ in Eq. (25), we obtain the implicit backward difference analog of Eq. (24), which, although stable for all possible values of R (i.e., unconditionally stable), is only first order accurate in time, $\bar{k}$ taking on the value $k+1$. In this case simultaneous systems of difference equations are generated in each time step containing as many as five unknowns each. Such systems are very time consuming to solve, usually requiring iterative procedures for most efficient treatment.

For $r = s = \frac{1}{2}$ and thus $\bar{k} = k+\frac{1}{2}$, Eq. (25) reduces to the well-known Crank-Nicolson method, which in addition to being unconditionally stable is second order accurate in time. The simultaneous systems of difference equations generated, however, as in the case of backward differences, require time consuming iterative methods for solution. As a matter of fact, it is evident that as long as r and s are both

nonzero, the systems of equations generated will be of the same form, requiring iterative solution. If, on the other hand, at least one of the parameters is 0 in each time step, the systems generated will be tridiagonal and admit of simple recursive solution without iteration (the form of the general tridiagonal system of equations is given below). In addition, as shown in Appendix D, it is necessary for unconditional stability that $\bar{k} \geq k+\frac{1}{2}$. Only when $\bar{k} = k+\frac{1}{2}$ does the time difference provide second order accuracy.

The only difference schemes which meet all three standards (of generating tridiagonal systems of equations, satisfying a necessary criterion for unconditional stability, and having second order local accuracy in the time difference) are those for which $r = 0$ and $s = 1$ or $r = 1$ and $s = 0$. If either of these assignments of values is used, however, and permitted to remain fixed, the resulting scheme still will not be unconditionally stable; although the assignment satisfies a necessary condition ($\bar{k} \geq k+\frac{1}{2}$), it is not sufficient to provide stability for all values of R. However, it is shown in Appendix D that, by choosing $r = 1$ and $s = 0$ in odd time steps and $r = 0$ and $s = 1$ in even steps, the difference scheme is unconditionally stable. By specifying r and s in such a manner, Eq. (25) reduces to the alternating-direction method of Peaceman and Rachford. The generalization of this scheme (given below) to Eq. (5) retains most of the advantages

described here. The systems of equations generated are tridiagonal and the value of $\bar{k}$ is $k+\frac{1}{2}$ (before linearization in which coefficients are taken at time τ_k). Although a full stability analysis has not been performed for the generalized scheme, it has usually been found in dealing with the conduction equation that, if a difference procedure is stable in the linear case, it will be stable for the nonlinear as well. As indicated earlier in the report, however, stability of a difference analog of the conduction equation does not necessarily extend in general to the coupled boundary procedure. It has been shown (Refs. 10 and 11) that for the linear equation in a bounded region, with values specified on the boundary, the alternating-direction method coupled with the known distribution on the boundary is unconditionally stable. In the case of boundary heat flux conditions, however, stability does not automatically follow and, in some cases, restriction of the size of $\Delta\tau$ is required, as discussed later in the report.

The results of the above discussion of the four schemes obtained from Eq. (25) in the linear case are summarized in Table 2 .

COMPUTATIONAL PROCEDURES

In each time step of the numerical solution of Eqs. (5) - (18), the major computational procedures are performed in the following order:

Table 2 . Comparison of difference schemes for solving the linear conduction equation

Case	Difference Scheme	Stability Criterion	Value of $\bar{k}$	Order of Time Difference
$r=s=0$	Forward (explicit)	$0 \leq R \equiv \frac{\alpha \Delta\tau}{h^2} \leq \frac{1}{4}$	k	1^{st}
$r=s=1$	Backward	$0 \leq R \leq \infty$	$k+1$	1^{st}
$r=s=\frac{1}{2}$	Crank-Nicolson	$0 \leq R \leq \infty$	$k+\frac{1}{2}$	2^{nd}
$r=1, s=0$ and $r=0, s=1$ alternately	Alternating-direction (Peaceman-Rachford)	$0 \leq R \leq \infty$	$k+\frac{1}{2}$	2^{nd}

first, new surface positions are predicted (when erosion occurs) at the hot gas boundary; second, the temperature distribution throughout the wall materials is obtained at the new time level; and, finally, gas mass flowrates of the generated gases are calculated within the charring material (after charring begins). The numerical methods employed in the program for each of these steps are described in the following paragraphs.

Prediction of New Surface Positions

First an iterative calculation of the values of the mass flowrates of the gases and liquids generated at the hot gas boundary by decomposition of the surface wall materials is made, as described in Appendix C. Then the following difference analog of Eq. (8) is used to predict the new radial position of the receding surface for each mesh line $x = x_i$ in the time step, $\tau_k \rightarrow \tau_{k+1}$:

$$\frac{f_{k+1}-f_k}{\Delta\tau} = -\left(\sum_i G_{i,k+\frac{1}{2}}\right)\sqrt{1+(\delta_x f_k)^2}\,/\,\rho_{k+\frac{1}{2}} \quad . \tag{29}$$

In Eq. (29), the summation index i ranges over the species generated and spatial subscripting is omitted for convenience of notation. The iteration described in Appendix C is performed in such a manner as to approximate the average value of the G_i and ρ during the time step.

Thus, the subscript $k+\frac{1}{2}$ is justified and we see that, except for the time level at which the space derivative of f is obtained, the left side of Eq. (29) is a central difference.

After prediction of the new positions during a time step, the new values are smoothed by a reordering process to insure the monotonicity of the converging and diverging portions of the thrust chamber as initially given in the program. In most cases, reordering will come close to preserving the volume of material lost and is much faster than any of the more sophisticated methods, such as curve-fitting. Moreover, because generally the raw predictions will themselves exhibit monotonicity, reordering will cause fewer unnecessary changes to be made in the predictions than will most curve-fitting procedures.

Derivatives at the new wall positions are approximated after smoothing through differencing as defined by Eqs. (19), (21), and (22), the latter two being required whenever recession takes place along the right or left extreme radial mesh lines, respectively. Finally, linear interpolation and extrapolation of the new radial positions and derivatives are used to obtain the corresponding positions and derivatives at the new intersections of the boundary with the axial mesh lines.

Finite Difference Analog of the Energy Equation

To illustrate the linearization of the generalized Peaceman-Rachford alternating-direction method used to discretize the energy equation, we rewrite Eq. (5) together with an accompanying symbolic scheme to indicate the time levels at which the differences have been taken. (Here k and k+2 represent even levels and k+1 an odd level):

$$(\rho C)\frac{\partial T}{\partial \tau} = K\left(\frac{\partial^2 T}{\partial x^2} + \frac{\partial^2 T}{\partial y^2} + \frac{1}{y}\frac{\partial T}{\partial y}\right) + \frac{dK}{dT}\left[\left(\frac{\partial T}{\partial x}\right)^2 + \left(\frac{\partial T}{\partial y}\right)^2\right] - \frac{dH}{dT}\left(G_x \frac{\partial T}{\partial x} + G_y \frac{\partial T}{\partial y}\right) \quad (30)$$

TIME STEP														
ODD:	(k)	($\bar{k}$)	(k)(k+1)	(k)	(k)	(k)	(k)x(k+1)	$(k)^2$	($\bar{k}$)(k)	(k+1)(k)	(k)			
EVEN:	(k+1)	($\bar{k}$+1)	($\bar{k}$+1)	(k+1)	(k+2)	(k+2)	(k+1)	$(k+1)^2$	(k+1)x(k+2)	(k+1)(k+1)	(k+1)(k+1)	(k+1)(k+2)		

For example, in either an odd or an even time step, the symbol (k+1) above means that the difference analog is taken at time level τ_{k+1}, the symbol (k)x(k+1) means that a product of derivatives has been differenced, one at time level τ_k and the other at τ_{k+1}, $(k+1)^2$ means both differences in a product taken at time level τ_{k+1}, and $\bar{k}$ is used as before to indicate a time level between k and k+1 at which a time difference has been taken.

The difference analogs of Eq. (30) at an interior point 0 (see Figs. 2 and 3), in odd and even time steps, as indicated in the symbolic

scheme, take the following forms, respectively (where the spatial subscript 0 is omitted for convenience but is understood to apply to each parameter appearing):

Odd Step.

$$(\rho C)_{eff,k}\frac{T_{k+1}-T_k}{\Delta\tau} = K_k\delta_x^2T_{k+1}+\left[K_k'\delta_xT_k-\frac{\delta_xH_k}{\delta_xT_k}(G_x)_k\right]\delta_xT_{k+1}$$
$$+K_k\delta_y^2T_k+\left[\frac{1}{j\Delta y}+K_k'\delta_yT_k-\frac{\delta_yH_k}{\delta_yT_k}(G_y)_k\right]\delta_yT_k \quad , \tag{31}$$

Even Step.

$$(\rho C)_{eff,k+1}\frac{T_{k+2}-T_{k+1}}{\Delta\tau} = K_{k+1}\delta_x^2T_{k+1}+\left[K_{k+1}'\delta_xT_{k+1}-\frac{\delta_xH_{k+1}}{\delta_xT_{k+1}}(G_x)_{k+1}\right]\delta_xT_{k+1}$$
$$+K_{k+1}\delta_y^2T_{k+2}+\left[\frac{1}{j\Delta y}+K_{k+1}'\delta_yT_{k+1}-\frac{\delta_yH_{k+1}}{\delta_yT_{k+1}}(G_y)_{k+1}\right]\delta_yT_{k+1} \quad . \tag{32}$$

In Eqs. (31) and (32), $(\rho C)_{eff}$ is an abbreviation for the coefficient of $\frac{\partial T}{\partial\tau}$ in Eq. (5) and is discretized as follows:

$$(\rho C)_{eff,k} = (\rho C)_k+Q_{py}\rho_v^*F_{res}\delta_{T_{max}}(F_{py})_{k-\frac{1}{2}}$$
$$+\rho_s^*\{Q_{sc}[\Gamma_{c,s}+\Gamma_{r,s}-1+F_{dec}(T_{max,k})]\delta_{T_{max}}(F_{sc})_{k-\frac{1}{2}} \tag{33}$$
$$+Q_{dec}F_{sc}(T_{max,k})\delta_{T_{max}}(F_{dec})_{k-\frac{1}{2}}\} \quad ,$$

where $\delta_{T_{max}}(F_i)_{k-\frac{1}{2}}$ is defined for each gas generation reaction i by

$$\delta_{T_{max}}(F_i)_{k-\frac{1}{2}} = \frac{F_i(T_{max,k}) - F_i(T_{max,k-1})}{T_{max,k} - T_{max,k-1}} \quad . \tag{34}$$

We use $\delta_{T_{max}}(F_i)_{k-\frac{1}{2}}$ in the discretization rather than the derivative of the known function $F_i(T_{max,k})$ despite the introduction of a third time level, the added computer storage requirements, and the reduction to first order local accuracy. This is to ensure obtaining the gas generation effect, even with a time lag, in the event of large jumps in temperature for which intervals of large values of $F_i'(T_{max})$ would be skipped entirely. This is especially likely when using an implicit method due to the possibility of using large time steps which would not be permitted for an explicit method because of stability considerations. Also, we use T_{max} as the argument of F_i because the gas generation reactions are not reversible and, in case of a drop in temperature at some point, no more generation can occur there until the temperature is raised back to the maximum thus far attained.

The use of $\delta_x H_k/\delta_x T_k$ and $\delta_y H_{k+1}/\delta_y T_{k+1}$ instead of $H'(T_k)$ and $H'(T_{k+1})$ in Eqs. (31) and (32) is similar in motivation to the use of $\delta_{T_{max}}(F_i)_{k-\frac{1}{2}}$. It ensures the inclusion of all heat absorption effects when the distance increments used are so large that intervals of large $H'(T)$ might be skipped. In this case, moreover, we are able to retain

second order local accuracy and the storage requirements are not increased.

It is evident from the definition of the difference operators δ and δ^2 that, for each interior point 0, Eq. (31) is a linear algebraic equation in the three unknown temperatures $T_{C,k+1}$, $T_{0,k+1}$, and $T_{A,k+1}$, and Eq. (32) is linear in the unknowns $T_{D,k+2}$, $T_{0,k+2}$, and $T_{B,k+2}$. Furthermore, since for all interior points 0, the adjacent points A, B, C, and D will ultimately include all boundary and interface points as well as the interior points, we will be left with many more unknowns than equations. In order to make up this deficit, we obtain difference analogs of the boundary and interface conditions at each of the respective boundary and interface points. The procedure used to do this, particularly in the case of curved surfaces, is the subject of the next section.

Normal Gradient Procedures at Curved Boundaries and Interfaces

As indicated above, difference analogs are required of the normal gradient conditions expressed by Eqs. (12) and (18) at the boundary and interface points in order to generate as many equations as there are unknown temperatures. In obtaining the added equations, we must be careful not to introduce any further unknowns to the system, or, if we

do, to provide a means for their elimination. In both Eq. (12) and Eq. (18), we may rewrite the normal derivative by making use of the following exact relationship, obtained through geometrical considerations:

$$\frac{\partial T}{\partial n} = \pm \left(\frac{\partial f}{\partial x} \frac{\partial T}{\partial x} - \frac{\partial T}{\partial y} \right) \Big/ \sqrt{1 + \left(\frac{\partial f}{\partial x} \right)^2} \quad . \tag{35}$$

Here $y = f(x,\tau)$ is the equation of the boundary or interface under consideration (and can only be time dependent at the hot gas boundary), and the plus (minus) sign is used at a lower (upper) boundary, i.e., when the outward normal has a positive (negative) component in the y-direction. We see that Eq. (35) holds even when the slope is infinite by taking the limit as $\frac{\partial f}{\partial x}$ approaches $\pm \infty$.

At a boundary point A formed by the intersection of a horizontal mesh line with a right lower boundary (see Fig. 4), for example, we substitute Eq. (35) in Eq. (12), obtaining

$$(h_{eff})_A \left[(T_{aw})_A - T_A \right] + \sum_i (\Delta H_i)_A (G_i)_A = K_A \frac{\left(\frac{\partial f}{\partial x}\Big|_A \frac{\partial T}{\partial x}\Big|_A - \frac{\partial T}{\partial y}\Big|_A \right)}{\sqrt{1 + \left(\frac{\partial f}{\partial x}\Big|_A \right)^2}} \quad . \tag{36}$$

To discretize Eq. (36), we replace $\frac{\partial f}{\partial x}\Big|_A$ to second order using $\delta_x^{(-)} T_A$, the left off-centered difference as given by Eq. (21). We have

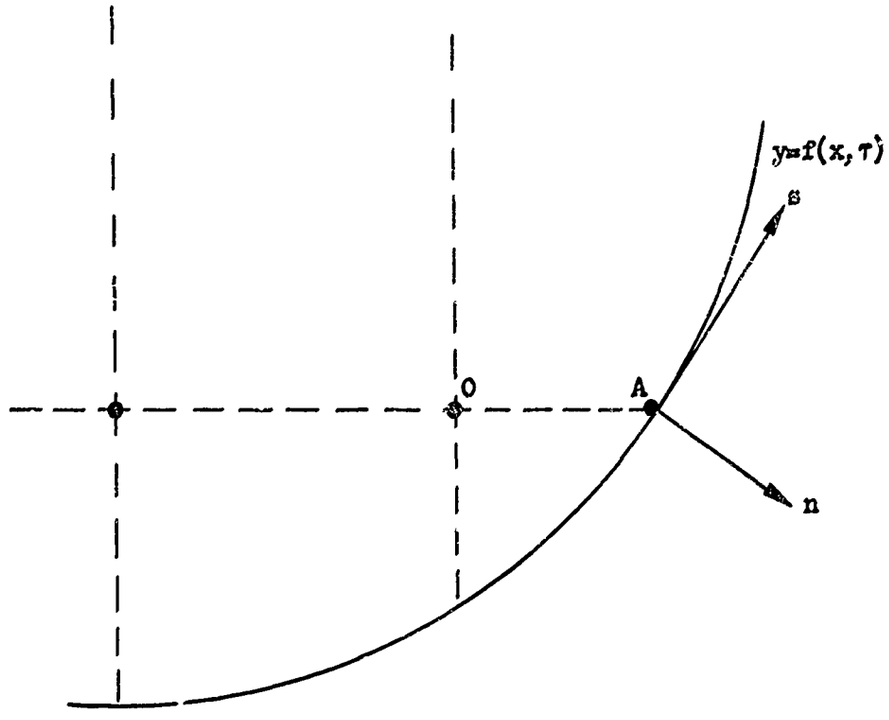

Fig. 4 Location of Boundary Point A Appearing in Eq. (36)

no similar expression for $\left.\frac{\partial T}{\partial y}\right|_A$, however. If, for example, we express $\left.\frac{\partial T}{\partial y}\right|_A$ about the adjacent interior point 0, which is in general its only adjacent interior point, we obtain (assuming T to be quadratic in x):

$$\left.\frac{\partial T}{\partial y}\right|_A = \left.\frac{\partial T}{\partial y}\right|_0 + d_A \left.\frac{\partial^2 T}{\partial x \partial y}\right|_0 \quad . \tag{37}$$

We see that our position is not improved by Eq. (37) due to the appearance of the mixed derivative at 0, for which no difference equivalent has been defined (the reason is given below).

The difficulty encountered at a right boundary point A in expressing $\left.\frac{\partial T}{\partial y}\right|_A$ or, equivalently, in expressing $\left.\frac{\partial^2 T}{\partial x \partial y}\right|_0$, can be circumvented in several ways. Those, however, which provide only a first order approximation to $\left.\frac{\partial T}{\partial y}\right|_A$ or are not compatible with the alternating-direction method (such as discretizing $\left.\frac{\partial^2 T}{\partial x \partial y}\right|_0$ directly) were not considered. A second order procedure for evaluating $\left.\frac{\partial T}{\partial y}\right|_A$, patterned after a method devised by R. V. Viswanathan for solving Poisson's equation by relaxation (see Ref. 12), was attempted in the program but was discarded due to the poorly conditioned system of difference equations it generated. This method, although not applicable here, might be quite useful when employed in conjunction with other schemes for solving the energy equation. A complete description of its use in connection with heat conduction problems can be found in Refs. 13 and 14.

The method finally employed to simulate normal gradient conditions at curved boundaries requires, in addition to the expression given by Eq. (35) for $\frac{\partial T}{\partial n}$ at a curved surface, a similar expression for $\frac{\partial T}{\partial s}$, the counterclockwise tangential derivative and a physical assumption about the local behavior of $\frac{\partial T}{\partial s}$. The first is the following exact expression relating $\frac{\partial T}{\partial s}$ to the axial and radial derivatives:

$$\frac{\partial T}{\partial s} = \pm \left(\frac{\partial T}{\partial x} + \frac{\partial f}{\partial x} \frac{\partial T}{\partial y} \right) \Big/ \sqrt{1 + \left(\frac{\partial f}{\partial x} \right)^2} \quad . \tag{38}$$

The physically based assumption is the vanishing of the tangential derivative at a curved surface

$$\frac{\partial T}{\partial s} = 0 \tag{39}$$

which is appropriate for most situations encountered in rocket engine applications due to the usual domination of $\frac{\partial T}{\partial s}$ by $\frac{\partial T}{\partial n}$. Then, from Eqs. (38) and (39), we obtain the following condition, which we use in Eq. (35) to eliminate $\frac{\partial T}{\partial y}$ $\left(\frac{\partial T}{\partial x} \right)$ in an odd (even) time step at a boundary or interface point lying on a horizontal (vertical) mesh line:

$$\frac{\partial T}{\partial x} = - \frac{\partial f}{\partial x} \frac{\partial T}{\partial y} \quad . \tag{40}$$

In an odd step, we combine Eqs. (35) and (40) to obtain

$$\frac{\partial T}{\partial x} = \pm \frac{\partial f}{\partial x} \frac{\partial T}{\partial n} \Big/ \sqrt{1 + \left(\frac{\partial f}{\partial x}\right)^2} \qquad (41)$$

and, in an even step, we obtain

$$- \frac{\partial T}{\partial y} = \pm \frac{\partial T}{\partial n} \Big/ \sqrt{1 + \left(\frac{\partial f}{\partial x}\right)^2} \quad , \qquad (42)$$

where the signs are employed as in Eq. (35).

Using Eqs. (41) and (42), we then obtain the following conditions, equivalent to Eqs. (12) and (18), for use at boundary and interface points on horizontal mesh lines in odd time steps and on vertical mesh lines in even steps:

Odd Step. At a right or left boundary point, we have

$$K \frac{\partial T}{\partial x} = \pm \frac{\partial f}{\partial x} \left[h_{eff}(T_{aw}-T) + \sum_i (\Delta H_i) G_i\right] \Big/ \sqrt{1 + \left(\frac{\partial f}{\partial x}\right)^2} \quad . \qquad (43)$$

At an interface point, we see that the derivative drops out entirely, yielding

$$K_I \left.\frac{\partial T}{\partial x}\right|_I = K_J \left.\frac{\partial T}{\partial x}\right|_J \quad , \qquad (44)$$

where the minus sign drops out of Eq. (18) because a non-vertical interface is both a lower and an upper boundary.

Even Step. At a boundary we have

$$- K \frac{\partial T}{\partial y} = \pm \left[h_{eff}(T_{aw}-T) + \sum_i (\Delta H_i) G_i \right] \Big/ \sqrt{1 + \left(\frac{\partial f}{\partial x}\right)^2} \tag{45}$$

and, at an interface,

$$K_I \left.\frac{\partial T}{\partial y}\right|_I = K_J \left.\frac{\partial T}{\partial y}\right|_J \quad . \tag{46}$$

We see that, aside from the physical assumption that $\frac{\partial T}{\partial s}$ vanishes, Eqs. (43) - (46) are exact.

The discretization of Eqs. (43) - (46) then follows quite readily. In an odd step, $\tau_k \to \tau_{k+1}$, we obtain the following.

Left Boundary Point C.

$$K_{C,\bar{k}} \delta_x^{(+)} T_{C,k+1} = \pm \left.\frac{\partial f}{\partial x}\right|_{C,k} \left\{ (h_{eff})_{C,\bar{k}} \left[(T_{aw})_C - T_{C,k+1} \right] + \sum_i (\Delta H_i)_C (G_i)_{C,\bar{k}} \right\} \Big/ \sqrt{1 + \left(\left.\frac{\partial f}{\partial x}\right|_{C,k}\right)^2} \quad . \tag{47}$$

Right Boundary Point A.

$$K_{A,\bar{k}} \delta_x^{(-)} T_{A,k+1} = \pm \left.\frac{\partial f}{\partial x}\right|_{A,k} \left\{ (h_{eff})_{A,\bar{k}} \left[(T_{aw})_A - T_{A,k+1} \right] + \sum_i (\Delta H_i)_A (G_i)_{A,\bar{k}} \right\} \Big/ \sqrt{1 + \left(\left.\frac{\partial f}{\partial x}\right|_{A,k}\right)^2} \quad . \tag{48}$$

Interface Point P (with region I on the left and J on the right).

$$(K_I)_{P,k}\,\delta_x^{(-)}T_{P,k+1} = (K_J)_{P,k}\,\delta_x^{(+)}T_{P,k+1} \quad . \tag{49}$$

In an even step, $\tau_{k+1} \rightarrow \tau_{k+2}$, the following equations result:

Lower Boundary Point D.

$$-K_{D,\bar{k}+1}\,\delta_y^{(+)}T_{D,k+2} = \{(h_{eff})_{D,\bar{k}+1}\,[(T_{aw})_D - T_{D,k+2}] + \sum_i (\Delta H_i)_D\,(G_i)_{D,\bar{k}+1}\} \Big/ \sqrt{1 + \left(\frac{\partial f}{\partial x}\Big|_{D,k+1}\right)^2} \tag{50}$$

Upper Boundary Point B.

$$-K_{B,\bar{k}+1}\,\delta_y^{(-)}T_{B,k+2} = -\{(h_{eff})_{B,\bar{k}+1}\,[(T_{aw})_B - T_{B,k+2}] + \sum_i (\Delta H_i)_B\,(G_i)_{B,\bar{k}+1}\} \Big/ \sqrt{1 + \left(\frac{\partial f}{\partial x}\Big|_{B,k+1}\right)^2} \quad . \tag{51}$$

Interface Point Q.

$$(K_I)_{Q,k+1}\,\delta_y^{(-)}T_{Q,k+2} = (K_J)_{Q,k+1}\,\delta_y^{(+)}T_{Q,k+2} \quad . \tag{52}$$

The use of $\bar{k}$ in Eqs. (47) - (52) indicates that, under certain heating conditions, local iterations are performed in order to obtain averaged

values. Except for the case of surface erosion which is discussed in Appendix C, these iterations are performed using the same boundary formula, but explicitly discretized. A new value of temperature is predicted at the boundary point and then h_{eff} and K are recomputed using an average of the predicted temperature and its value at the old time level. For the present version of the computer program, the last term of Eq. (51) vanishes, surface erosion only being permitted at the hot gas boundary.

In an odd time step, then, we see that Eq. (31) with Eqs. (47) - (49) provides complete linear systems of algebraic equations (one for each horizontal mesh line) with as many equations as unknowns. Similarly Eqs. (32), (50) - (52) generate complete systems on vertical mesh lines in even steps.

Only two steps in the method used to obtain values for temperature at all the mesh points in each time step remain to be described. First, we will treat the tridiagonalization of the systems of equations generated by the above procedures and the recursive solution of each transformed system. Secondly, a brief discussion is included of the methods used to calculate the temperatures not obtained by the recursive solution, that is, the temperatures at the irregular points on vertical (horizontal) mesh lines in odd (even) time steps (in the case illustrated by Fig. 2, for example, we require additional procedures to obtain T_C in even steps).

Tridiagonalization and Recursive Solution

In order to take advantage of simple recursive procedures for solving systems of linear equations, we wish to transform the systems generated by the procedures discussed above into tridiagonal systems of equations. A tridiagonal system is one whose coefficient matrix contains nonzero elements only along the main diagonal and its immediately adjacent diagonals. Such a system, say consisting of n equations in the n unknowns, u_i, $i=1,\ldots,n$, can be characterized as follows:

$$
\begin{aligned}
b_1u_1 + c_1u_2 &= d_1 \\
a_2u_1 + b_2u_2 + c_2u_3 &= d_2 \\
a_3u_2 + b_3u_3 + c_3u_4 &= d_3 \\
\text{- -} & \\
a_\ell u_{\ell-1} + b_\ell u_\ell + b_\ell u_{\ell+1} &= d_\ell \\
\text{- -} & \\
a_{n-1}u_{n-2} + b_{n-1}u_{n-1} + c_{n-1}u_n &= d_{n-1} \\
a_nu_{n-1} + b_nu_n &= d_n
\end{aligned}
\qquad (53)
$$

The solution to system (53) is obtained by the following recursion scheme (also defined in Refs. 3 and 15), which can be easily derived using a direct Gaussian elimination scheme such as the compact Crout method:

$$
\begin{aligned}
r_1 &= b_1 \\
r_\ell &= b_\ell - \frac{a_\ell c_{\ell-1}}{r_{\ell-1}} \quad , \ \ell = 2,\ldots, n \\
z_1 &= \frac{d_1}{r_1} \\
z_\ell &= \frac{d_\ell - a_\ell z_{\ell-1}}{r_\ell}, \quad \ell = 2,\ldots, n \qquad (54) \\
u_n &= z_n \\
u_\ell &= z_\ell - \frac{c_\ell u_{\ell+1}}{r_\ell} \ , \quad \ell = n-1,\ldots, 1
\end{aligned}
$$

For a given mesh line in, say an odd time step we see that the system of equations generated by Eqs. (31) and (47)-(49) complies with the conditions for tridiagonality as given by system (53) at each interior point (using Eq. (31)) and does not at either boundary point (points 1 and n of system (53)) or at an interface point. If, say, the i^{th} point on the mesh line is an interface point, then the system generated above has the following form (for n points):

$$
\begin{aligned}
&A_1u_1 + B_1u_2 + C_1u_3 &&= d_1\\
&a_2u_1 + b_2u_2 + c_2u_3 &&= d_2\\
&\text{- -}\\
&a_{i-1}u_{i-2} + b_{i-1}u_{i-1} + c_{i-1}u_i &&= d_{i-1}\\
&A_iu_{i-2} + B_iu_{i-1} + C_iu_i + D_iu_{i+1} + E_iu_{i+2} &&= d_i\\
&a_{i+1}u_i + b_{i+1}u_{i+1} + c_{i+1}u_{i+2} &&= d_{i+1}\\
&\text{- - - - - - - - - - - - - - - - - -}\\
&a_{n-1}u_{n-2} + b_{n-1}u_{n-1} + c_{n-1}u_n &&= d_{n-1}\\
&A_nu_{n-2} + B_nu_{n-1} + C_nu_n &&= d_n
\end{aligned}
\tag{55}
$$

In order to remedy this situation we must eliminate u_3 from the first equation of system (52), both u_{i-2} and u_{i+2} from the i^{th} equation, and u_{n-2} from the n^{th} equation. This is accomplished through use of two general elimination schemes, as follows: For the first and last of these required eliminations we consider the system

$$
\begin{aligned}
\alpha_1x + \beta_1y + \gamma_1z &= \sigma_1\\
\alpha_2x + \beta_2y + \gamma_2z &= \sigma_2 \quad ,
\end{aligned}
\tag{56}
$$

the eliminant, after removing z from the system, can be written as

$$
(\alpha_1\gamma_2 - \alpha_2\gamma_1)x + (\beta_1\gamma_2 - \beta_2\gamma_1)y = \gamma_2\sigma_1 - \gamma_1\sigma_2 \tag{57}
$$

To eliminate u_{i-2} and u_{i+2} from the i^{th} equation we observe that for the system of three equations

$$\begin{aligned} \alpha_1 v + \beta_1 w + \gamma_1 x &= \sigma_1 \\ \alpha_2 v + \beta_2 w + \gamma_2 x + \delta_2 y + \epsilon_2 z &= \sigma_2 \\ \gamma_3 x + \delta_3 y + \epsilon_3 z &= \sigma_3 \ , \end{aligned} \tag{58}$$

the eliminant to remove v and z may take the following form:

$$\begin{aligned} (\alpha_1\beta_2 - \alpha_2\beta_1)\epsilon_3 w + [(\alpha_1\gamma_2 - \alpha_2\gamma_1)\epsilon_3 - \alpha_1\gamma_3\epsilon_2]x + \alpha_1(\delta_2\epsilon_3 - \delta_3\epsilon_2)y \\ = (\alpha_1\sigma_2 - \alpha_2\sigma_1)\epsilon_3 - \alpha_1\epsilon_2\sigma_3 \ . \end{aligned} \tag{59}$$

Application of Eq. (57) twice and Eq. (59) for as many interfaces as appear in system (55) (only one is shown) will transform system (55) into a tridiagonal system as given by system (53). Then the system is solved using the recursive procedure given by Eqs. (54). This is carried out for each successive mesh line, horizontal in odd time steps and vertical in even steps.

Obtaining Temperatures at Irregular Points

In order to complete the temperature calculation in each step, a separate method was devised and coded for obtaining temperatures at the irregular boundary and interface points in alternate time steps, i.e., at irregular points on vertical (horizontal) mesh lines in odd (even) time

steps. This procedure entails the use of linear and "constant" interpolation and extrapolation (within a single material region only) to obtain temperatures at the irregular points from those already calculated at the new level in the tridiagonal systems described above. At all interface points, linear or constant extrapolation is performed from both sides and the average is taken. Linear extrapolation is used where possible, when at least two successive interior points are adjacent on the same side of the interface point, and constant extrapolation if only one interior point is available (in Fig. 5 , in an even time step, for example, linear extrapolation is used from the left at point P and constant extrapolation from the right). Two types of boundary points are considered: those exposed to engine firing and those not exposed. In the latter case, extrapolation from the interior is used applying the same rule as at an interface, but without taking an average. At an irregular point on a boundary exposed to firing, we use linear surface interpolation or constant surface extrapolation from temperatures already calculated in the tridiagonal systems at similarly exposed boundary points of the same material. Thus, taking examples from Fig. 5 , in an even time step, T_{B_5} is extrapolated from T_{B_4} and T_{B_2} interpolated from T_{B_1} and T_{B_3}, while, in an odd time step T_{B_1} is extrapolated from T_{B_2} and both T_{B_3} and T_{B_4} are interpolated from T_{B_2} and T_{B_5}.

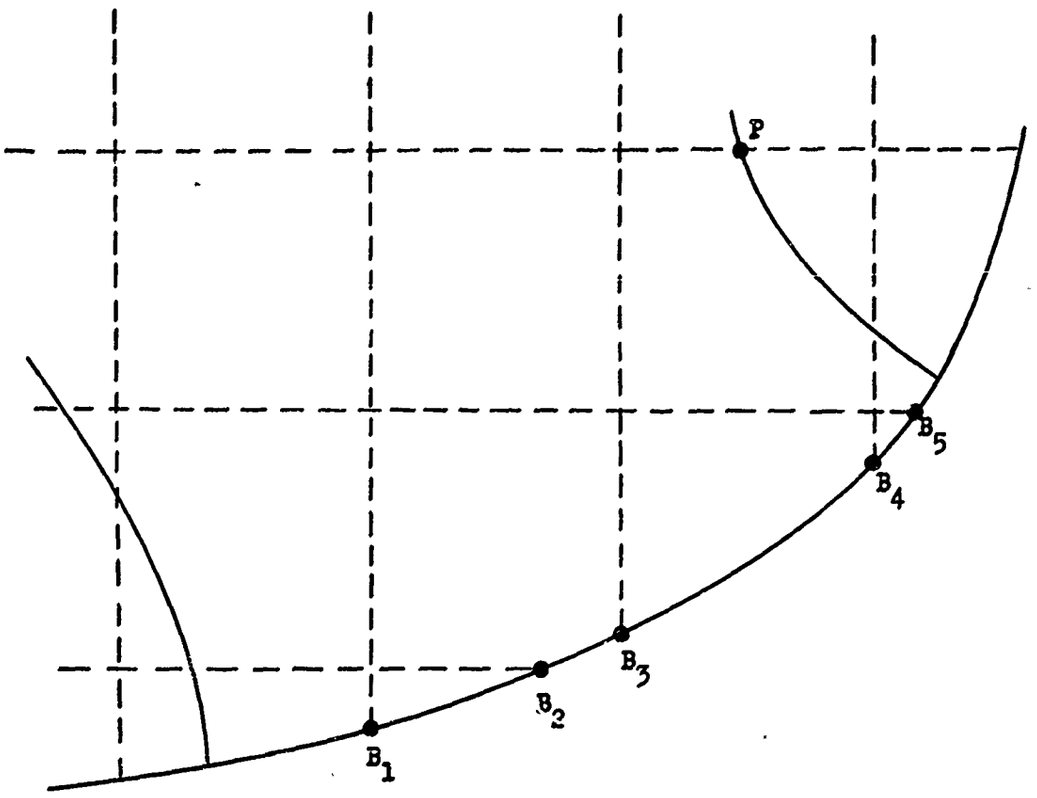

Fig. 5 Point Arrangement Illustrating Interior and Surface Interpolation and Extrapolation of Temperatures at Irregular Mesh Points

Because the method adopted for irregular points does not directly utilize any of the equations comprising the model, some further discussion of the approach would seem to be in order. Apart from the fact that the method has worked in the cases attempted, it should be noted that it does simulate, to what is usually a first order approximation, the thermal behavior of adjacent points, which was in turn obtained from the model equations. Care, however, should be taken, in selecting the mesh lines for the analysis, to prevent extrapolation over relatively long distances. This is especially true in the use of surface extrapolation at boundaries exposed to firing.

Discretization and Solution of the Continuity Equation

Coupled to the solution of the energy equation (5) for the temperature distribution is the solution of the continuity equation (6) for the mass flowrate of the generated gases in the charring material. After substitution of the simplifying assumption given by Eq. (7) into Eq. (6), the continuity equation takes the following form:

$$\frac{\partial(xG_x)}{\partial x} + \frac{1}{y}\frac{\partial(yG_y)}{\partial y} = -\frac{\partial \rho}{\partial \tau}, \qquad (60)$$

where ρ is the density of the charring material whose time derivative is given by the left side of Eq. (6).

In the numerical solution of the basic equations, the mass flowrate analysis is uncoupled from the temperature calculation by solving the energy equation first in each time step and then using the calculated values of temperature in the solution of the continuity equation. This is achieved in the discretization of Eq. (60) by expressing the time derivative as a backward difference. Spatially the discretization is somewhat simplified in that the mass flowrate analysis is performed only at regular points. Thus, the following discretization of Eq. (60), obtained in terms of mass flowrates and temperatures at the four points (x_i,y_j), (x_{i+1},y_j), (x_i,y_{j+1}), and (x_{i+1},y_{j+1}) (or, more conveniently, the points 1, 2, 3, and 4 as pictured in Fig. 6), is second order in distance and first order in time and is assumed to hold at the point $(x_{i+\frac{1}{2}},y_{j+\frac{1}{2}})$ at time τ_k:

$$\frac{1}{2}\left\{\frac{R_{2,k}G_{2,k}-R_{1,k}G_{1,k}}{\Delta x}+\frac{R_{4,k}G_{4,k}-R_{3,k}G_{3,k}}{\Delta x}\right.$$

$$\left.+\frac{2}{(2j+1)\Delta y}\left[\frac{(j+1)\Delta yG_{3,k}-j\Delta yG_{1,k}}{\Delta y}+\frac{(j+1)\Delta yG_{4,k}-j\Delta yG_{2,k}}{\Delta y}\right]\right\}$$

$$=\frac{1}{4}\sum_{\ell=1}^{4}\left\{\rho_v^*F_{res}\left(F_{py,\ell,k}-F_{py,\ell,k-1}\right)\right. \qquad (61)$$

$$+\rho_{sL}^*\left[\left(\Gamma_{c,s}+\Gamma_{r,s-1}+F_{dec,\ell,k}\right)\left(F_{sc,\ell,k}-F_{sc,\ell,k-1}\right)\right.$$

$$\left.\left.+F_{sc,\ell,k}\left(F_{dec,\ell,k}-F_{dec,\ell,k-1}\right)\right]\right\}/\Delta\tau$$

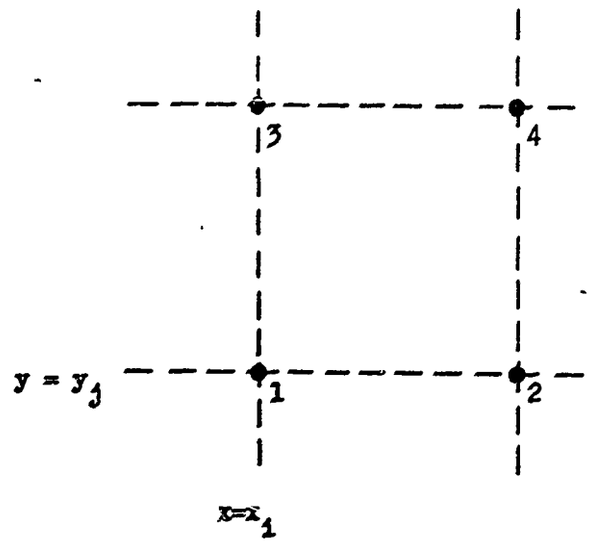

Fig. 6 Point Arrangement for Discretizing Continuity Equation

where, for convenience, the subscripts y and i have been dropped from G_y and Δx_i, respectively. In Eq. (61), for each reaction i, $F_{i,\ell,k}$ and $F_{i,\ell,k-1}$ are evaluated at $T_{max,\ell,k}$ and $T_{max,\ell,k-1}$, respectively, as in Eqs. (33) and (34). For each set of points 1, 2, 3, and 4, such that at least point 2 is in the charring material, Eq. (61) is rewritten in the following form and solved explicitly for $G_{2,k}$:

$$\left(1-\frac{1}{2j+1}-R_{2,k}\frac{\Delta y}{\Delta x}\right)G_{2,k}=\left(1+\frac{1}{2j+1}+R_{4,k}\frac{\Delta y}{\Delta x}\right)G_{4,k}$$

$$+\left(1+\frac{1}{2j+1}-R_{3,k}\frac{\Delta y}{\Delta x}\right)G_{3,k}-\left(1-\frac{1}{2j+1}+R_{1,k}\frac{\Delta y}{\Delta x}\right)G_{1,k} \qquad (62)$$

$$-\frac{\Delta y}{2}\sum_{\ell=1}^{4}\delta_{\tau}^{(F)}\rho_{\ell,k}$$

where $\delta_{\tau}^{(F)}\rho_{\ell,k}$ is a symbolic representation of the ℓ^{th} term of the summation in Eq. (61). Equation (62) is used to sweep across each horizontal mesh line from left to right starting with the topmost mesh line and going down from line to line. The boundary conditions are simulated by the following interpretations of Eq. (62):

a) If an interface common to the charring material and one of the other materials cuts through the rectangle formed by points 1, 2, 3, and 4, then both G and F_i vanish at all points in the other material. If any of the points ℓ (other than point 2) happens to be on the interface, then G_ℓ is set equal to 0, but $F_{i,\ell}$ can still be nonzero. If point 2

is on an interface (in which case at least one of the other points must be in the charring material), both G_2 and $F_{i,2}$ can be nonzero. b) If a boundary cuts through the rectangle, again both G and F_i are zero at points outside the material, and again F_i can be nonzero on the boundary. G is zero at an upper boundary, but can be nonzero at a noninsulated lower boundary. c) If either $T_{max,2}$ or $T_{max,4}$ is less than T_{py} or if point 4 is outside the charring material, then G_2 is set equal to 0. If G_1 is 0, then G_2 is obtained from the following two-point formula instead of Eq. (62):

$$G_{2,k} = \frac{j+1}{j} G_{4,k} - \frac{(2j+1)\Delta y}{4j} \delta_\tau^{(F)} (\rho_{2,k} + \rho_{4,k}) \tag{63}$$

In practice, a modification of Eq. (7) is used to obtain $R_{\ell,k}$ at each point ℓ for use in Eq. (62). Because we know that the direction of the mass flowrate vector to the right of the throat plane should be downward to the right, we limit the range of allowable values of $R_{\ell,k}$ to the closed interval $[-1,0]$. $R_{\ell,k}$ is obtained at first as the ratio of $\delta_x T_{\ell,k}$ to $\delta_y T_{\ell,k}$ and then is (a) set to zero if the ratio is positive, (b) set to -1 if the ratio is less than -1, and (c) left unchanged otherwise. To the left of the throat, we similarly restrict $R_{\ell,k}$ to the range $[0,1]$ with one exception. Because $R_{\ell,k}$ is nonnegative to the left of the throat we must be sure that the coefficient of $G_{2,k}$ in Eq. (62) does not vanish. This is done in the computer program by automatically

calculating the minimum value $\mu = (1 - \frac{1}{2j+1}) \frac{\Delta x_i}{\Delta y}$ for all values of j and Δx_i to the left of the throat and then restricting $R_{\ell,k}$ to the range $[1,r]$ where $r = \min \{f\mu, 1\}$, where $0 < f < 1$.

The temporal stability of the mass flowrate solution procedure given by Eq. (62) is assured due to the backward time difference employed, provided that the schemes used to solve both the energy equation and its boundary conditions are also stable. The stability with respect to distance of the procedure as used explicitly in each time step from point to point is, however, another matter. A complete stability analysis of the latter type has not been performed, but it can be shown (by methods similar to those used in Appendix D) that a homogeneous linearization of Eq. (62) is unconditionally unstable in the y direction and in the x direction to the right of the throat. To the left of the throat, on the other hand, it is unconditionally stable. These results should not, however, be surprising because we know (due to the restrictions on $R(x,y,\tau)$) that the solution must grow, to the right of the throat, in the same axial and radial directions in which the numerical solution is marched out; whereas to the left of the throat, the solution must grow in the same radial direction but in the opposite axial direction. No steps have been taken to introduce at least conditional stability to the numerical procedure because in practice it has proved to be quite satisfactory when used in conjunction with the temperature calculation. Only a

relatively few distance steps are taken in performing the calculation and the values generated are probably small enough that local instability will not affect the overall stable time step calculation. In any case, it is felt by the writers that no usable modification of the numerical scheme would provide stability in the axial direction to the right of the throat due to the sign of $R(x,y,\tau)$, now would any be stable radially on either side of the throat because we must march from higher to lower values of j due to the available boundary conditions.

Control of Size of Time Increments

In the one-dimensional code completed in Phase 1 of the present program (see Ref. 2), the approach taken to the maximization of the time step was to start with a very small increment and allow it to increase periodically during the program run provided that several built-in criteria are satisfied. Two options are available in the two-dimensional program, one similar in approach to the Phase 1 program and the other rather different. The first, which we shall call Option A, consists simply of scheduling a variable array of time-steps directly as input. (Option A was exercised for the second checkout case described in the Results Section below and is given in Table 4. Option B, discussed below, was used for the first checkout case.)

In Option B, on the other hand, a single large (input) time step is employed wherever possible throughout the program run and is only reduced

temporarily as required. Such reductions are scheduled within the program in accordance with a stability criterion based upon the intensity of engine firing as simulated in representative periods by the fraction of "on" time, $F_{on}(\tau)$ (defined below Eq. (16)).

It has been shown by previous investigators (see Ref. (16), p. 47-49, for example) that instability can be introduced in a numerical solution by the intensity of heating at the boundary. For the one and two dimensional forward difference methods used to solve the heat conduction equation, the following inequalities must be satisfied, respectively, to ensure a stable solution:

$$R \equiv \frac{\alpha \Delta\tau}{(\Delta x)^2} < \frac{1}{2(1+N)} \tag{64}$$

$$R < \frac{1}{2(2+N)} \tag{65}$$

where $N = (h\Delta x)/K$, $\Delta x = \Delta y$, and h and K are constants. In the present program the following analogous criterion is used to limit the size of $\Delta\tau$ when Option B is exercised:

$$R \equiv \frac{\alpha \Delta\tau}{(\Delta z)^2} < \frac{C}{1+N_z} \tag{66}$$

where $\Delta z = \min[\min_i(\Delta x_i), \Delta y]$, $N_z = (h_{eff}\Delta z)/K$, and C is an empirically determined constant.* In order to be able, within the program, to schedule

*C was taken to be .4 or .6 in all checkout runs using Option B.

all time-step reductions based on inequality (66) before the numerical calculation begins, a reference temperature, equal to 60% of the throat value of $T_{aw}(x)$, is used to compute values for h_{eff} and K.

There is one other criterion for temporary time-step reduction, based upon amount of surface recession, which is employed with either Option A or B when surface erosion takes place. The purpose is to prevent excessive radial recession in any one time step. This is accomplished in the program by specifying as input a fraction of the radial increment Δy as the maximum allowable amount of radial surface recession along any mesh line $x = x_i$ in a time step. When this criterion is violated, the program automatically reduces the time step, through multiplication by an input constant less than one in magnitude, and then begins the time step again (this does not involve much recalculation because recession is the first mechanism in each time step).

One other means of time step control is provided in the program by permitting the optional partition of the first time step (only) into as many smaller steps as desired. This may be done in conjunction with either Option A or B.

An excellent feature of the Phase 1 code is its capability of varying the distance increment with time. This was not considered feasible in the Phase 2 code because of the excessive amount of recalculation which

would be required to establish the new mesh. However, in the two-dimensional program, added flexibility is provided by the variable spacing permitted on the radial mesh lines.

DESCRIPTION OF THE COMPUTER PROGRAM

GENERAL REMARKS

The numerical procedures developed above for solving the two-dimensional ablation and heat conduction model given by Eqs. (5) - (18) were coded in Fortran IV for automatic computation on the EDPM 7094. The computer program has been given the designation "2D-ABLATE."

Input to the program is handled by a very sophisticated input routine which was adapted from a current Rocketdyne procedure. Its advantages include reading all input into a single data array (which is allocated within the program), which can thus be conveniently augmented as required, and a particularly efficient method of handling multiple runs or updating data from run to run through use of single cards to replace the contents of specific locations in the data array.

In order to take advantage of the overlay feature of the Fortran IV system, the program was written in several links. In addition to the main control link, Link 0, two other links are provided for: (a) Link 1, which handles all execution prior to the time-step calculation, and (b) Link 2, the time-step calculation, which carries out the numerical procedures described earlier.

Link 1 includes allocation of the input data array, imposition of mesh lines on the input curved boundaries and interfaces resulting in the regular and irregular mesh points defined earlier, generation of descriptive arrays characterizing these points, linear interpolation at the positions $x_i = x_{i-1} + \Delta x_i$ of the input axially varying tabular data, piecewise linear and quadratic fitting of the input temperature dependent material properties, piecewise constant and linear fitting of the time varying data (e.g., $F_{on}(\tau)$, which is defined earlier), and scheduling temporary reductions of the input computational time-step (as required by Inequality (66)) for use in periods of strong surface heating unless the option is exercised of scheduling variable time steps directly as input.

In order to acquaint the reader with the scope of the program, a discussion follows of the input data required for its operation, brief descriptions are given of the execution performed in Links 1 and 2, overall flowcharts are presented of the main program logic, and the output options available in the program are outlined.

INPUT REQUIRED FOR THE COMPUTER PROGRAM

The input data required for operation of the 2D-ABLATE computer code include the following:

(a) Thrust chamber wall geometry.

Piecewise quadratic functions are used to describe the configuration of

all material boundaries and interfaces. Because the materials are numbered from 1 to a maximum of 5, each quadratic piece must also be identified by the number assigned to the material or materials (in case of an interface) which it bounds. The kind of boundary condition assumed must also be read in; possibilities include insulation, engine firing, radiation to the surroundings, environmental heating, or some combination of these. A maximum of 40 quadratic pieces may be used in describing the wall geometry.

(b) Discretization parameters.

The only required parameters for the discretization are the basic time increment $\Delta\tau$ (Option B) or an array of time increments (Option A) scheduled as described in (g) below, the radial distance increment Δy, and the axial increments Δx_i, where i goes from 1 to a maximum of 15. It is not necessary to read in the coordinates of any mesh points; these are all automatically determined in Link 1. Due to storage requirements, Δy must be chosen so that no more than 35 horizontal mesh lines will intersect the wall boundaries.

(c) Temperature dependent material properties.

The product, ρC, of density and specific heat is read in as a piecewise linear function of temperature for each wall material and the conductivity, K, as a piecewise quadratic. The effective enthalpy of the gases generated internally in the charring material is also read in

as a piecewise linear function of temperature. Each of the gas-generation reactions which take place within the charring ablator (a maximum of three is permitted) is characterized by the temperature range in which it occurs and by the maximum value of $F_1(T)$ (see Nomenclature or Appendix B) which is attained during the reaction. These values are then used within the program to generate a trigonometric function which is employed to describe the variation of $F_1(T)$ within the reaction range.

(d) Constants for gas generation reactions in the charring material. The constants required to characterize the reactions are F_{res}, Q_{py}, Q_{sc}, Q_{dec}, ρ_v, ρ_s, $\Gamma_{c,s}$, and $\Gamma_{r,s}$.

(e) Hot wall erosion parameters.

Included in the input data array is a list of all the parameters required to perform the calculations given in Appendix C. They include

(1) flow constants of the combustion gas: specific heat ratio, molecular weight, chamber pressure, throat radius, radius of curvature of the throat boundary, and parameters used in computing the blocking effect.

(2) melting rate constants for each exposed material: thermal conductivity of the melt, viscosity parameters, specific heat of the melt, heat of fusion, and melting temperature.

(3) vaporization constants for each material: mass diffusion coefficient at standard conditions, molecular weight of the vapors, vapor pressure parameters, heat of vaporization, and density of the material.

(4) chemical reaction constants for each material: molecular weight of reactant gas, mol fraction of reacting gas, rate equation constants, enthalpy change for the reaction, mass diffusion coefficient at standard conditions, and specific heat of the reaction products.

(f) Parameters affecting the heat flux.

Values are required for each of the following parameters at various prespecified axial positions: T_{aw}, h_{conv}, β_f, and q_{env}. In addition, two radiation constants are required: σ and T_{env}.

(g) Time varying parameters.

To characterize intermittent firing and pulsing with soakback, an array of values of $F_{on}(\tau)$ is read in, each of which is held constant during a preassigned time interval. If Option A is exercised, an input array of time steps is similarly associated with these intervals. An array of weighting constants is also read in to permit piecewise linear variation of q_{env} with time. None of these arrays may contain more than 40 elements.

(h) Initial temperature.

The initial wall temperature is required as an input constant.

LINK 1 PROCEDURES

Input Processing and General Procedure

All data for the program are arranged in a matrix format which is input as a single array and stored on tape by the program so as to be made available if needed at the completion of the problem run. Thus to perform multiple runs it is only necessary to read in those data elements (along with their array positions) whose values change from run to run.

Error checks are made extensively in Link 1 and, in the event of an error, execution continues in an attempt to check for other errors prior to termination. Data input which defines the geometrical configuration is especially critical, and it is important that certain rules (discussed in the next section) be strictly followed in choosing axial and radial increments to be used by the program in imposing a mesh on the wall configuration. The mesh imposition essentially consists of determining intersections of the functions describing the input boundary and interface geometry with the horizontal and vertical mesh lines. Arrays are generated and stored consisting of these locations along with the derivatives of the boundary and interface functions at these locations, boundary types, and region numbers associated with them.

Temperature dependent data are then processed, including enthalpy, ρC, and thermal conductivity. The first two sets are fitted by several linear segments over the temperature range while thermal conductivity is fitted by quadratic segments.

Further processing is required in Link 1 to linearly interpolate the axially varying input parameters, β_f, T_{aw}, h_{conv}, and q_{env}, at the axial positions of the vertical mesh lines.

Then, unless Option A is exercised of scheduling variable time steps as input, a schedule of computational time increments is generated in accordance with the stability criterion given by Inequality (66) above, which depends upon the input values of $F_{on}(\tau)$ used to simulate intensity of engine firing in prespecified time intervals.

Finally, initialization of certain Link 2 parameters is performed. This terminates Link 1 and program control is then transferred to Link 2.

A flowchart of the overall Link 1 logic is shown in Fig. 7 .

Some Rules Governing Thrust Chamber Geometry Definition

1. A mesh line which intersects the configuration must contain exactly two boundary points which are terminal points of the line.

2. A mesh line may contain as many as eight boundary and interface points.

Fig. 7 Link 1 Procedure
Flow Diagram

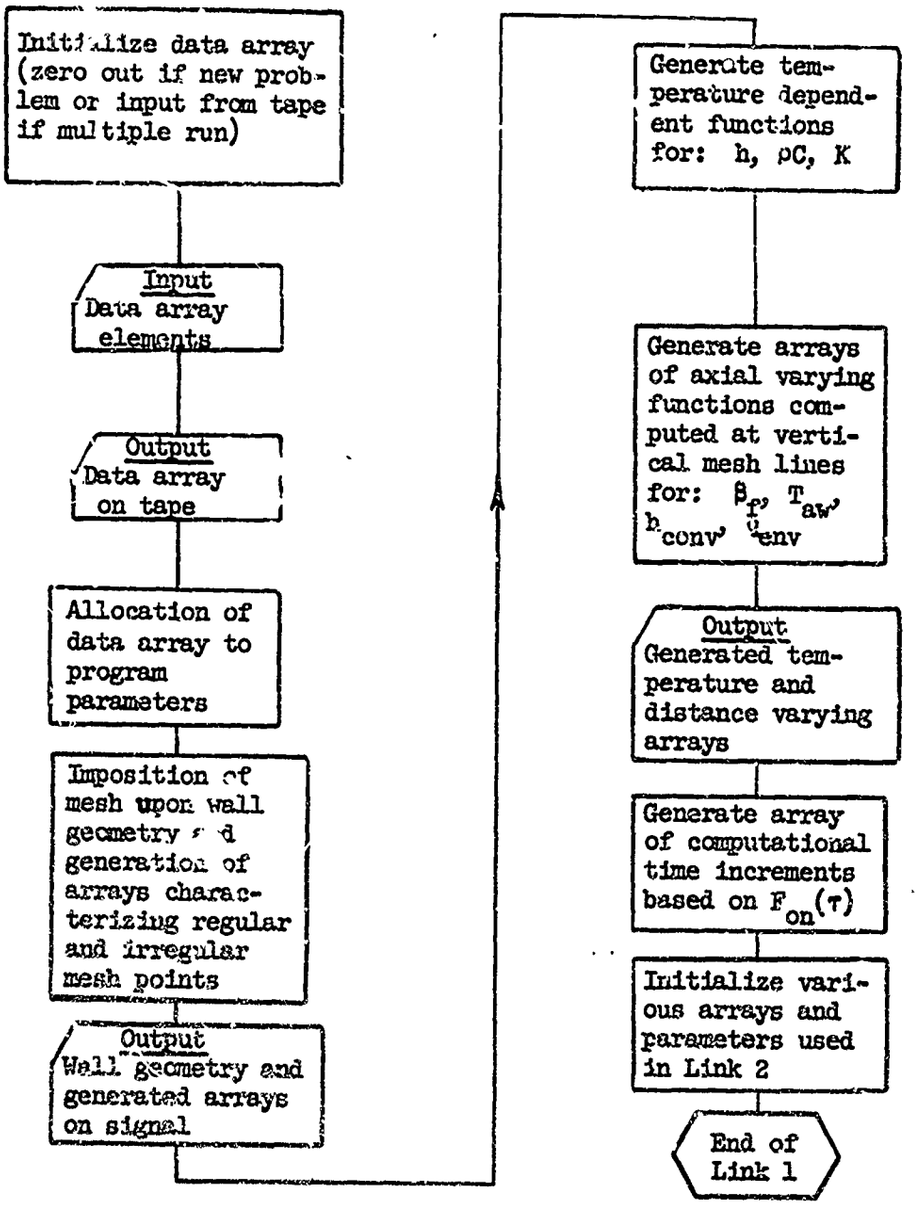

3. A horizontal mesh line may contain as many as 23 points of all kinds. A vertical mesh line may contain as many as 43 points.

4. A mesh line which intersects the configuration must contain a minimum of four points; these may be any combination of boundary, interface, and regular mesh points.

5. At least one regular mesh point must lie between successive boundary and interface points.

6. No common intersection of three or more quadratic boundary or interface segments may lie on a mesh line.

7. No mesh line may coincide with a vertical or horizontal boundary or interface.

LINK 2 EXECUTION

In Link 2 of the program, the entire time-step calculation is performed as described earlier in the section on numerical procedures. The program flow is iterative in nature, calculations being performed in one time step at a time in the following order: an iterative procedure (see Appendix C) is used to determine the erosion characteristics at the hot gas boundary and predict the resulting surface recession, the temperature distribution is obtained using the alternating-direction

method, and the gas mass flowrate calculation is performed for gases generated in the charring ablator.

Of these calculations, the temperature computation requires the most intricate program flow due to the need for alternately converting horizontal arrays (at both regular and irregular points) and irregularly located vertical arrays at odd time levels to and from the corresponding vertical and irregularly located horizontal arrays at even levels.

A flowchart of the overall calculation is given in Figure 8.

OUTPUT PROCEDURES

Output from the Phase 2 code 2D-ABLATE is printed out in both Link 1 and 2 using several program options.

In Link 1, the input data array is always printed out in matrix form as well as are the generated arrays characterizing the boundary and interface points. Upon an input signal, a descriptive printout is given of the allocated data array and the remaining generated parameters.

In Link 2, at regularly spaced time intervals (the spacing may change with each change in $F_{on}(\tau)$), the following computed values are printed out:

Fig. 8 Link 2 Procedure
Flow Diagram

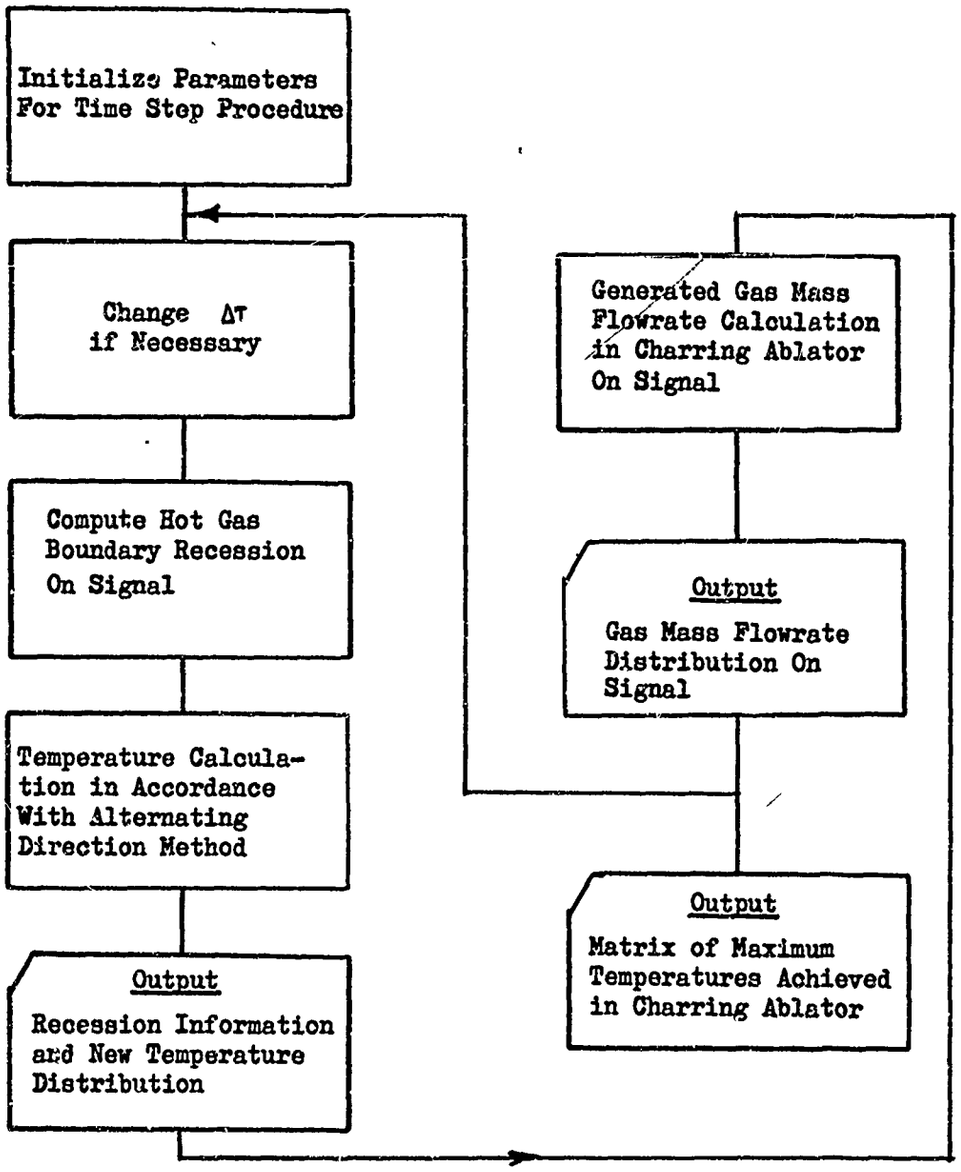

(a) Surface data at each intersection of the hot gas boundary with a radial mesh line, including mass flowrate of gases generated within the ablative region, new positions of the surface, and surface recession rates.

(b) Temperatures at all points, regular and irregular, which lie on a horizontal (vertical) mesh line in an odd (even) time step.

The following information is available for optional printout at the same times:

(a) Values of effective heat transfer coefficients at both ends of each horizontal (vertical) mesh line in an odd (even) time step.

(b) Temperatures at irregular boundary and interface points lying on vertical (horizontal) mesh lines in odd (even) time steps.

(c) Values of $G_y(x,y,\tau)$ and $R(x,y,\tau)$ at every regular point of the charring ablator which has reached the minimum pyrolysis temperature.

Finally, a listing is printed out at the end of the run of the maximum temperature achieved at each regular point of the charring ablator.

RESULTS

In order to provide a broad base for evaluating the capabilities of the two-dimensional computer program, 2D-ABLATE, developed in Phase II of this study, checkout of the program included comparisons both with theoretical and with test data, as follows:

1. Simulation of transient one-dimensional (radial) conduction in a hollow cylinder, with no charring or recession. The exact solution for this problem is known and is presented in the form of temperature response curves in Ref. 21, the "CYLHEAT" handbook.

2. Comparison with test data obtained from an engine firing at Edwards AFB. Here it was necessary to simulate two-dimensional charring and conduction in a two-material thrust chamber, the exposed material being a carbon cloth-phenolic backed up by a stainless steel shell.

Cases 1 and 2 above comprised only a portion of the checkout performed for the 2D-ABLATE program, which for purposes of debugging included treatment of an assortment of wall configurations, material arrangements and properties, and external heating conditions. Cases 1 and 2, however, were treated in depth and, being representative of the two classes of problems handled, are discussed here in detail.

COMPARISON WITH AN EXACT SOLUTION OF A CONDUCTION PROBLEM

Despite the complexity of the 2D-ABLATE program and the many physical and chemical mechanisms it treats, its basic function, nevertheless, is the prediction of transient temperature distributions resulting from the conduction of heat in solids. Consequently, before the program could be used with any real degree of confidence, it was necessary to determine its capabilities for handling pure conduction problems. Furthermore, because an implicit method of solution was employed for the energy equation, it was especially important to show that sufficiently accurate and stable results can be obtained using large distance increments and relatively large time steps, i.e., large (for a given distance increment) compared to the step size required for an explicit method. For this purpose, the best standard for comparison is an exact solution. Although the case chosen of a hollow cylinder is only one-dimensional, the spatial coordinate is radial (the direction of greatest heat flux in most engine firings) and provides the closest approximation to an axisymmetric thrust chamber for which an exact solution is available.

The conduction problem whose solution is given in the CYLHEAT handbook can be expressed (in our notation) as follows:

$$\frac{1}{\alpha}\frac{\partial T}{\partial \tau} = \frac{\partial^2 T}{\partial y^2} + \frac{1}{y}\frac{\partial T}{\partial y} \quad , \quad r_i \leq y \leq r_o \, , \quad \tau > 0 \tag{67}$$

$$K\frac{\partial T}{\partial n} = -K\frac{\partial T}{\partial y} = h(T_{aw}-T) \quad , \quad y = r_i \tag{68}$$

$$K\frac{\partial T}{\partial n} = K\frac{\partial T}{\partial y} = 0 \quad , \quad y = r_o \tag{69}$$

$$T = T_o \quad , \quad \tau = 0 \tag{70}$$

where α, K, and h are known constants and where r_i and r_o are the inner and outer radii, respectively, of the cylinder (see Fig. 9 for axial and radial cross-sections).

In order to assess the 2D-ABLATE conduction capabilities under extreme conditions, the program was run for the cases of both high and low thermal conductivity materials, such as an ATJ graphite throat insert and a carbon cloth-phenolic ablator, respectively. The numerical data used as input for the two cases are given in Table 3. Only a single list of data is given to cover both cases because the values chosen differ only in thermal conductivity. The numerical solution was obtained in both cases using a distance increment of $\Delta y = .11$ inches. Multiple runs were made in each case for several different constant values of $\Delta\tau$, ranging from .125 to 8 seconds in Case 1 (the high conductivity case) and from .5 to 8 seconds in Case 2. The results are presented (for $\Delta\tau = 1$

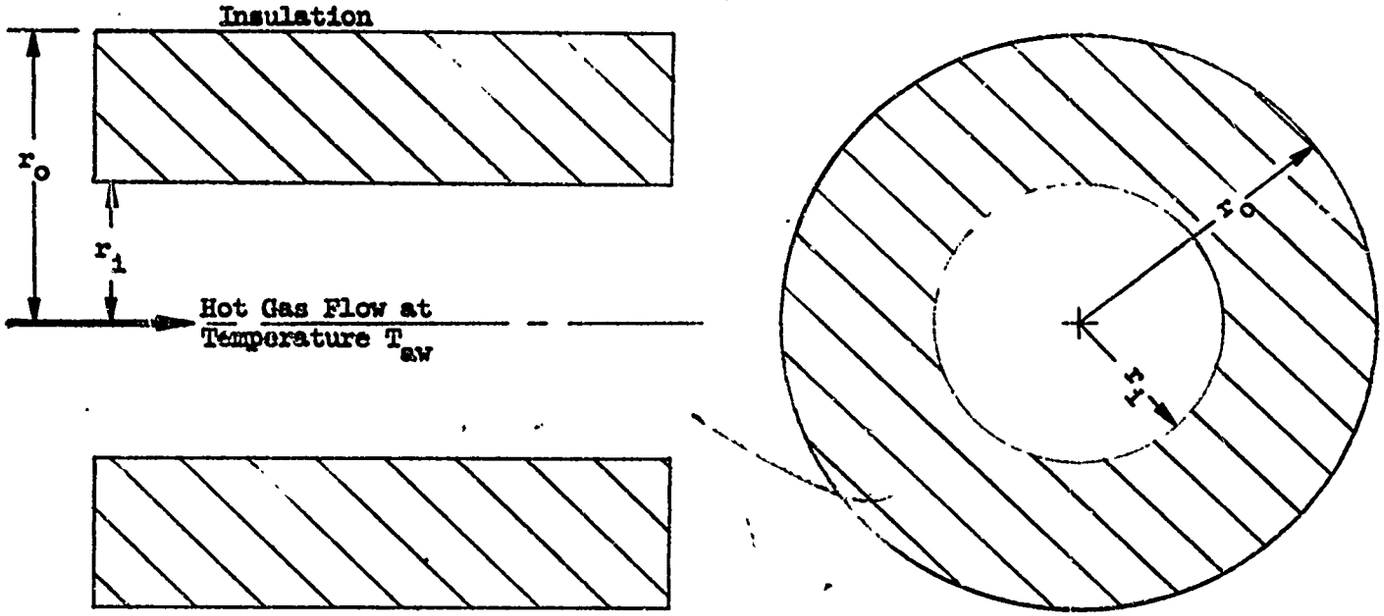

FIG. 9. AXIAL AND RADIAL CROSS-SECTIONS OF HOLLOW CYLINDER

$r_i = 1$ in
$r_o = 3$ in
$T_{aw} = 5500^{\circ}R$
$h = 1.335 \times 10^{-3}$ Btu/in^2-sec-$^{\circ}R$
$\rho C = .025$ Btu/in^3-$^{\circ}R$
$T_o = 500^{\circ}R$
$K = \left\{ \begin{matrix} 5 \times 10^{-4} \\ 1 \times 10^{-5} \end{matrix} \right\}$ Btu/in-sec-$^{\circ}R$ for the $\left\{ \begin{matrix} \text{high} \\ \text{low} \end{matrix} \right\}$ conductivity material

Table 3. Properties and Conditions Used for the Hollow Cylinder Runs

and 8 seconds only in Case 1 and for $\Delta\tau = 2$ and 8 seconds in Case 2) in Figs. 10 to 13 in the form of surface temperature histories and temperature profiles at fixed time levels.

The power of using an implicit method is strikingly illustrated here, especially in the high conductivity case. Had we used the explicit method, we see from Inequality (65) that, to ensure a stable solution, we would have been forced to use a value of $\Delta\tau$ less than or equal to .132 seconds in Case 1 and .906 seconds in Case 2. Yet, as shown in Figs. 10 and 12, we were able to obtain a stable solution (and quite accurate - especially at the surface) using a time step as much as 60 times as large. Theoretically we can use as large a time step as we

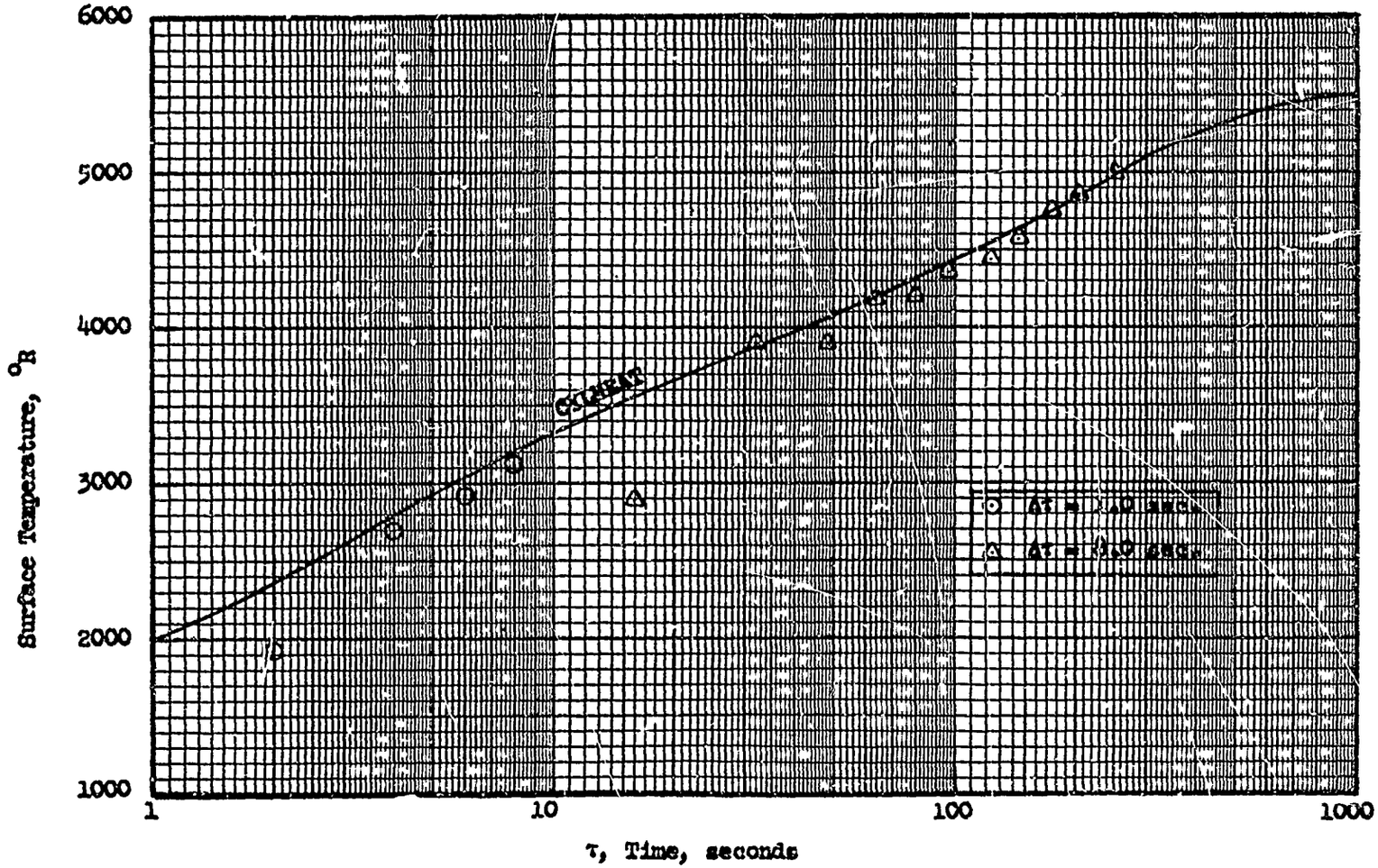

Fig. 10. HOLLOW CYLINDER

Thermal Response of Surface - High Thermal Diffusivity Material

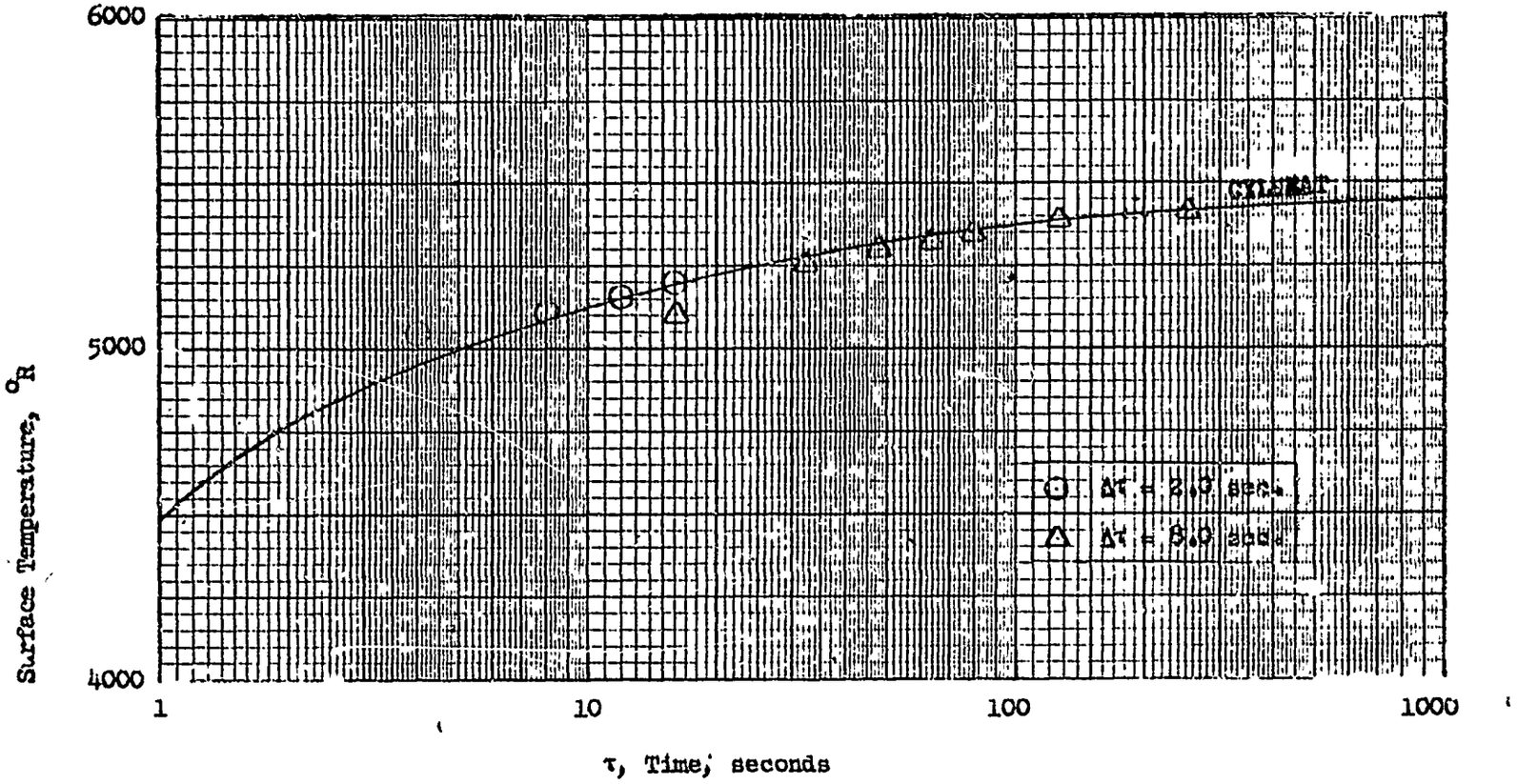

FIG. 11. HOLLOW CYLINDER

Thermal Response of Surface - Low Thermal Diffusivity Material

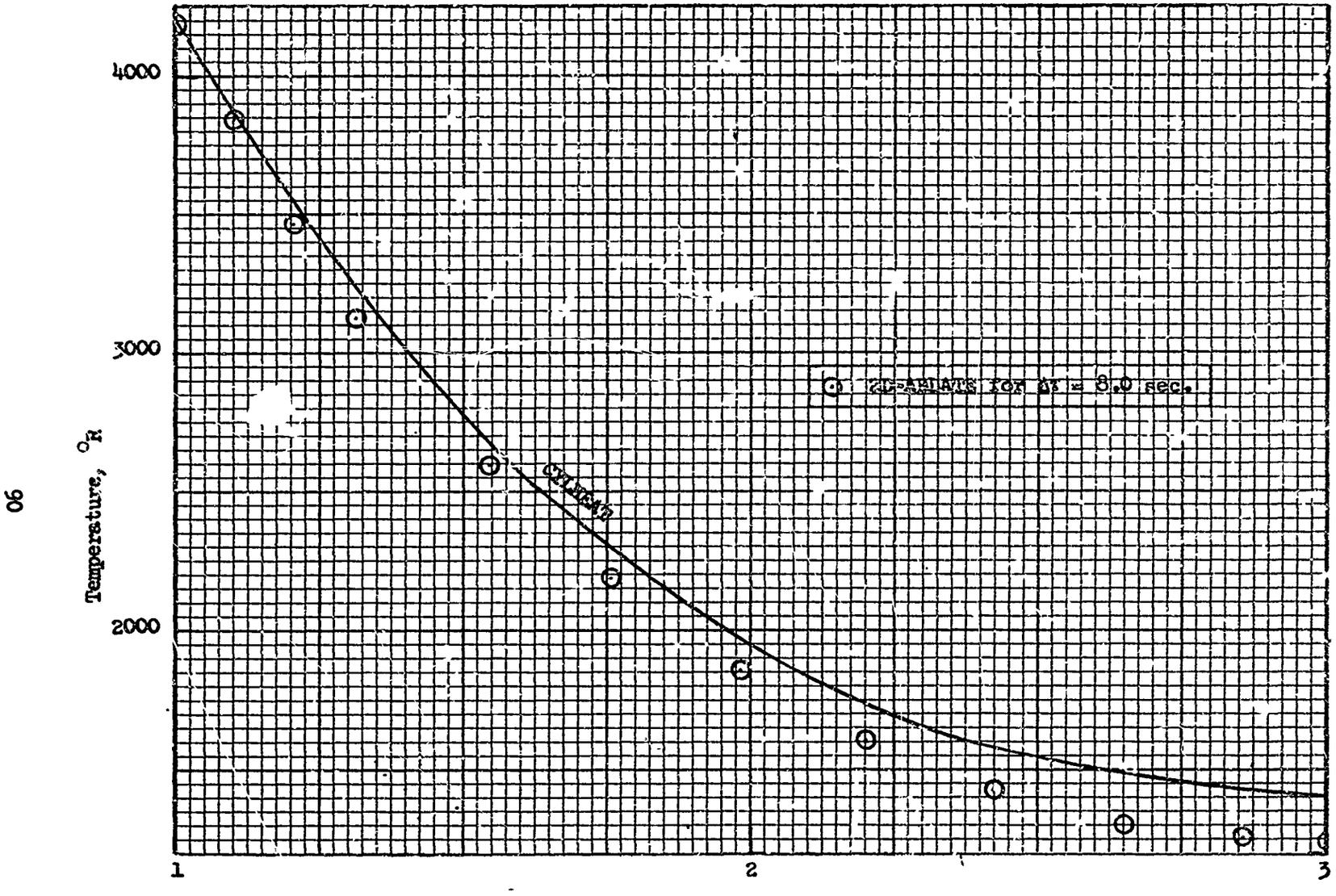

FIG. 12. HOLLOW CYLINDER

Thermal Response of Interior at 64 seconds - High Thermal Diffusivity Material

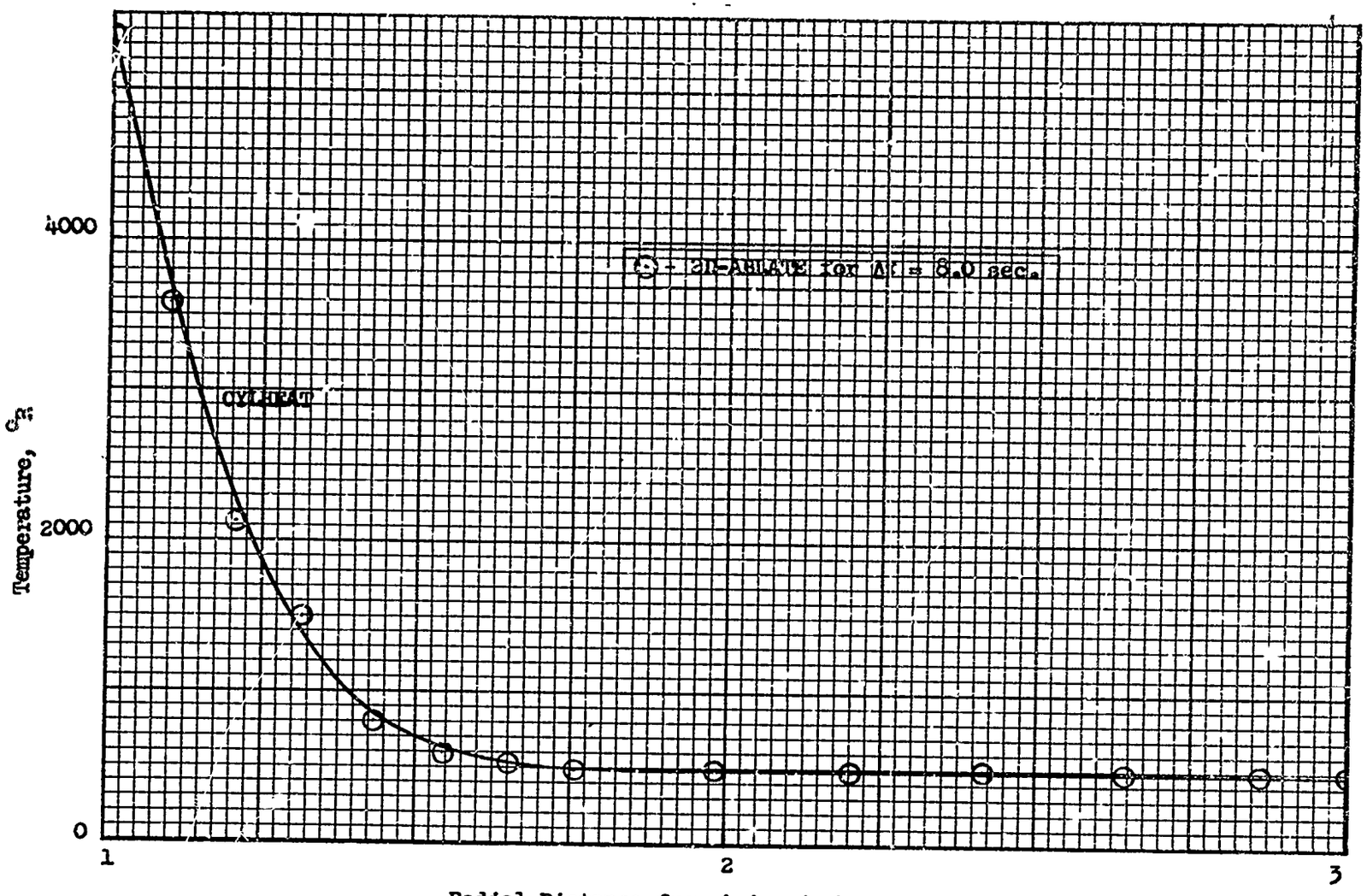

FIG. 13. HOLLOW CYLINDER

Thermal Response of Interior at 60 seconds - Low Thermal Diffusivity Material

please and still expect a stable convergent* solution - it would just take longer to home in.

In Fig. 10, for both $\Delta\tau = 1$ second and $\Delta\tau = 8$ seconds, we see that the calculated surface temperatures begin below the exact curve and approach it asymptotically with time. Simultaneously, a small error is evident in the numerical solution in the form of a slight oscillation which damps with time. The larger one-sided error is truncation error due to discretization of the continuous Eq. (67), whereas the oscillatory behavior is characteristic of the numerical procedure itself independent of the differential equation. In particular, the damping of the oscillations with time illustrates the stability of the procedure. The computer run made with $\Delta\tau = 1$ second was terminated after 8 seconds due to the expected early convergence of the numerical with the exact solution. For the run performed with so large a time step as 8 seconds, on the other hand, it was considered advisable to carry out the computations for almost 130 seconds to ensure convergence. As can be seen in Fig. 10, this proved to be overcautious; for, despite an error of over $500^{\circ}R$ at 16 seconds (the first available surface calculation), most of the early error has been eliminated shortly after 30 seconds and the correspondence

*Although the criteria given above for size of the time step were derived in terms of stability of the numerical procedure, it can be shown that this is intimately related to convergence. Indeed, in the case of a linear problem such as that defined by Eqs. (67) - (70), a proof is given in Ref. 22 that stability and convergence are equivalent for a consistent numerical scheme, i.e., one for which the difference equation at each point approaches the differential equation in the limit as the space and time increments go to zero.

is good considering the size of the time and space increments.

The numerical results obtained for the low conductivity material are pictured in Fig. 11. The closer approximation to the exact solution is to be expected because an 8 second time step here is not as large relative to that required for the explicit method as it was in the high conductivity case. The reason for the reversed direction of the early error in the 2 second time step run is not evident.

Figures 12 and 13 compare temperature profiles computed by 2D-ABLATE for $\Delta\tau = 8$ seconds with the exact solution at fixed representative intermediate time levels selected late enough to avoid early gross truncation error but before most of the error has been damped out. Again, the errors, although not excessive, are greater in the case of the high conductivity material. In particular, the error can be seen to increase with depth into the material in the high conductivity case, whereas this behavior is not particularly evident for the low conductivity material. This should not be too unexpected because, with increased distance from the surface exposed to heating, the stability (and thus convergence) criterion given by Inequality (65) becomes less applicable and is replaced by Inequality (28), which covers conduction in the interior unaffected by external heating. On the basis of Inequality (28), the upper bound for $\Delta\tau$ required in the explicit method remains virtually

unchanged for the high conductivity material but increases significantly for the low conductivity material, taking on values of .151 seconds and 7.56 seconds, respectively. Thus we see that, for internal conduction, a time step of 8 seconds for the high conductivity material is still more than 50 times as large as that required for the explicit method, but is only slightly larger for the low conductivity material. Thus we expect much more accurate results in the latter case. Indeed, for a low conductivity material, aside from reduced local temporal truncation error, there is little advantage in the use of an implicit method as long as the spatial temperature gradients are not too steep. When large gradients occur, however, small distance increments are required for local spatial accuracy and an implicit method would permit correspondingly larger time steps when desirable than would the explicit.

In summary, Figs. 10 through 13 show that 2D-ABLATE can provide very accurate results for a pure conduction problem using relatively large distance and time increments. Increased accuracy would undoubtedly result from exercising the program option of varying the time step during a computer run, using a small step at early times and larger steps later.

COMPARISON WITH ABLATIVE ENGINE TEST DATA

After establishing the adequacy of the 2D-ABLATE program in performing its basic function, i.e., in the treatment of heat conduction, the next step was to evaluate its usefulness in practice. For a real engine firing, the program must be able to predict transient temperature distributions with a reasonable degree of accuracy within the limits of a) the applicability of the mechanisms simulated in the program and b) the accuracy of the values used as input for the physical and chemical properties. Furthermore, in order to justify the use of an implicit scheme for the numerical solution, the time steps employed in the program must be larger than those required for the explicit method. To demonstrate this capability, a case was run on 2D-ABLATE for which test data were available (supplied by Edwards Air Force Base). Reasonably good agreement with the measured temperatures and char depths was obtained, at least in the throat region, as is shown below. The data supplied were for a thrust chamber firing F_2/N_2H_4 blend (66.7% N_2H_4, 24% MMH, and 9.3% H_2O, by weight) at a chamber pressure of 116 psia to develop a thrust of 3900 pounds. The thrust chamber walls consisted of two materials including a phenolic-carbon cloth ablative, exposed to engine firing, backed up by a stainless steel shell (see Fig. 14). The external heating (and cooling) conditions included heating of the inner surface by the hot combustion gases, radiative cooling at the outer

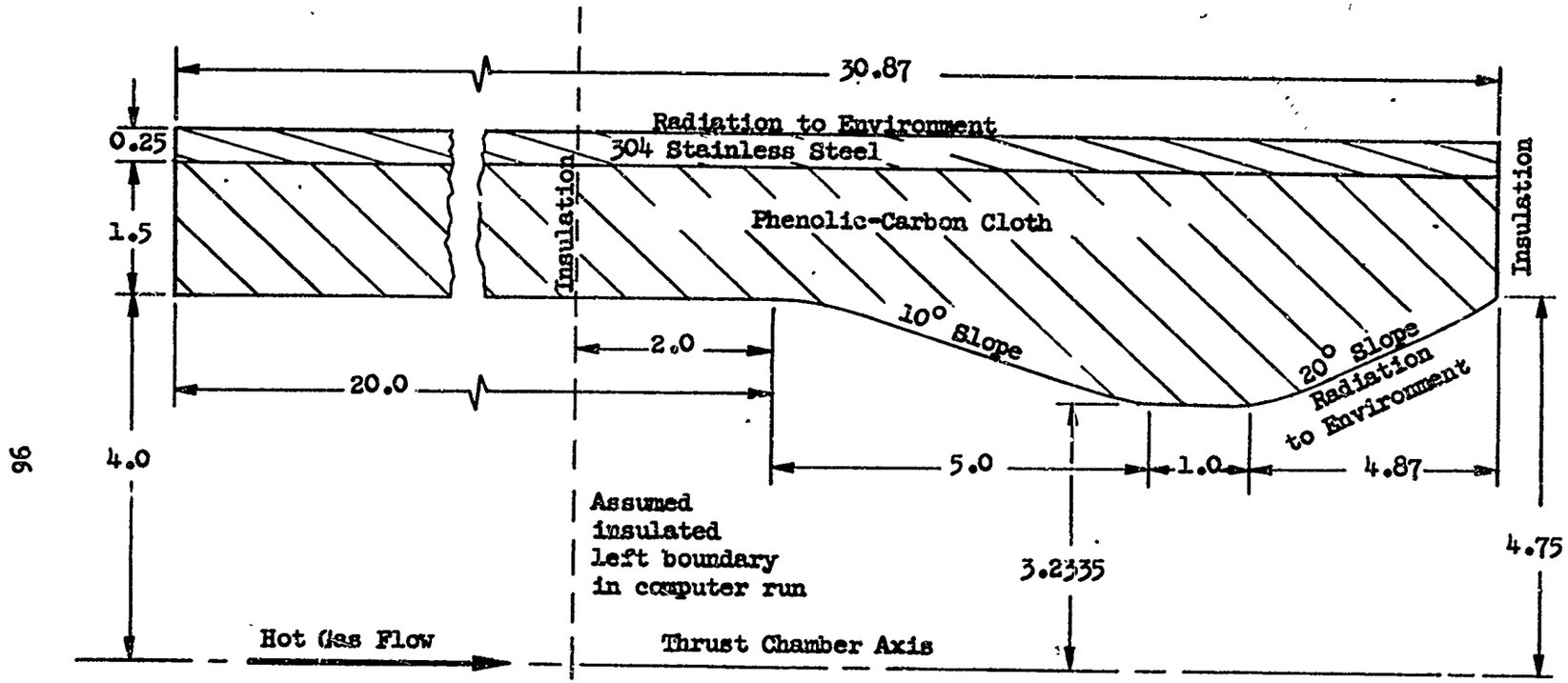

FIG. 14. THRUST CHAMBER WALL CONFIGURATION USED FOR EAFB FIRING

surface and at the diverging portion of the inner nozzle surface, convective cooling (simulated in the radiation term) at the outer surface, and insulation elsewhere as indicated in Fig. 14. Engine firing was steady for the first 60 seconds, followed by engine shutdown and soakout for the remainder of the run. The axial heat flux in the combustion chamber wall was assumed to be so slight that an effective insulated left boundary was employed at an axial position 18 inches from the injector for the computer run, as shown by the dotted line in Fig. 14; i.e., results to the left of the assumed boundary were assumed to be identical to those obtained to the right (in the combustion chamber only). Table 4 is a list of the other pertinent data required to describe the firing and used as input to the computer program. Included are material and gas properties, both physical and chemical, as well as the operating conditions, heating parameters, erosion data, and the space and time increments used to obtain a finite difference solution.

The values used were based on information supplied by EAFB supplemented by additional Rocketdyne data and experience. The density-specific heat product employed for the ablative material accounts for both the transition from virgin material to char and the increase of the specific heat of the char with temperature. The thermal conductivity of the ablative reflects similar effects in addition to a radiation contribution at high temperatures. Pyrolysis of the ablative resin occurs over a

TABLE 4. PROPERTIES AND CONDITIONS USED TO SIMULATE REAL ENGINE FIRING

MATERIAL PROPERTIES

Phenolic-Carbon Cloth Ablative (and generated pyrolysis gas):

$$\rho C = \begin{cases} 1.38\times10^{-2}\ \text{Btu/in}^3\text{-}^\circ\text{R}, & 460^\circ \le T \le 960^\circ\text{R}, \\ .42\times10^{-5}T + .9768\times10^{-2}, & 960^\circ \le T \le 1960^\circ, \\ .3\times10^{-5}T + 1.212\times10^{-2}, & 1960^\circ \le T \le 3460^\circ, \\ 2.25\times10^{-2}, & 3460^\circ \le T \le 6960^\circ. \end{cases}$$

$$K = \begin{cases} .8\times10^{-8}T + .732\times10^{-5}\ \text{Btu/in-sec-}^\circ\text{R}, & 460^\circ \le T \le 960^\circ\text{R}, \\ 1.\times10^{-8}T + .54\times10^{-5}, & 960^\circ \le T \le 3160^\circ, \\ .5\times10^{-8}T + 2.12\times10^{-5}, & 3160^\circ \le T \le 6960^\circ. \end{cases}$$

$$H = .5T - .023\ \text{Btu/lb}_m, \quad 460^\circ \le T \le 6960^\circ\text{R}.$$

$$F_{res} = .335$$

$$F_{py} = \begin{cases} 0, & T \le 960^\circ, \\ .3\left[1 - \frac{\cos(T-960)}{1000}\right], & 960^\circ \le T \le 1960^\circ, \\ .6, & 1960^\circ \le T. \end{cases}$$

$$Q_{py} = 250\ \text{Btu/lb resin}$$

$$\rho_v^* = .0542\ \text{lb}_m/\text{in}^3$$

TABLE 4 (Cont'd.)

304 Stainless Steel:

$\rho C = .031$ Btu/in^3-$^\circ$R , $460^\circ \leq T \leq 6960^\circ$R ,

$K = 1.\times10^{-7}T + 1.54\times10^{-4}$ Btu/in-sec-$^\circ$R , $460^\circ \leq T \leq 6960^\circ$R .

EROSION CONSTANTS AND COMBUSTION GAS CONDITIONS
(See Nomenclature in Appendix C)

Gas Flow Constants:

$\gamma = 1.312$

$(M_w)_\infty = 18.374$ lb$_m$/lb$_{mole}$

$P_c = 116$ psia

$(C_p)_\infty = .452$ Btu/lb$_m$-$^\circ$R

$r_c = 3.2335$ in.

Vaporization Constants:

$D_{vap} = .02$ in^2/sec

$(M_w)_{vap} = 12$

$k_{vap} = .12\times10^9$ psia

$E_{vap} = .206\times10^5$ Btu/lb$_{mole}$

$\Delta H_{vap} = 4000$ Btu/lb$_m$

$\rho_{wall\ material} = .045$ lb$_m$/in^3

TABLE 4 (Cont'd.)

Reaction Constants ($C_{(s)} + H_{2(g)} \rightarrow CH_{4(g)} + C_2H_{2(g)}$):

$(M_w)_{\text{reactant gas}} = 2\ lb_m/lb_{mole}$

$Y_{\text{reactant gas}} = .173$

$k_w = .0089$ in/sec

$E_{\text{reaction}} = .44 \times 10^5$ Btu/lb_{mole}

$\Delta H_{\text{reaction}} = 5000$ Btu/lb_m

$D_{\text{reaction}} = .118$ in^2/sec

$(C_p)_{\text{products}} = .3$ Btu/lb_m-$^\circ R$

OPERATING CONDITIONS AND HEATING PARAMETERS (axially varying)

$T_c = 530^\circ R$

$T_{env} = 0^\circ R$

$B = .4$

$(C_p)_\infty = .452$ Btu/lb_m-$^\circ R$

$n_{py} = 1.$ (for pyrolysis gases ejected at surface)

$\sigma\varepsilon = 3.3 \times 10^{-15}$ Btu/in^2-sec-$(^\circ R)^4$

x(in)	0.	1.	2.	4.	6.	7.5	8.5	10.	11.5	12.87
β_c (hot wall)	0.	0.	0.	0.	0.	0.	0.	.2	.3	.5
β_f (cold wall)	2.	2.	2.	2.	2.	2.	2.	2.	2.	2.
T_{aw} ($^\circ$R)	5875.	6375.	6875.	6875.	6875.	6875.	6875.	6875.	6875.	6875.
$\bar{h}_{conv}$ † up to 60 sec	$.38\times10^{-3}$	$.38\times10^{-3}$	$.38\times10^{-3}$	$.42\times10^{-3}$	$.5\times10^{-3}$	$.55\times10^{-3}$	$.55\times10^{-3}$	$.39\times10^{-3}$	$.29\times10^{-3}$	$.22\times10^{-3}$
$\bar{h}_{conv}$ after 60 sec	0	0	0	0	0	0	0	0	0	0

† (Btu/in^2-sec-$^\circ$R)

TABLE 4 (Cont'd.)

TABLE 4 (Cont'd.)

FINITE DIFFERENCE INFORMATION

Space Increments:

$y = 0$, at axis of thrust chamber

$\Delta y = .1$ in, axial mesh lines at $y = y_j = 3.3 + (j-1)\Delta y$, $j = 1, \cdots, 25$

$x = 0$, .1 in. to left of chamber cut-off position

radial mesh lines at $x = x_{i+1} = x_1 + \Delta x_i$, $i = 1, \cdots, 14$, $x_1 = .35$

i	1	2	3	4	5	6	7	8	9	10	11	12	13	14
Δx_i (in.)	.75	.75	.75	1.25	1.25	1.25	1.	.5	.25	.25	.5	.75	1.5	1.1

Variable Time Steps (Option A):

k	1	2	3	4	5	6	7	8	9	10	11	12
$\Delta\tau_k$(sec)	.1	.2	.5	1.	2.	5.	1.	2.	5.	10.	20.	30.
$F_{on,k}(\tau)$	1.	1.	1.	1.	1.	1.	0.	0.	0.	0.	0.	0.
τ	0.	.3	.5	1.	10.	30.	60.	70.	80.	100.	200.	400.

where τ is initial time for use of $\Delta\tau_k$

temperature range extending from 500 to 1500°F with an average heat of pyrolysis of 250 Btu/lb $_{sin}$. The pyrolysis gases generated were assumed in this case to undergo no further high temperature cracking or gas-char reactions during passage through the porous char. The gas-side heat transfer coefficient distribution used in the program is based on the Bartz equation. Thermodynamic and kinetic constants are given in Table 4 to account for possible vaporization of the char and reaction of the char with hydrogen in the combustion gas. As noted, a variable axial distance increment, Δx, was used with closest spacing in the throat. A variable time step, $\Delta\tau$, was specified to obtain sufficient accuracy with a minimum of computer time.

The pertinent results of the computer run of the 2D-ABLATE program, for the data listed in Table 4, are presented in Figs. 15 to 19 in the form of temperature and radial char depth histories, temperature profiles, and contours of the char front at fixed time levels. Although the computer run included erosion constants as input data, no surface recession was predicted. This was in agreement with the results of the engine test firing.

Figure 15 compares computed char depth histories at the throat, combustion chamber, and exit (at axial positions 4.87, 11.87, and .67 inches, respectively, from the exit plane) with two experimental throat values

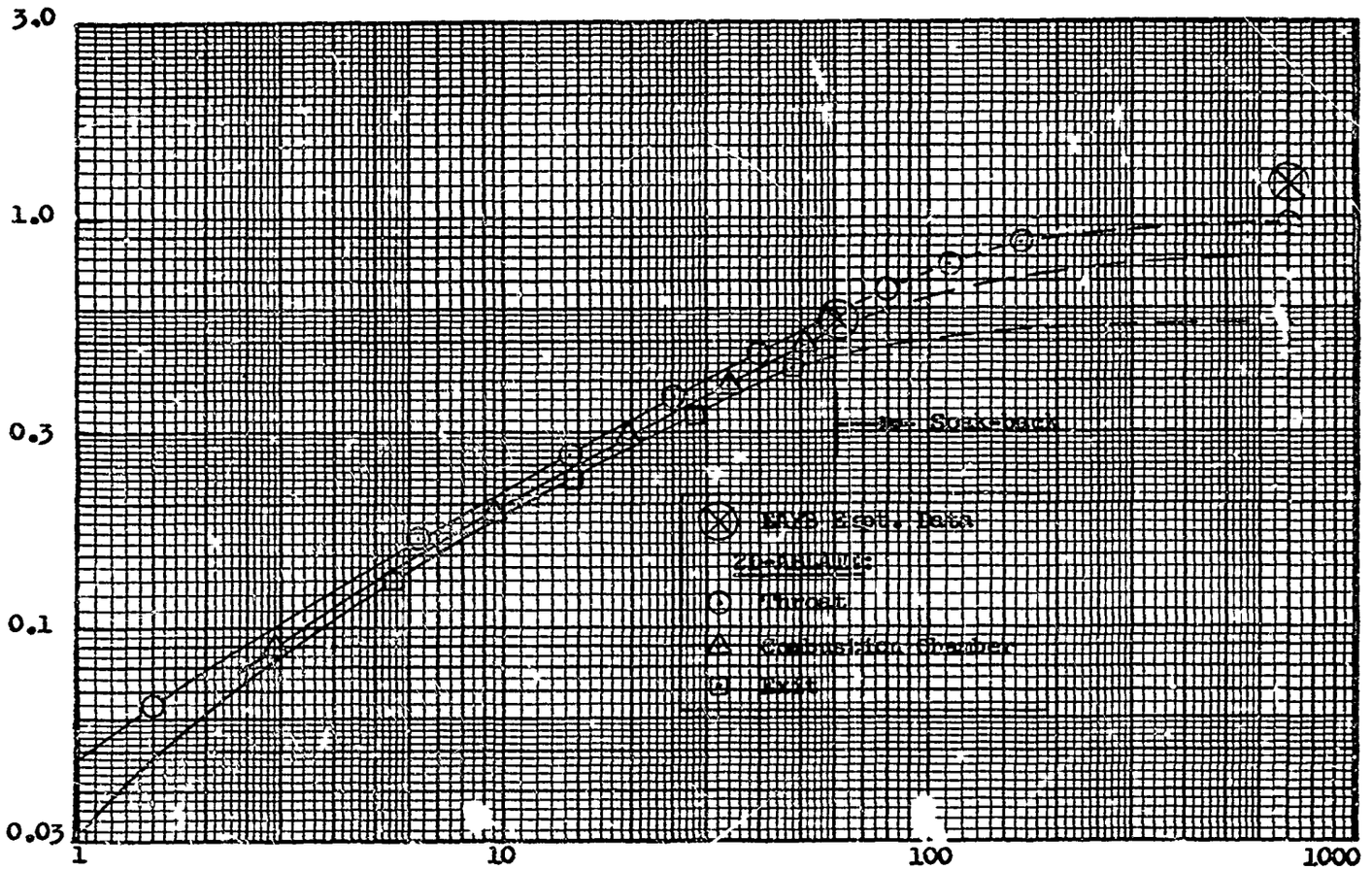

FIG. 15. RADIAL CHAR DEPTH (1460°R Isotherm)
No Surface Erosion Predicted

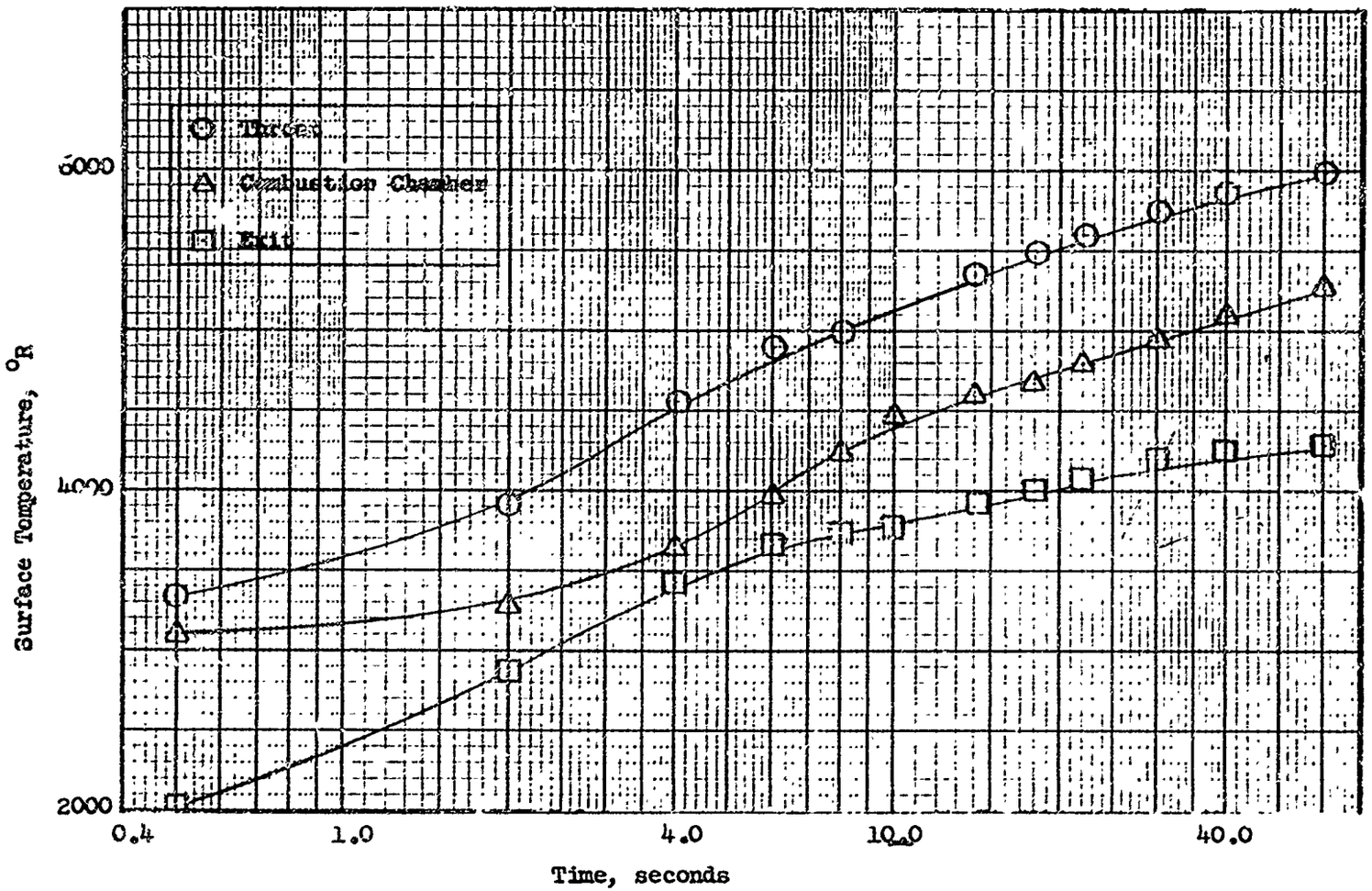

FIG. 16. SURFACE TEMPERATURE RESPONSE

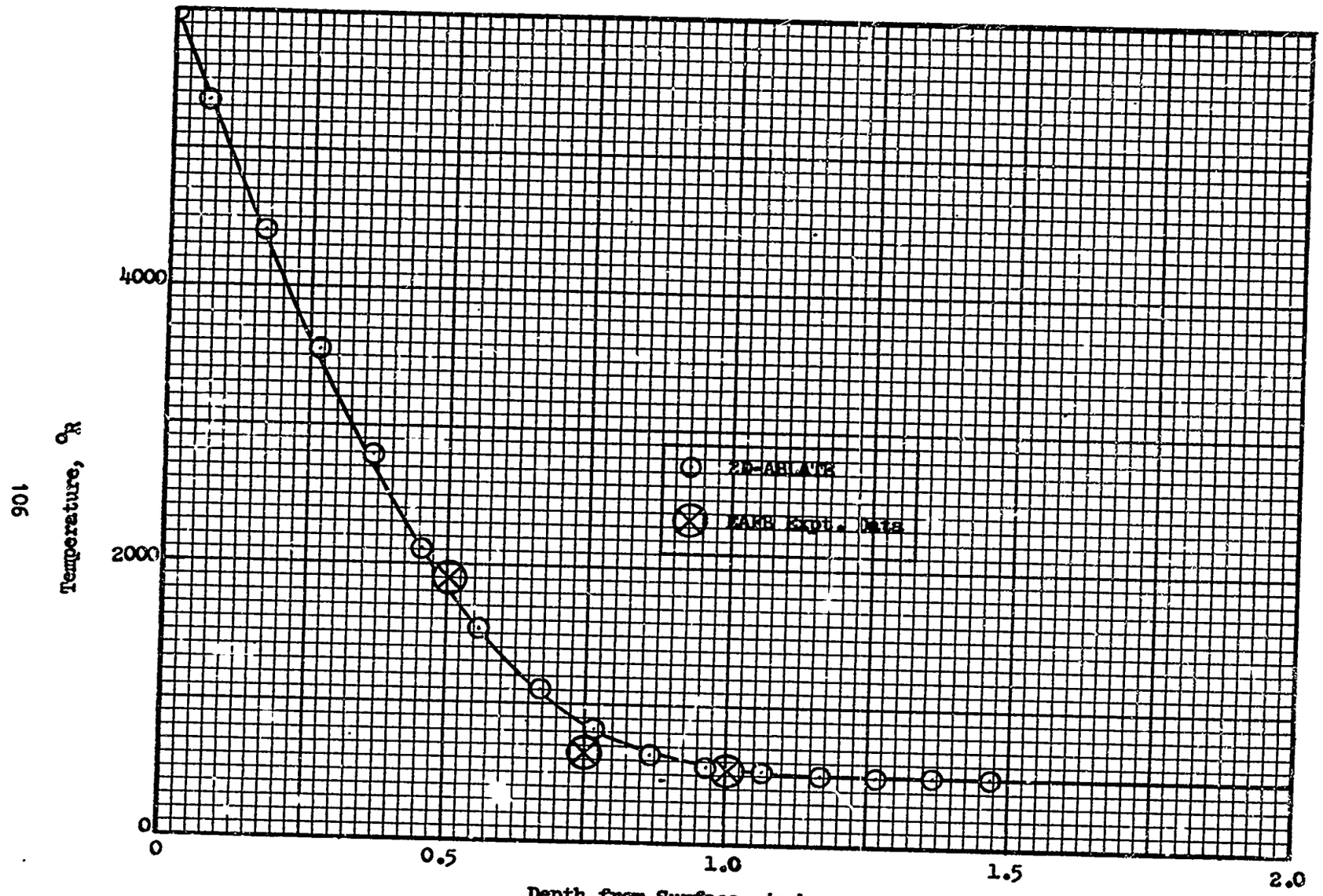

FIG. 17. THROAT TEMPERATURE PROFILE AT 60 SECONDS

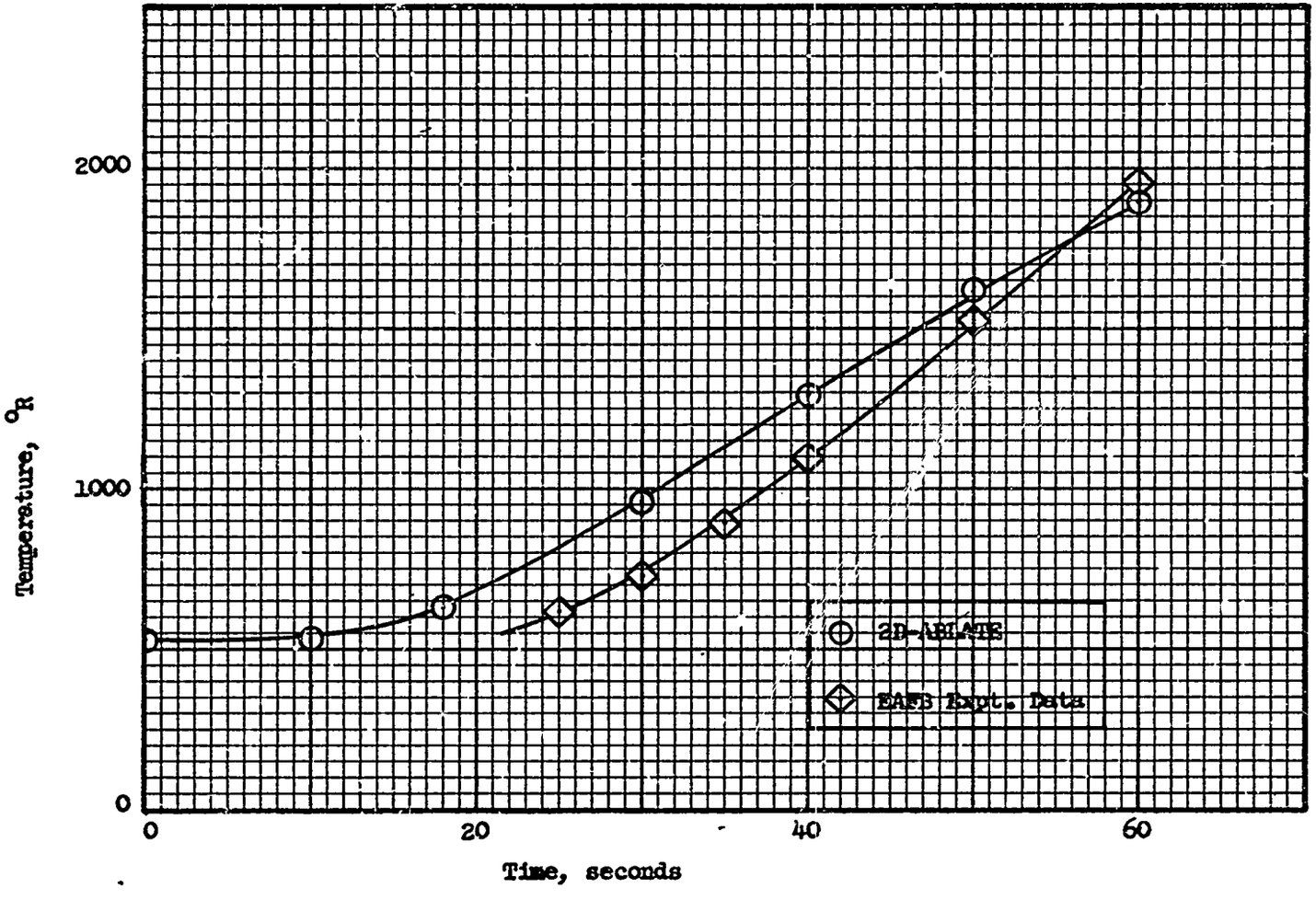

FIG. 18. THROAT TEMPERATURE HISTORY AT DEPTH OF 0.5 INCHES

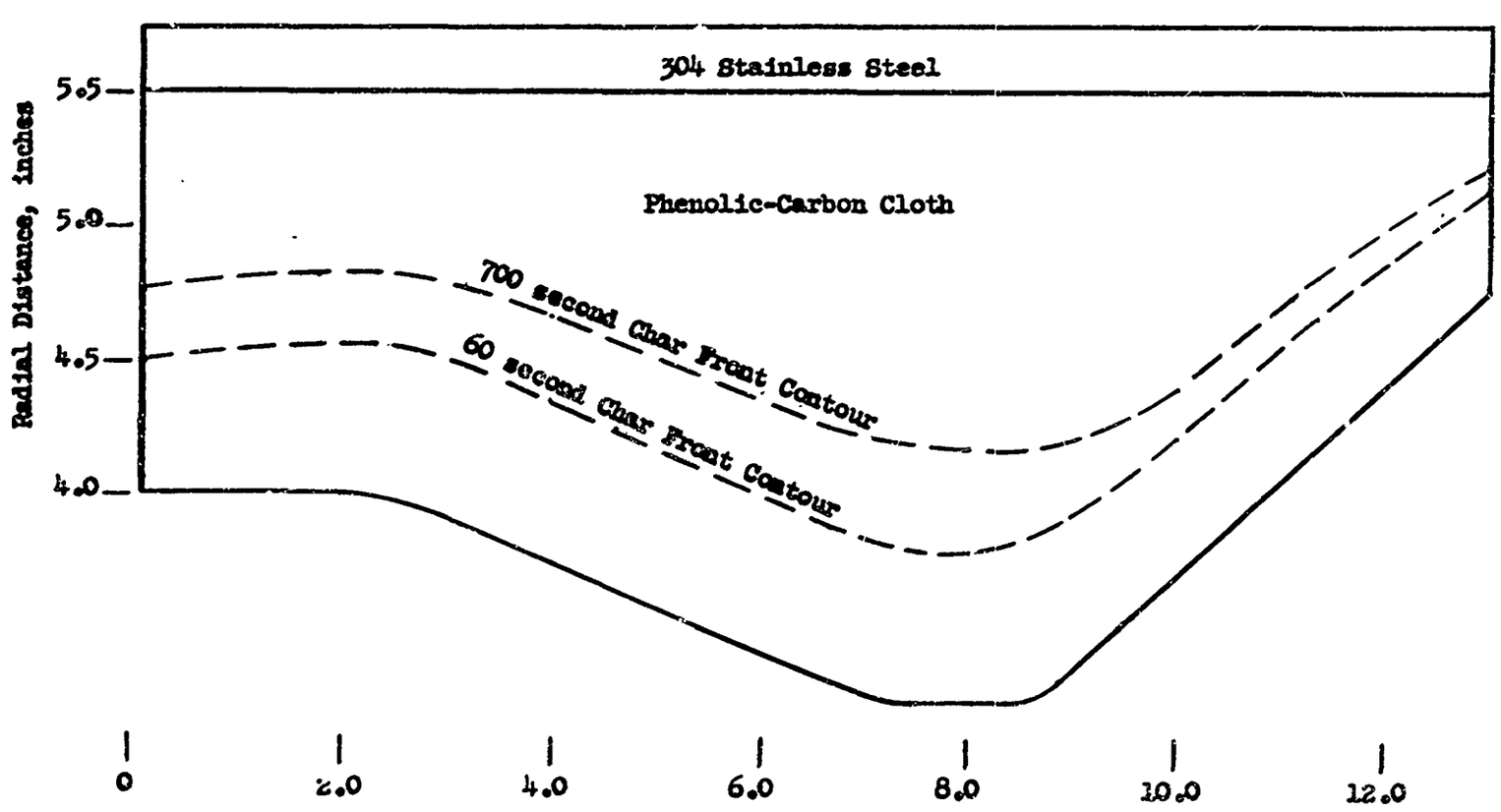

FIG. 19. CONTOUR OF CHAR FRONT (1460°R ISOTHERM) AT 60 SECOND AND 700 SECOND LEVELS

obtained from measured test data. For all plotted points except the measured throat value at 700 seconds (a depth of 1.2 inches), char depth for a given axial position at any time was defined to be the radial distance from the surface of the point whose maximum temperature attained up until that time was 1460°R, the midpoint of the charring temperature range (the 60 second experimental value was obtained by interpolation from throat temperatures measured at several radial positions). The measured value at 700 seconds, on the other hand, was not based on the location of a temperature level but instead on a visual judgment which placed it in the initial portion (considerably below 1460°R) of the charring temperature range. The extrapolated experimental char depth at the throat (based on the 1460°R definition) at 700 seconds thus should appear much closer to the computed value. For the throat, chamber, and exit values of T_{aw} and $\bar{h}_{conv}$ employed in the program, the relative positions of the corresponding computed char depth histories are consistent with expected results.

In Fig. 16, surface temperature histories are presented for the same three axial positions (throat, chamber, and exit). Although no measurements were made of surface temperature during the real engine firing, the curves shown in Fig. 16 provide further grounds for evaluation of the run based on 1) their positions relative to each other, 2) how closely the magnitudes attained correspond to expected results, and

3) the compatibility of the shapes assumed by the curves. The results seem reasonable on the basis of all three criteria (in assessing the compatibility of the shapes assumed, it must be remembered that, due to axial ordering, the chamber and exit curves should not be compared directly with each other, but only through comparisons of each with the throat curve).

Figure 17 is a comparison with experimental data of a computed temperature profile at the throat after 60 seconds of firing (comparable data at the chamber and exit were not available in depth). In general, the agreement is reasonably good. No comparison is possible until a depth of .5 inches, where the computed value is 50°R less than the measured. Proceeding into the material, the computed temperature does not drop off as quickly and is above the next measured value (at a depth of .75 inches) by over 150°R. Beyond that point, there is not enough thermal penetration for a meaningful comparison.

In Fig. 18, a comparison is given of the computed temperature history with the measured at a depth of .5 inches. Again the correspondence is reasonably good. The slopes are close and the values differ by at most 250°R. The computed curve rises sooner than the measured, the difference between the curves reaching a maximum after about 30 seconds of firing. At this time, the slope of the measured curve has just about

caught up with and, thenceforth, exceeds that of the computed curve. The curves cross at about 55 seconds and the computed curve has dropped below the measured by about 60°R at 60 seconds, the end of firing.

Similar comparisons are not pictured for the chamber and exit temperature histories (no similar test data are available at the exit). The correspondence in the chamber was not good, there being almost a 30 second delay in the beginning of the rise of the measured temperature values after that of the computed values. No physical explanation has been found for this lag unless some other heat transfer mechanism, such as film cooling from the injector, was present in the combustion chamber to cause the delay. The computed chamber values, on the basis of past experience, seem to be more compatible with both the computed and measured throat values. After the initial lag, the slope of the curve of the measured values is relatively steep and, by the end of the 60 second firing cycle, the measured value is within 50°R of the computed.

Finally, in Fig. 19, contours are pictured of the char front (based on a 1460°R isotherm) obtained from the computer run for two fixed time levels: at $\tau = 60$ seconds, the end of firing, and at $\tau = 700$ seconds, after 640 seconds of soakout. It is of interest to note that, although the radial char depth at 60 seconds is nearly uniform for all axial positions (see Fig. 15 as well), the additional radial penetration of the char

front during soakout is considerably greater at the throat than elsewhere, the least additional penetration occurring at the exit position. This is mainly due to the greater heat content in the throat volume below the char front at 60 seconds than in the exit or chamber. In addition, the particularly small change at the exit is probably due in part to axial conduction losses from the exit to the throat plane and possibly to greater proximity of the exit portion (and the chamber portion as well) of the char front to the radiating sink at the outer surface of the stainless steel shell. In the first 60 seconds, on the other hand, these effects are dominated by the strong, almost uniform heat flux along the exposed inner surface. Although no contours of measured data are available for comparison, the computed contours agree with the 60 second experimental point pictured in Fig. 15, they assume shapes which are in agreement with the relative locations of the adjacent thermal sources and sinks, and they are compatible with each other.

To summarize, the results of using the 2D-ABLATE program to simulate a real engine firing corresponded reasonably well to measured test data, and, where measured data were not available, the computed results were compatible with expected results and with each other. They were obtained for a 700 second run using time steps which varied from .1 to 30 seconds in size (see Table 4), 79 steps in all. The machine time required for the run can be broken down as follows: 30 seconds to load, 20 seconds

for the Link 1 preliminary execution, and 120 seconds for the time-step calculation (at 1½ seconds of machine time per time step), for a total of 170 seconds of machine time. On the basis of Inequality (28) (applied to the backup material, due to its high thermal diffusivity) the explicit method would have required a value of $\Delta\tau$ less than or equal to .5 seconds. Even assuming as little as ½ second of machine time per time step, this would mean a minimum of 700 seconds for execution alone using the explicit method. Furthermore, the number of time steps and thus the machine time used by 2D-ASTRA for this case could probably have been reduced significantly without appreciable changes in the results. This was substantiated by making another 700 second run identical to the first, but for which each time step was cut in half. The temperatures obtained at comparable times and positions were uniformly within 1% of each other from run to run (except in the first few steps of both the firing and cooling periods when they differed by at most 3%) and generally differed by considerably less than 1%. This is well within the usual convergence standards and indicates that larger steps than those used in the first run could have been safely employed.

CONCLUSIONS

In Phase 2 of the subject program, it has been demonstrated by means of a digital computer code that the nonlinear equations of a comprehensive two-dimensional transient ablation (including both surface erosion and internal charring) and heat conduction model for the multimaterial walls of a rocket engine thrust chamber can be solved using numerically stable implicit finite difference procedures. The analysis was performed in cylindrical coordinates (axial and radial) assuming axisymmetric walls with temperature dependent physical and chemical properties and arbitrarily curved material boundaries and interfaces. Chemical reactions within the charring material were treated in depth and include three gas generation reactions plus cracking of the generated gases. Surface erosion effects handled at the hot combustion gas boundary were melting, vaporization, and chemical reactions. Blocking of the combustion gas due to injection of gases generated within the wall materials and at the surface was also accounted for. Other heat flux mechanisms included in the model and handled by the program included: engine firing, environmental heating, radiation from the walls to the environment, insulation at the boundaries, and convective cooling within the charring ablator. Engine firing may be steady or intermittent with soakout, the latter consisting of either multiple-start operation or pulsing. All heat

fluxes at the boundaries and interfaces were expressed in terms of normally directed temperature gradients.

A time step procedure was employed to uncouple and solve the continuous equations, finite differences being used for the discretization. Of particular interest was a generalization of the unconditionally stable alternating method of Peaceman and Rachford used for the energy equation in conjunction with special second order accurate techniques developed to simulate the normal gradient conditions at curved surfaces. The numerical procedures developed were incorporated in the Fortran IV computer program, 2D-ABLATE, used for the solution.

The program capabilities were evaluated by comparison with 1) an exact solution of the transient one-dimensional pure conduction problem for a hollow cylinder heated at the inner surface and insulated at the outer, and 2) test data from an engine firing with two-dimensional transient charring and conduction taking place in the two-material thrust chamber. Comparisons were made at various axial positions with respect to char depth (in the second case only), temperature profiles, and both surface and interior temperature histories. Excellent agreement was obtained with results of the exact solution and reasonably good agreement with the measured test data obtained from the engine firing. Moreover, the program exhibits a high degree of self-consistency and compatibility of results obtained.

RECOMMENDATIONS FOR FUTURE EFFORTS

The Phase 1 effort of the subject program has led to the development of numerical procedures and a computer code for solving comprehensive two-dimensional transient ablation and heat conduction problems. There are, however, several extensions to the program which should be made in addition to both practical and theoretical investigations to delimit the program capabilities and provide analytical tools for future rocket nozzle designs. A summary of recommendations for future effort follows.

1. Many materials of current interest are strongly anisotropic. The existing computer program should be extended to handle materials with differing temperature dependent conductivities in the x and y directions.

2. Provision should be made in the program to permit more than one of the wall materials to be charring ablators.

3. It has been well-established that, for many cases of engine firing, radiative exchange between opposing surfaces of the hot gas boundary has a significant effect on the transient temperature distribution. The program should be extended to account for the effect of this mechanism.

4. A comprehensive study should be made of several of the parameters in the analysis to ascertain their significance in the overall heat

transfer process. The goal of such a study would be the generation of graphs and tables which summarize the variation of thermal penetration, char depth, and surface erosion in rocket engine walls with the essential parameters governing the material properties and arrangement as well as the thermal environment. Such results would provide basic information required for the design of thrust chambers and would serve to establish detailed guidelines for the subsequent use of the computer program.

5. Investigation should be made to develop alternative finite-difference procedures which provide greater accuracy by reducing both temporal and spatial local truncation errors. The principal motivation of an improved scheme would be its ability to reduce the machine time required to achieve a given standard of accuracy by increasing the size of the computational increments required. A three-level (in time) alternating direction method, for example, which has recently been developed by the present investigators, might be employed. This procedure is second order in time, requiring no linearization for its application to the nonlinear energy equation. Unconditional stability has already been established for this method when used to discretize the linear energy equation.

6. A theoretical investigation should be made of the finite difference procedures utilized in the program and any of its extensions or modifications (in accordance with recommendations 1, 2, 3, and 5 above) with

main emphasis given to a study of their numerical stability and convergence properties. The value of such an investigation would be as a tool to eliminate expensive experimentation with the program to establish detailed quantitative stability and convergence criteria for each change in materials and thermal environment. In the event, however, that a theoretical investigation is not made, then an empirical determination of stability and convergence criteria should be conducted.

REFERENCES

1. "Final Report, Theoretical and Applied Research in a Transpiration-Cooled Thrust Chamber," Rocketdyne Report R-5279, October 1963, under Contract AF04(611)-8190 and issued as RTD-TDR-63-1087 (Confidential).

2. Rivers, W. J., Van Wyk, R., Seader, J. D., Friedman, H. A., Chu, H. N. "Final Report, Effect of Rocket Engine Combustion on Chamber Materials, Part I: One-Dimensional Computer Program," Rocketdyne Report R-6050-2, issued as Technical Documentary Report No. AFRPL-TR-65-13, Air Force Rocket Propulsion Laboratory, Edwards, Calif., prepared under Contract No. AF04(611)-9714, January 1965.

3. Peaceman, D. W. and Rachford, H. H. Jr., "The Numerical Solution of Parabolic and Elliptic Differential Equations," J. Soc. Ind. Appl. Math., Vol. 3, No. 1, 28-41, 1955.

4. Bray, A. P. and Mac Cracken, S. J., "TIGER II, An IBM 7090 Digital Computer Program: Temperatures from Internal Generation," General Electric Company Report KAPL-2044, Knolls Atomic Power Laboratory, Schenectady, New York, 29 May 1959.

5. Abrahams, R. S. and Fick, J. L., "Engineering Utilization Manual-Thermal Network Analyzer Program - IBM 709-7090 Computer," Lockheed Aircraft Corporation Missiles and Space Division Report TM 59-24-1, 28 April 1965.

6. Hurwicz, H., "Aerothermochemistry Studies in Ablation," paper presented at Fifth AGARD Combustion and Propulsion Colloquium, Braunschweig, 9-13, April 1962.

7. Hurwicz, H., Fifer, S., and Kelley, M., "Multidimensional Ablation and Heat Flow During Re-Entry," Journal of Spacecraft and Rockets, Vol. 1, No. 3, 235-242 (1964).

8. McCuen, P. A., Schaefer, J. W., Lundberg, R. E., and Kendall, R. M., "A Study of Solid-Propellant Rocket Motor Exposed Materials Behavior," Final Report, AFRPL-TR-65-33, Vidya Report No. 149, February 26, 1965.

9. Mc Farland, B. L., internal Rocketdyne Report in process of completion.

10. Douglas, J. Jr., "A Note on the Alternating Direction Implicit Method for the Numerical Solution of Heat Flow Problems," Proc. Amer. Math. Soc., 1955, 409-412.

11. Lees, Milton, "Alternating Direction and Semi-Explicit Difference Methods for Parabolic Partial Differential Equations," NYU Tech. Report NYO 9494, Institute of Mathematical Sciences, 1 March 1961.

12. Viswanathan, R. V., "Solution of Poisson's Equation by Relaxation Method--Normal Gradient Specified on Curved Boundaries," Math Tables and Other Aids to Computation, Vol. 11, No. 58, 67-78, 1958.

13. Friedman, H. A., "Numerical Solution of the Nonlinear Transient Two-Dimensional Heat Conduction Problem in Composite Solids with Curved Boundaries and Interfaces," Rocketdyne Research Memorandum RM 964-351, October 1963.

14. Friedman, H. A., "The Numerical Solution of Nonlinear Heat Transfer Problems in Regions with Fixed or Free Curved Material Interfaces and Curved Boundaries," Rocketdyne Report R-5361F, October 1963.

15. deSoto, S. and Friedman, H. A., "Flame Spreading and Ignition Transients in Solid Grain Propellants, "Rocketdyne Research Report RR 63-4, Appendix A, 1963.

16. Mc Adams, W. H., "Heat Transmission," Mc Graw-Hill Book Co., New York, p. 47-49, 1954.

17. Mc Farland, B. L. and Harmon, D. B., "Heat Transfer Through a Melt Layer with External Gas Flow," 1961 Heat Transfer and Fluid Mechanics Institute, p. 208, June 1961.

18. Sauer R., "General Characteristics of the Flow Through Nozzles at Near Critical Speeds," NACA TM-1147, June 1947.

19. Rosner, D. E., "Convective Diffusion as an Intruder in Kinetic Studies of Surface Catalyzed Reactions," AIAA Journal, Vol. 2, No. 4, p. 593, April 1964.

20. Van Wyk, R., Dickerson, R., and Friedman, H. A., "A Rocket Engine Combustion Model for the Analytical Evaluation of Unstable Combustion Damping Devices: Preliminary Report," Rocketdyne Research Memorandum RM 997-351, January 1964.

21. Desmon, L. G. and Avis, G. B., "CYLHEAT Handbook - Vol. I. Transient Body Temperature Response Curves for Hollow Cylinders with Heated Interior and Insulated Exterior," Report No. AEL/X-123, Allegany Ballistics Lab., Hercules Powder Co., Cumberland, Maryland, sponsored by Advanced Research Projects Agency Propellant Chemistry Office and Bureau of Naval Weapons Special Projects Office, July 1964.

22. Lax, P. D. and Richtmyer, R. D., "Survey of the Stability of Linear Finite Difference Equations," Comm. Pure Appl. Math., Vol. 9, 1956.

APPENDIX A

DEVELOPMENT OF ENERGY AND CONTINUITY EQUATIONS

The following form of the mass continuity equation has been employed in the char region of the charring ablative material:

$$\frac{\partial \rho_g}{\partial x} + \frac{\partial \rho}{\partial \tau} + \frac{\partial G_x}{\partial x} + \frac{1}{y}\frac{\partial}{\partial y}(yG_y) = 0 \quad . \tag{A-1}$$

Using the thermodynamic methods given in Appendix B to express the density ρ of the charring material, we can rewrite Eq. (A-1) as

$$-\frac{\partial \rho_g}{\partial \tau} - \sum_1 \frac{\partial \rho}{\partial F_1}\frac{\partial F_1}{\partial \tau} = \frac{\partial G_x}{\partial x} + \frac{1}{y}\frac{\partial}{\partial y}(yG_y) \quad . \tag{A-2}$$

By assuming the time rate of change of gas density to be dominated by the other terms, we obtain the form of the continuity equation given earlier (Eq. (2)).

Making use of Eq. (A-2), we can further derive the form of the energy equation given previously by Eq. (1). We begin by assuming a form for the energy equation, as follows (again using the thermodynamic approach):

$$\frac{\partial(\rho H)}{\partial \tau} + \frac{\partial(\rho_g H_g)}{\partial \tau} = \sum_i \Delta Q_i \frac{\partial \rho}{\partial F_i} \frac{\partial F_i}{\partial \tau} - \frac{\partial}{\partial x}(G_x H_g) - \frac{1}{y}\frac{\partial}{\partial y}(y G_y H_g) + \frac{\partial}{\partial x}\left(K \frac{\partial T}{\partial x}\right) + \frac{1}{y}\frac{\partial}{\partial y}\left(yK \frac{\partial T}{\partial y}\right) \quad . \tag{A-3}$$

Then, multiplying Eq. (A-2) by H_g and adding Eq. (A-3) with enthalpy derivatives expanded, we obtain after combining terms appropriately (and making use of the fact that $\frac{\partial \rho}{\partial \tau} = \sum_i \frac{\partial \rho}{\partial F_i}\frac{\partial F_i}{\partial \tau}$) the following expression:

$$\rho \frac{\partial H}{\partial \tau} + \rho_g \frac{\partial H_g}{\partial \tau} = \sum_i (\Delta Q_i + H_g - H) \frac{\partial \rho}{\partial F_i} \frac{\partial F_i}{\partial \tau} - G_x \frac{\partial H_g}{\partial x} - G_y \frac{\partial H_g}{\partial y} + \frac{\partial}{\partial x}\left(K \frac{\partial T}{\partial x}\right) + \frac{1}{y}\frac{\partial}{\partial y}\left(yK \frac{\partial T}{\partial y}\right) \quad . \tag{A-4}$$

By noting that ρ_g is dominated by ρ, we can suppress the second term on the left side of Eq. (A-4). In addition, the first term can be rewritten as follows:

$$\frac{\partial H}{\partial \tau} = \frac{dH}{dT}\frac{\partial T}{\partial \tau} = C \frac{\partial T}{\partial \tau} \quad , \tag{A-5}$$

where C is the specific heat at constant pressure of the solid material in the char region. We may similarly rewrite $\frac{\partial F_i}{\partial \tau}$ as $\frac{dF_i}{dT}\frac{\partial T}{\partial \tau}$. Finally we may take $\Delta Q_i + H_g - H$ to be a constant Q_i by assuming that the composition of the gas generated in each reaction remains unchanged as it is being formed; i.e., for each i,

$$\frac{\partial \Delta Q_i}{\partial T} = - \frac{\partial (H_g - H)}{\partial T} \quad . \tag{A-6}$$

This l[illegible]s by integration to the following expression

$$\Delta Q_i + H_g - H = \text{constant} \equiv Q_i \quad . \tag{A-7}$$

Then [illegible]ay write Eq. (A-4) with the above modifications as

$$\left(\rho C - \frac{\partial \rho}{\partial F_i} \frac{dF_i}{dT}\right) \frac{\partial T}{\partial \tau} = \frac{\partial}{\partial x}\left(K \frac{\partial T}{\partial x}\right) + \frac{1}{y} \frac{\partial}{\partial y}\left(yK \frac{\partial T}{\partial y}\right) - G_x \frac{\partial H_g}{\partial x} - G_y \frac{\partial H_g}{\partial y} \quad , \tag{A-8}$$

which i[illegible]exactly Eq. (1). (The subscript g has been dropped for convenienc[illegible]from the symbol for gas enthalpy.)

APPENDIX B

DERIVATION OF EQUATION FOR DENSITY OF CHARRING LAMINATE

The derivation of the expression given previously by Eq. (4) for the density of the solid portion of the charring material is based on a thermodynamic simulation of all internally occurring chemical reactions, and in particular on the assumption that all chemically reacting systems within the material are in thermodynamic equilibrium. Required for the development are the following known functions of temperature:

$F_{py}(T)$ - fraction of mass converted from resin to vapor by the pyrolysis reaction (then $1-F_{py}$ would be the fraction converted to char, i.e., the fraction of solid mass remaining after pyrolysis)

$F_{sc}(T)$ - fraction of mass (of char and reinforcement combined) remaining as the solid product of the char-reinforcement reaction

$F_{dec}(T)$ - fraction of mass converted from the solid product (of the char-reinforcement reaction) to gas by further decomposition.

Other symbols used are defined in the Nomenclature Section of this report.

If all these chemical conversions are taken into account, the following expression for the density of the solid material for any degree of gas

generation results from a mass balance:

$$\rho = \rho_v^* - \rho_{g1} - \rho_{g2} - \rho_{g3} \quad . \tag{B-1}$$

Since each F_i can be treated as a ratio of densities as well as a ratio of mass increments, we can immediately write by definition

$$\rho_{g1} = \rho_{res}^* F_{py} = \rho_v^* F_{res} F_{py} \tag{B-2}$$

and

$$\rho_{g3} = \rho_s F_{dec} = \rho_s^* F_{sc} F_{dec} \quad . \tag{B-3}$$

The density of the intermediately formed gas is obtained in somewhat different fashion because we ultimately express it in terms of the density of the solid product instead of the reactants. Thus we first write

$$\rho_{g2} = \rho_c + \rho_r - \rho_s \quad . \tag{B-4}$$

But $\rho_c = \Gamma_{c,s} \rho_s$ and $\rho_r = \Gamma_{r,s} \rho_s$. Therefore we obtain

$$\rho_{g2} = (\Gamma_{c,s}+\Gamma_{r,s}-1)\rho_s = (\Gamma_{c,s}+\Gamma_{r,s}-1)\rho_s^* F_{sc} \quad . \tag{B-5}$$

Finally, substituting Eqs. (B-2), (B-3), and (B-5) in (B-1) yields

$$\rho = \rho_v^*(1-F_{res}F_{py}) - (\Gamma_{c,s}+\Gamma_{r,s}-1)\rho_s^* F_{sc} - \rho_s^* F_{sc} F_{dec} \tag{B-6}$$

from which we obtain Eq. (4) by combining terms.

APPENDIX C

SURFACE RECESSION CALCULATIONS

As the surface temperature of the thrust chamber wall at the hot gas boundary increases, several modes of surface removal become possible. They include melting, vaporization (or decomposition), and chemical reactions between the wall material and certain combustion gas components. These modes of surface recession were considered in order to be able to handle two cases: (1) surface removal occurs only by melting and/or vaporization, typical of glass-reinforced ablative materials; (2) surface removal occurs only by vaporization and/or chemical reaction with the combustion gas, typical of carbon or graphite cloth-reinforced ablative materials or solid graphite.

For both cases, the energy balance at the hot gas boundary can be written in the following form, equivalent to Eq. (12) (using $G_i = -\rho v_i^*$ for each mode i):

$$K \left.\frac{\partial T}{\partial n}\right|_s = h_{eff}(T_{aw}-T_s) - \rho \sum_i v_i \Delta H_i \quad , \qquad \text{(C-1)}$$

where, for case (1) above, $\sum_i v_i \Delta H_i$ is interpreted as $v_{vap}\Delta H_{vap} + v_w\left[\Delta H_m + \frac{2}{3}(C_p)_m(T_s-T_m)\right]$.

*Nomenclature for this Appendix appears at the end of the section.

Each of the chemical reaction modes is governed by a "kinetic rate" equation that defines the temperature dependence. A solution for the surface recession can therefore be obtained by a simultaneous solution of the energy and kinetic rate equations. A one-dimensional (radial coordinate y), constant-property form of the energy equation can be written in the form

$$K \frac{\partial^2 T}{\partial y^2} + \frac{K}{y} \frac{\partial T}{\partial y} = G_g (C_p)_g \frac{\partial T}{\partial y} + \rho C \frac{\partial T}{\partial \tau} \quad . \tag{C-2}$$

Integrating Eq. (C-2) from the gas surface y_s to a position into the wall material, given by y_s+s_1, yields (with Eq. (C-1))

$$\rho \sum v_i \Delta H_i = h_{eff}(T_{aw}-T_s) + \left\{ \left[K \left. \frac{\partial T}{\partial y} \right|_{s_1} - \left(\frac{K}{y} - G_g (C_p)_g \right) (T_s - T_1) \right] \right.$$
$$\left. - \rho C \int_{y_s}^{y_s+s_1} \frac{\partial T}{\partial \tau} \, dy \right\} \Big/ \sqrt{1 + \left(\frac{\partial f}{\partial x} \right)^2} \tag{C-3}$$

where

$$\frac{\partial T}{\partial n} \simeq - \frac{\partial T}{\partial y} \Big/ \sqrt{1 + \left(\frac{\partial f}{\partial x} \right)^2} \tag{C-4}$$

and $\frac{1}{y}$ is a constant in the integration, since y changes only slightly in the interval (y_s, y_s+s_1). To evaluate the integral of Eq. (C-3) it is assumed that the temperature profile in the wall

material can be approximated by the quadratic form, $T = T_s - a(y-y_s) + b(y-y_s)^2$, with coefficients determined by the temperatures at the surface and the first and second mesh points on each vertical line. Leibnitz's rule gives

$$\int_{y_s}^{y_s+s_1} \frac{\partial T}{\partial \tau}\, dy = \frac{\partial}{\partial \tau} \int_{y_s}^{y_s+s_1} T dy + \sum v_i\, T_s \qquad (C\text{-}5)$$

where Σv_i is defined by Eq. (C-30) or (C-31) below. Then the integral on the right side of Eq. (C-5) can be obtained as follows:

$$\int_{y_s}^{y_s+s_1} T dy = s_1\left(T_s - \frac{as_1}{2} + \frac{bs_1^2}{3}\right) \quad , \qquad (C\text{-}6)$$

where

$$a = (T_s - T_1)/s_1 + \frac{[s_2 T_s + s_1 T_2 - (s_1+s_2)T_1]}{s_2(s_1+s_2)} \qquad (C\text{-}7)$$

and

$$b = (as_1 + T_1 - T_s)/s_1^2 \quad . \qquad (C\text{-}8)$$

A forward time difference (which we abbreviate here using the operator δ_τ) is used to evaluate the time derivative giving

$$\rho \Sigma v_i \Delta H_i = h_{eff}(T_{aw} - T_s) - \left\{\rho C\left[\delta_\tau \int_{y_s}^{y_s+s_1} T dy + T_s \Sigma v_i\right] + (a - 2bs_1)K\right. \qquad (C\text{-}9)$$

$$\left. + \left[\frac{K}{y} - G_\pi (C_p)_g\right](T_s - T_1)\right\} \Big/ \sqrt{1 + \left(\frac{\partial f}{\partial x}\right)^2}$$

Iteration is then performed on the value of surface temperature until Eq. (C-9) gives the same recession rate Σv_i as the kinetic rate equation (C-27) discussed below.

MELTING ABLATION

An estimate for the removal of material by melting can be obtained in simple form only at the axial position for which the surface heating is a maximum or minimum in whose neighborhood the surface temperature of the melt can be considered constant.

The differential equation governing the flow of the melt layer can be written in the following form, neglecting the effect of pressure gradients (Ref. 17):

$$v_w - v_{vap} = \frac{\delta_m^2}{2} \frac{\partial}{\partial \nu} \left(\frac{g_c \tau_{sh}}{\mu_m} \right) \quad . \tag{C-10}$$

where δ_m is obtained as the ratio of $K_m(T_s - T_m)$ and $h_{eff}(T_{aw} - T_s)$. When the tangential derivatives of heating rate are zero, Eq. (C-10) can be written in the simpler form,

$$v_w - v_{vap} = \frac{g_c \delta_m^2}{2\mu_m} \frac{\partial \tau}{\partial \nu} \quad . \tag{C-11}$$

Reynolds' Analogy can be used to relate shear stress to the local heating conditions:

$$\tau_{sh} = \frac{c_f}{2} \frac{\rho_e U_e^2}{g_c} = \frac{h_{conv} U_e Pr^{2/3}}{g_c (C_p)_e} \quad . \tag{C-12}$$

Therefore

$$\frac{\partial \tau_{sh}}{\partial v} = \frac{h_{conv} Pr^{2/3}}{g_c (C_p)_e} \frac{\partial U_e}{\partial v} \quad . \tag{C-13}$$

In the throat region of a nozzle, Sauer's Analysis (Ref. 18) can be used to estimate the velocity gradient, yielding

$$\frac{\partial U_e}{\partial v} = a^* \left(1 + \frac{r_t}{2r_c}\right) \left[\frac{2}{(\gamma+1) r_t r_c}\right]^{1/2} \quad . \tag{C-14}$$

In addition, the melting rate equation for the throat can be written as

$$v_w - v_{vap} = \frac{h_{conv} Pr^{2/3} \delta_m^2 a^*}{2\mu_m (C_p)_e} \left(1 + \frac{r_t}{2r_c}\right) \left[\frac{2}{(\gamma+1) r_t r_c}\right]^{1/2} \quad . \tag{C-15}$$

For purposes of the present analysis, we assume that Eq. (C-11) holds for the entire chamber and nozzle regions as well. Finally, the free stream velocity gradient is estimated on the basis of one-dimensional flow to yield

$$\frac{\partial U_e}{\partial v} = \left(\frac{\gamma+1}{2}\right)^{\frac{1}{2(\gamma+1)}} \frac{a^* M^{*3/2} \left(1 - \frac{\gamma-1}{\gamma+1} M^{*2}\right)^{\frac{2\gamma-1}{2(\gamma-1)}} \sin\beta}{r_t (1 - M^{*2})} \quad . \tag{C-16}$$

For use in Eqs. (C-10) - (C-16) in addition to the equations appearing below, the following parameters are required:

$$Pr = \frac{4\gamma}{9\gamma-5} \tag{C-17}$$

$$\mu_e = 5 \times 10^{-9} M_w^{0.5} T_{aw}^{0.6} \tag{C-18}$$

$$\mu_m = k_m \exp(-E/RT_s) \tag{C-18a}$$

$$(C_p)_e = \frac{2\gamma}{(\gamma-1)M_w} \tag{C-19}$$

$$\Delta = \frac{(C_p)_e \mu_e}{h_{conv} Pr} \tag{C-20}$$

$$\left(\frac{r_t}{r}\right)^2 = \left(\frac{\gamma+1}{2}\right)^{\frac{\gamma+1}{\gamma-1}} \frac{M}{\left(1+\frac{\gamma-1}{2}M^2\right)^{\frac{\gamma+1}{\gamma-1}}} \tag{C-21}$$

$$\frac{\rho_e}{P_c} = \frac{M_w}{RT_{aw}} \left(1+\frac{\gamma-1}{2}M^2\right)^{-\frac{\gamma}{\gamma-1}} \tag{C-22}$$

MASS TRANSFER EFFECTS

In computing the amount of surface recession for reacting or vaporizing materials, the diffusion of the reactants and/or products of the reaction or vaporization through the boundary layer must be considered.

For this analysis, a frozen composition boundary layer is assumed where the species in question diffuses through the boundary layer without reaction. In this case, the steady state mass flux of the species is

governed by the following differential equation (see Ref. 19), where the subscript 1 is omitted for convenience:

$$\rho_e D \frac{\partial^2 Y}{\partial n^2} - \rho_e V \frac{\partial Y}{\partial n} = 0 \quad . \tag{C-23}$$

For a constant mass diffusion coefficient, Eq. (C-23) has the solution

$$Y = Y_w + (Y_\infty - Y_w) \left[\frac{1 - e^{\frac{Vn}{D}}}{1 - e^{\frac{V\Delta}{D}}} \right] \quad . \tag{C-24}$$

As the blowing velocity V approaches zero, we obtain the following familiar expression through differentiation of Eq. (C-24) and use of l'Hopital's rule:

$$\frac{\partial Y}{\partial n} = \frac{Y_\infty - Y_w}{\Delta} \quad . \tag{C-25}$$

This combined with a particular integral of Eq. (C-23) yields

$$\rho v = -\rho_e V = - \frac{\rho_e D (Y_\infty - Y_w)}{\Delta} \tag{C-26}$$

provided the solution is restricted to $V \ll D/\Delta$ in the boundary layer.

When vaporization or decomposition occurs as the mode of surface removal, the diffusing component is considered to be the component vaporized or decomposed at the surface. Equation (C-26) is used to compute the recession rate because the mole fraction at the wall is

known, as discussed in the next section. When a chemical reaction occurs between the exhaust gases and the wall material, the diffusing component is the reactant in the combustion gas. In this case the mole fraction of reactant at the wall must be computed.

The recession rate of the wall is given by

$$\dot{r} = k_w Y_w e^{-E/RT_s} \quad . \tag{C-27}$$

In this case the wall concentration is computed from the following relation obtained from Eqs. (C-26) and (C-27)

$$D \frac{\partial Y}{\partial n} = \frac{\rho}{\rho_e} k_w Y_w e^{-E/RT_s} \quad . \tag{C-28}$$

Therefore, from Eqs. (C-25) and (C-28) we obtain

$$Y_w = Y_\infty \left[1 + \frac{\rho k_w \ell e^{-E/RT_s}}{\rho_e D} \right]^{-1} \quad . \tag{C-29}$$

Equation (C-28) automatically accounts for diffusion limited reactions and gives a smooth transition between kinetic controlled and diffusion controlled reactions.

In its current form, the computer program written to perform the surface recession calculation can accommodate a maximum of

three chemical reactions occurring independently at the material surface. Total erosion is computed as the sum of the individual reactions plus vaporization, or melting plus vaporization,

$$\Sigma v_i = v_1+v_2+v_3+v_{vap} \quad \text{(chemical reactions)} \tag{C-30}$$

or

$$\Sigma v_i = v_w \quad \text{(melting)} \ . \tag{C-31}$$

VAPORIZATION OR DECOMPOSITION

When the material does not melt, and the exhaust gases are non-reactive to the parent material, surface removal is assumed to occur only by vaporization (in the case of graphite) or thermal decomposition (in the case of Teflon, silicon carbide, etc.).

The generation of vapor is handled as a zero-order reaction by computing an equilibrium vapor pressure. These data are then used to determine a vapor pressure equation of the form

$$P_{vap} = k_{vap} e^{-E/RT_s} \ . \tag{C-32}$$

The latent heat of vaporization (or decomposition) is then equal to E and the rate of surface removal estimated by diffusion of the products of decomposition through the boundary layer using Eq. (C-26).

NOMENCLATURE

Capital Letters

C	Specific heat of wall material
C_p	Specific heat at constant pressure
D	Coefficient of mass diffusion
E	Activation energy of reaction
G	Mass flow rate per unit area
ΔH	Enthalpy change during reaction
K	Thermal conductivity
M	Mach number
M_w	Molecular weight
P	Pressure
Pr	Prandtl number
R	Universal gas constant
T	Temperature
T_{aw}	Adiabatic wall temperature
T_1	Temperature at first interior mesh point
T_2	Temperature at second interior mesh point
U	Gas velocity
V	Blowing velocity of ejected gas ($= -\rho v/\rho_e$)
Y	Mole fraction of gas

Lower Case Letters

a^*	Sonic velocity
c_f	Coefficient of friction
$f(x,\tau)$	Radial position of hot gas boundary
g_c	Gravitational constant
h_{conv}	Convective heat transfer coefficient
h_{eff}	Effective heat transfer coefficient
k_m	Constant factor in melt viscosity equation
k_{vap}	Constant factor in vapor pressure equation
k_w	Constant factor in rate equation
n	Normal coordinate to surface
r_c	Radius of curvature of the throat
r_t	Throat radius (value of y at the throat)
v	Normal recession rate of surface $\left(= \frac{\partial f}{\partial \tau} / \sqrt{1 + (\partial f/\partial x)^2}\right)$
x	Axial coordinate
y	Radial coordinate

Greek Letters

β	Angle of wall surface
γ	Specific heat ratio of gases
δ_m	Melt layer thickness
Δ	Effective thickness of boundary layer
ν	Tangential coordinate to surface

μ	Viscosity
ρ	Density
τ	Time
τ_{sh}	Shear stress

Subscripts

c	Chamber conditions
e	Conditions at edge of boundary layer
g	Conditions in gas generated within charring ablator
i	Index ranging over modes of wall erosion
m	Melt properties or conditions
s	Gas-liquid interface (or gas-wall interface if no liquid is present)--often referred to as "surface" in text
s_1	Distance from surface to first interior mesh point
s_2	Distance from first to second interior mesh point
vap	Vapor properties or conditions
w	Wall surface
∞	Free stream conditions

Superscript

*	Sonic conditions

APPENDIX D

STABILITY ANALYSIS FOR THE FINITE DIFFERENCE ANALOG OF THE LINEAR CONDUCTION EQUATION

A difference scheme, such as that obtained by assigning values to r and s in Eq. (25) above, will be termed stable, for given values of the space and time increments if initial, truncation, or boundary errors introduced into the analysis do not grow without bound as the number of time steps increases. Thus a sufficient condition for stability is that the ratio of the total error at the end of any computational step to that at the beginning does not exceed one in modulus. A stability analysis will be performed for Eq. (25) for varying r and s to determine which values provide stable schemes. Stability will be further characterized as conditional or unconditional according to whether or not it depends upon the boundedness of the ratio $R = \frac{\alpha \Delta \tau}{h^2}$.

Using Eq. (20) above and its radial analog for $d_A=d_B=d_C=d_D=h$, we can rewrite Eq. (25) in the following form (the indices m and n are used to indicate spatial subscripting rather than i and j to avoid confusion below with the imaginary number $i = \sqrt{-1}$):

$$\left\{1-h^2R(r\delta_x^2 + s\delta_y^2)\right\}T_{m,n,k+1} = \left\{1+h^2R[(1-r)\delta_x^2+(1-s)\delta_y^2]\right\}T_{m,n,k} \quad (D\text{-}1)$$

If we ignore the effect of boundary conditions and lump all errors introduced into the analysis at any point (x_m, y_n, τ_k) into a single variable,

$\epsilon_{m,n,k}$, then we see that $\epsilon_{m,n,k}$ will satisfy Eq. (D-1) within terms of order $h^2+(r+s-1)\Delta\tau + \Delta\tau^2$. Assuming a separated solution for $\epsilon_{m,n,k}$ (see Ref. 20, for example) of the form

$$\epsilon_{m,n,k} = \sum_{p,q} A_{p,q}\eta_{p,q}^{k} e^{im\alpha_p h} e^{in\beta_q h}, \qquad (D-2)$$

where p,q take on integral values, then if we can show that $|\eta_{p,q}| \leq 1$ for all p and q this will imply that $\frac{\epsilon_{m,n,k+1}}{\epsilon_{m,n,k}} \leq 1$. This is the sufficient condition stated earlier for stability.

Substituting Eq. (D-2) into (D-1), equating terms of like indices p and q and eliminating common factors we obtain:

$$\left\{1-h^2R\left[r\delta_x^2+s\delta_y^2\right]\right\} e^{im\alpha_p h} e^{in\beta_q h}\eta_{p,q} = \left\{1+h^2R\left[(1-r)\delta_x^2+(1-s)\delta_y^2\right]\right\}e^{im\alpha_p h} e^{in\beta_q h} \qquad (D-3)$$

Then using the identities

$$h^2\delta_x^2 e^{im\alpha h} = -4e^{im\alpha h}\sin^2\frac{\alpha h}{2}, \qquad (D-4)$$

$$h^2\delta_y^2 e^{in\beta h} = -4e^{in\beta h}\sin^2\frac{\beta h}{2}, \qquad (D-5)$$

Eq. (D-3) can be rewritten in the following form:

$$\eta = \frac{1-4R\left[(1-r)\sin^2\frac{\alpha h}{2} + (1-s)\sin^2\frac{\beta h}{2}\right]}{1+4R\left[r\sin^2\frac{\alpha h}{2} + s\sin^2\frac{\beta h}{2}\right]}. \qquad (D-6)$$

We wish to see when $|\eta| \leq 1$ or $-1 \leq \eta \leq 1$. Because $r, s \leq 1$, we see that $\eta \leq 1$ is satisfied for all permissible values of r,s, and R; $\eta \geq -1$ is satisfied when

$$R\left[(1-2r)\sin^2 \frac{\alpha h}{2} + (1-2s)\sin^2 \frac{\beta h}{2}\right] \leq \frac{1}{2} . \tag{D-7}$$

It is easy to see that (D-7) holds for all $R > 0$ if

$$r, s \geq \frac{1}{2} . \tag{D-8}$$

Thus, if r and s satisfy (D-8), Eq. (D-1) determines an unconditionally stable scheme. If $r,s < \frac{1}{2}$, then (D-7) holds only for

$$R \leq \frac{1}{4[1-(r+s)]} \tag{D-9}$$

and we have only conditional stability. We may similarly show that for one of the parameters, say r, less than $\frac{1}{2}$ and $s \geq \frac{1}{2}$, (D-7) is satisfied when $R \leq \frac{1}{2(1-2r)}$ and again we have only conditional stability. These cases cover all possible schemes determined by Eq. (25) for which r and s are invariant and we therefore see that the only ones which satisfy the sufficient condition of non-amplification for all values of R are those given by (D-8).

There is another class of schemes in which values for r and s are switched after every time step, which we term "alternating schemes". In particular, we will consider a restricted class of alternating schemes

for which $s = 1-r$ and $r > \frac{1}{2}$ in odd time steps. The alternating direction method of Peaceman and Rachford falls within this class and is obtained when $r = 1$ and $s = 0$ in odd time steps and $r = 0$ and $s = 1$ in even. To analyze the stability of this restricted class of alternating schemes, we investigate the following two expressions, one for an odd step and one for an even which are analogous to Eq. (D-6):

$$\eta_{odd} = \frac{1-4R\left[(1-r_o)\sin^2\frac{\alpha h}{2} + r_o\sin^2\frac{\beta h}{2}\right]}{1+4R\left[r_o\sin^2\frac{\alpha h}{2} + (1-r_o)\sin^2\frac{\beta h}{2}\right]}, \qquad \text{(D-10)}$$

$$\eta_{even} = \frac{1-4R\left[r_o\sin^2\frac{\alpha h}{2} + (1-r_o)\sin^2\frac{\beta h}{2}\right]}{1+4R\left[(1-r_o)\sin^2\frac{\alpha h}{2} + r_o\sin^2\frac{\beta h}{2}\right]}, \qquad \text{(D-11)}$$

where r has the value r_o in odd steps and $1-r_o$ in even. It has already been demonstrated that neither $|\eta_{odd}|$ nor $|\eta_{even}|$ are bounded by 1 for all values of $R > 0$ but only for values of $R \leq \frac{1}{2(2r-1)}$ and $\leq \frac{1}{2(1-2r)}$, respectively. However, it can readily be shown that $|\eta_{odd}\eta_{even}| \leq 1$ for all $R > 0$, provided that R has the same value in both Eq. (D-10) and Eq. (D-11), i.e., provided that $\Delta\tau$ be held constant for two time steps. Therefore, we can assert the

unconditional stability of all such restricted alternating schemes for solving Eq. (D-1).* The simplest for computational purposes and therefore the one we have chosen is the Peaceman-Rachford method, since it is the only one which generates tridiagonal system of equations.

*Since the writing of this report a stability analysis was performed covering all possible alternating schemes, removing the restriction $r + s = 1$. The criterion determined for unconditional stability of an alternating scheme is $r + s \geq 1$ provided that each value of $\Delta\tau$ employed be held constant for at least two time steps. It can further be shown that, when $r + s < 1$, the condition on R required for stability is just inequality (D-9). Clearly, alternating schemes provide no advantage over those for which r and s are invariant, with the single exception of the alternating-direction method which is computationally more convenient.

Unclassified
Security Classification

DOCUMENT CONTROL DATA - R&D

(Security classification of title, body of abstract and indexing annotation must be entered when the overall report is classified)

1. ORIGINATING ACTIVITY (Corporate author) Rocketdyne, A Division of North American Aviation, Inc.	2a. REPORT SECURITY CLASSIFICATION Unclassified 2b. GROUP

3. REPORT TITLE
FINAL REPORT
EFFECT OF ROCKET ENGINE COMBUSTION ON CHAMBER MATERIALS, PART II: TWO-DIMENSIONAL COMPUTER PROGRAM

4. DESCRIPTIVE NOTES (Type of report and inclusive dates)

5. AUTHOR(S) (Last name, first name, initial)
Friedman, H. A., Persselin, S. F., Mc Farland, B. L., and Seader, J. D.

6. REPORT DATE	7a. TOTAL NO. OF PAGES	7b. NO. OF REFS
September 1965	146 & xv	22

8a. CONTRACT OR GRANT NO.	9a. ORIGINATOR'S REPORT NUMBER(S)
AF04(611)-9714 b. PROJECT NO. 3058 c. Task No. 305802 d. Program Structure No. 750G	AFRPL-TR-65-176 9b. OTHER REPORT NO(S) (Any other numbers that may be assigned this report) Rocketdyne No. R-6050-2

10. AVAILABILITY/LIMITATION NOTICES
Qualified requesters may obtain copies of this report from DDC.

11. SUPPLEMENTARY NOTES	12. SPONSORING MILITARY ACTIVITY
	Air Force Rocket Propulsion Laboratory, Edwards, California

13. ABSTRACT

An alternating direction implicit finite difference procedure is developed for solving a general class of two-dimensional transient non-linear ablation and heat conduction problems for rocket engine thrust chamber walls. Engine firing may be steady or can consist of multiple start or pulsing type modes. The analysis is performed in cylindrical coordinates (axial and radial) assuming an axisymmetric multi-material wall having arbitrarily curved boundaries and interfaces. A maximum (due only to computer storage limitations) of five different wall materials may be treated in a given problem including one charring ablative material. Temperature dependent properties may be specified for each material. Chemical reactions within the ablative material are handled in depth; also surface erosion due to chemical reactions or melting at the hot gas boundary is treated and the resulting surface recession is predicted. The numerical procedures have been programmed in Fortran IV for automatic computation on the IBM 7094 digital computer. Comparison of the results of sample computations with actual engine test firing data is included in this report.

DD FORM 1 JAN 64 1473

Unclassified
Security Classification

14. KEY WORDS	LINK A		LINK B		LINK C	
	ROLE	WT	ROLE	WT	ROLE	WT
Heat Transfer						
Mass Transfer						
Ablation						
Heat Conduction						
Ablative Materials Response						
Pyrolysis						
Charring						
Liquid Rocket Chamber Materials						
Mathematical Model						
Energy Equation						
Continuity Equation						
Two-Dimensional Heat Transfer Program						
Numerical Procedures						
Implicit Finite Difference Method						
Numerical Stability						
Curved Boundaries						
Char Depth						
Surface Recession						

INSTRUCTIONS

1. ORIGINATING ACTIVITY: Enter the name and address of the contractor, subcontractor, grantee, Department of Defense activity or other organization *(corporate author)* issuing the report.

2a. REPORT SECURITY CLASSIFICATION: Enter the overall security classification of the report. Indicate whether "Restricted Data" is included. Marking is to be in accordance with appropriate security regulations.

2b. GROUP: Automatic downgrading is specified in DoD Directive 5200.10 and Armed Forces Industrial Manual. Enter the group number. Also, when applicable, show that optional markings have been used for Group 3 and Group 4 as authorized.

3. REPORT TITLE: Enter the complete report title in all capital letters. Titles in all cases should be unclassified. If a meaningful title cannot be selected without classification, show title classification in all capitals in parenthesis immediately following the title.

4. DESCRIPTIVE NOTES: If appropriate, enter the type of report, e.g., interim, progress, summary, annual, or final. Give the inclusive dates when a specific reporting period is covered.

5. AUTHOR(S): Enter the name(s) of author(s) as shown on or in the report. Enter last name, first name, middle initial. If military, show rank and branch of service. The name of the principal author is an absolute minimum requirement.

6. REPORT DATE: Enter the date of the report as day, month, year, or month, year. If more than one date appears on the report, use date of publication.

7a. TOTAL NUMBER OF PAGES: The total page count should follow normal pagination procedures, i.e., enter the number of pages containing information.

7b. NUMBER OF REFERENCES: Enter the total number of references cited in the report.

8a. CONTRACT OR GRANT NUMBER: If appropriate, enter the applicable number of the contract or grant under which the report was written.

8b, 8c, & 8d. PROJECT NUMBER: Enter the appropriate military department identification, such as project number, subproject number, system numbers, task number, etc.

9a. ORIGINATOR'S REPORT NUMBER(S): Enter the official report number by which the document will be identified and controlled by the originating activity. This number must be unique to this report.

9b. OTHER REPORT NUMBER(S): If the report has been assigned any other report numbers *(either by the originator or by the sponsor)*, also enter this number(s).

10. AVAILABILITY/LIMITATION NOTICES: Enter any limitations on further dissemination of the report, other than those imposed by security classification, using standard statements such as:

(1) "Qualified requesters may obtain copies of this report from DDC."

(2) "Foreign announcement and dissemination of this report by DDC is not authorized."

(3) "U. S. Government agencies may obtain copies of this report directly from DDC. Other qualified DDC users shall request through _____."

(4) "U. S. military agencies may obtain copies of this report directly from DDC. Other qualified users shall request through _____."

(5) "All distribution of this report is controlled. Qualified DDC users shall request through _____."

If the report has been furnished to the Office of Technical Services, Department of Commerce, for sale to the public, indicate this fact and enter the price, if known.

11. SUPPLEMENTARY NOTES: Use for additional explanatory notes.

12. SPONSORING MILITARY ACTIVITY: Enter the name of the departmental project office or laboratory sponsoring *(paying for)* the research and development. Include address.

13. ABSTRACT: Enter an abstract giving a brief and factual summary of the document indicative of the report, even though it may also appear elsewhere in the body of the technical report. If additional space is required, a continuation sheet shall be attached.

It is highly desirable that the abstract of classified reports be unclassified. Each paragraph of the abstract shall end with an indication of the military security classification of the information in the paragraph, represented as *(TS), (S), (C), or (U)*.

There is no limitation on the length of the abstract. However, the suggested length is from 150 to 225 words.

14. KEY WORDS: Key words are technically meaningful terms or short phrases that characterize a report and may be used as index entries for cataloging the report. Key words must be selected so that no security classification is required. Identifiers such as equipment model designation, trade name, military project code name, geographic location, may be used as key words but will be followed by an indication of technical context. The assignment of links, rules, and weights is optional.